QA protocol: P2A_C3H_M10

Johannes Müller[1,2,†], Theresa Suckert[1,3,†], Elke Beyreuther[1, 4], Moritz Schneider[1], Marc Boucsein[5], Elisabeth Bodenstein[1, 2], Liane Stolz-Kieslich[1, 2], Mechthild Krause[1,2,3, 6, 7], Cläre von Neubeck[1, 3, 8], Robert Haase[9], Armin Lühr[1, 2, 3, 10 #], and Antje Dietrich[1,3,*,#]

[1] *OncoRay - National Center for Radiation Research in Oncology, Faculty of Medicine and University Hospital Carl Gustav Carus, Technische Universität Dresden, Helmholtz-Zentrum Dresden-Rossendorf, Dresden, 01309, Germany*
[2] *Helmholtz-Zentrum Dresden-Rossendorf, Institute of Radiooncology - OncoRay, Dresden, 01309, Germany*
[3] *German Cancer Consortium (DKTK), Partner Site Dresden, and German Cancer Research Center (DKFZ), Heidelberg, 69120, Germany*
[4] *Helmholtz - Zentrum Dresden - Rossendorf, Institute of Radiation Physics, Dresden, 01328, Germany*
[5] *Clinical Cooperation Unit Radiation Oncology, German Cancer Research Center (DKFZ), and Department of Radiation Oncology, Heidelberg University Hospital, Heidelberg, 69120, Germany*
[6] *Department of Radiotherapy and Radiation Oncology, Faculty of Medicine and University Hospital Carl Gustav Carus, Technische Universität Dresden, Dresden, Germany*
[7] *National Center for Tumor Diseases (NCT) Dresden, Dresden, 01307, Germany*
[8] *Department of Particle Therapy, University Hospital Essen, University of Duisburg-Essen, Essen, Germany*
[9] *DFG Cluster of Excellence Physics of Life, TU Dresden*
[10] *TU Dortmund, Dortmund, Germany*
[†] *these authors share first-authorship*
[#] *these authors share last-authorship*

March 13, 2021

Contents

1 CBCT image data **3**

2 Simulation image data **3**

3 Atlas image data **4**

4 MRI image data **5**
4.1 Denoising . . . 5
4.1.1 Sequence type: T1 . . . 5
4.1.2 Sequence type: T2 . . . 20
4.2 Registration (timepoints) . . . 34
4.2.1 Sequence type: T1 . . . 34
4.2.2 Sequence type: T2 . . . 35
4.3 Warping to CBCT . . . 37

5 Histology image data **38**
5.1 Bundle registration . . . 38
5.1.1 0001_Scene_1 . . . 38
5.1.2 0001_Scene_2 . . . 39
5.1.3 0002_Scene_1 . . . 40
5.1.4 0002_Scene_2 . . . 40
5.1.5 0003_Scene_1 . . . 41
5.1.6 0003_Scene_2 . . . 42
5.1.7 0004_Scene_1 . . . 43
5.1.8 0004_Scene_2 . . . 43
5.1.9 0005_Scene_1 . . . 44
5.1.10 0005_Scene_2 . . . 44
5.1.11 0006_Scene_1 . . . 45
5.1.12 0006_Scene_2 . . . 46
5.1.13 0007_Scene_1 . . . 47
5.1.14 0007_Scene_2 . . . 48
5.1.15 0008_Scene_1 . . . 48
5.1.16 0008_Scene_2 . . . 49
5.1.17 0009_Scene_1 . . . 50
5.1.18 0009_Scene_2 . . . 51
5.1.19 0010_Scene_1 . . . 51
5.1.20 0010_Scene_2 . . . 52
5.1.21 0011_Scene_1 . . . 53
5.1.22 0011_Scene_2 . . . 54
5.1.23 0012_Scene_1 . . . 54
5.1.24 0012_Scene_2 . . . 55
5.1.25 0013_Scene_1 . . . 56
5.1.26 0013_Scene_2 . . . 56
5.2 Slice2Volume . . . 57
5.3 Histology close-up . . . 59

1 CBCT image data

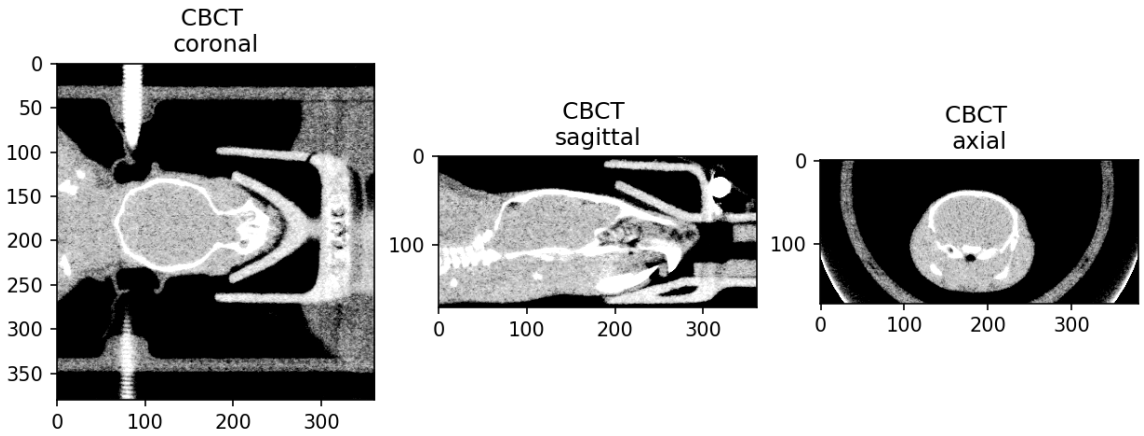


Figure 1.1: Multi-view cutplanes of CBCT serving as anatomical reference

2 Simulation image data

Received dose (mean dose within $0.9 \cdot D_{max}$): $60\,Gy$

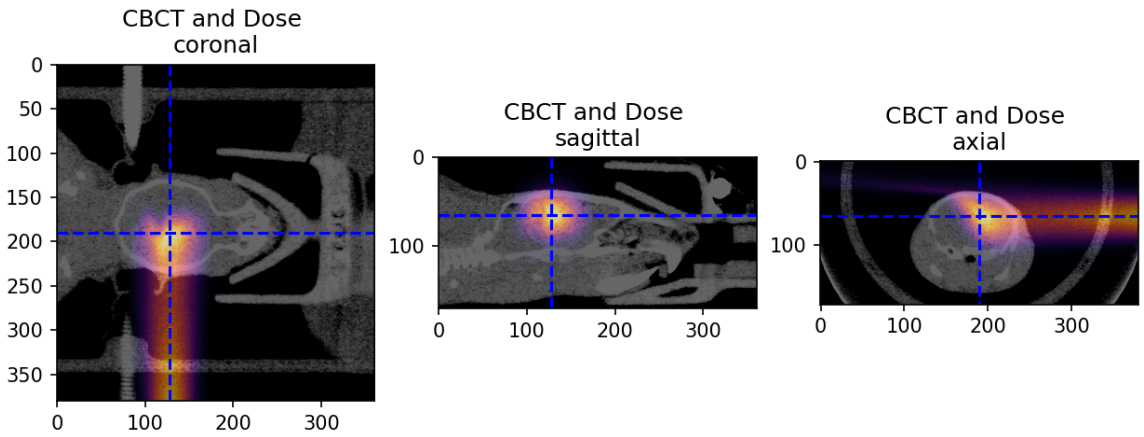


Figure 2.1: Overlay of CBCT and simulated dose distribution

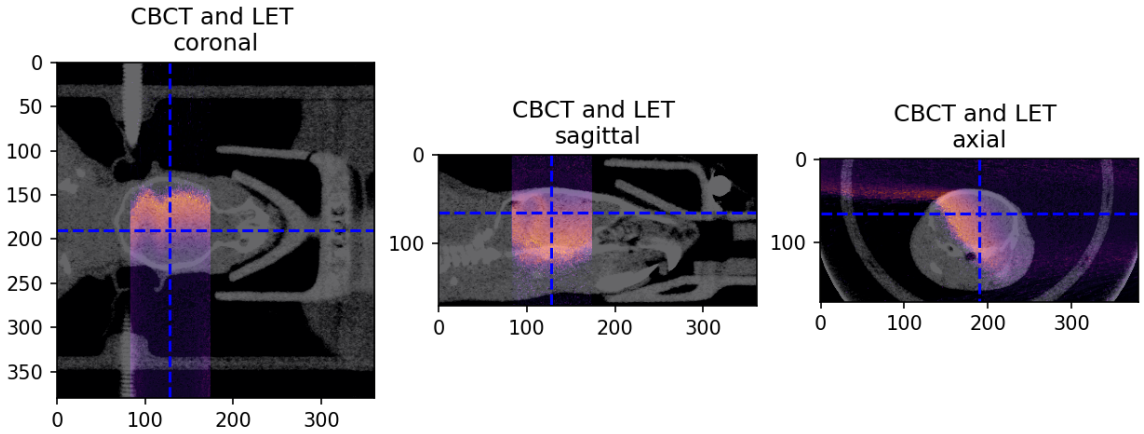


Figure 2.2: Overlay of CBCT and simulated LET distribution

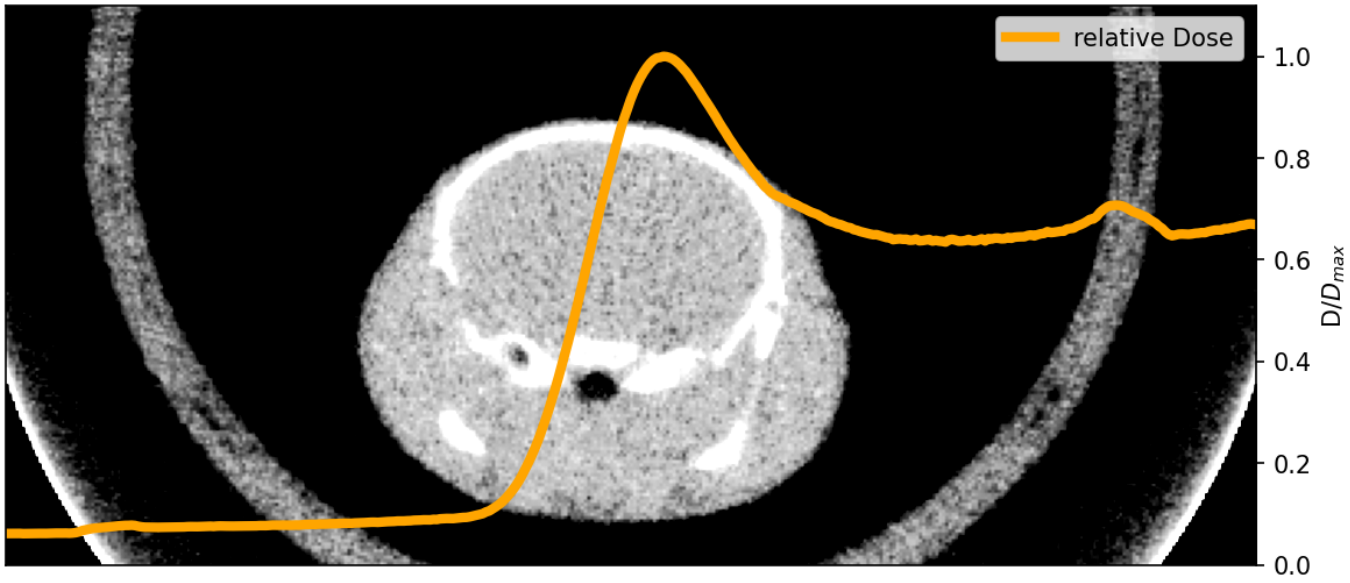


Figure 2.3: Axial CBCT slice with overlaid summed and normalized proton dose (orange).

3 Atlas image data

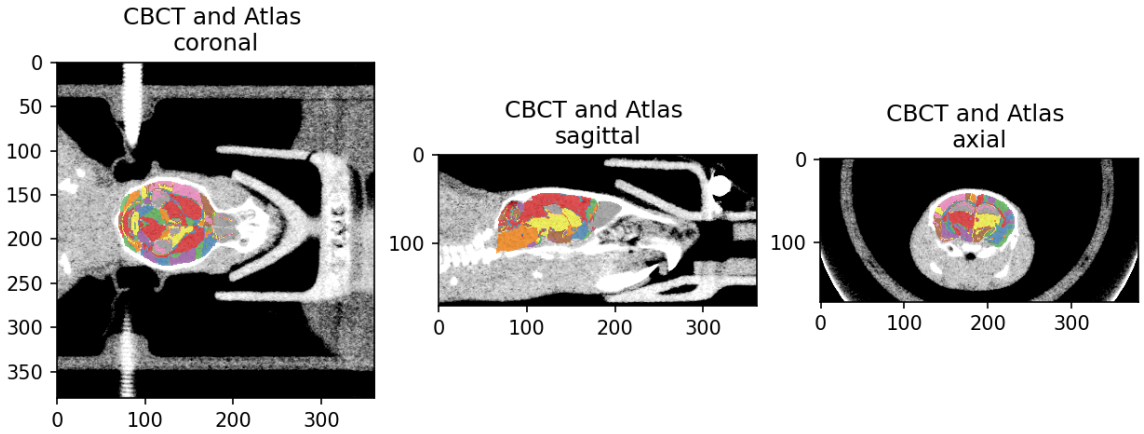


Figure 3.1: Overlay of CBCT and registered DSURQE brain atlas

4 MRI image data

4.1 Denoising

4.1.1 Sequence type: T1

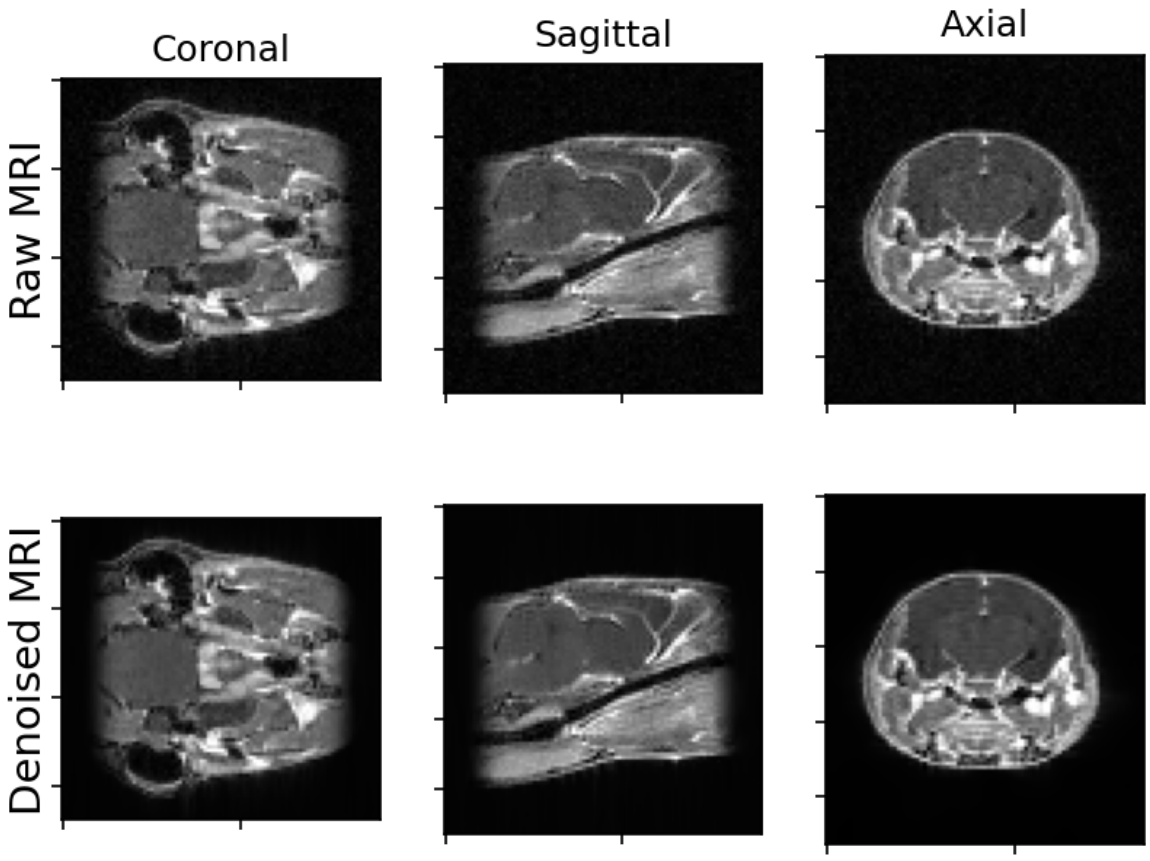


Figure 4.1: Raw and denoised MRI image, Timepoint:Week_00, Sequence type: T1, Signal-to-noise ratio (raw)= 41.76, Signal-to-Noise ratio (denoised) = 59.12

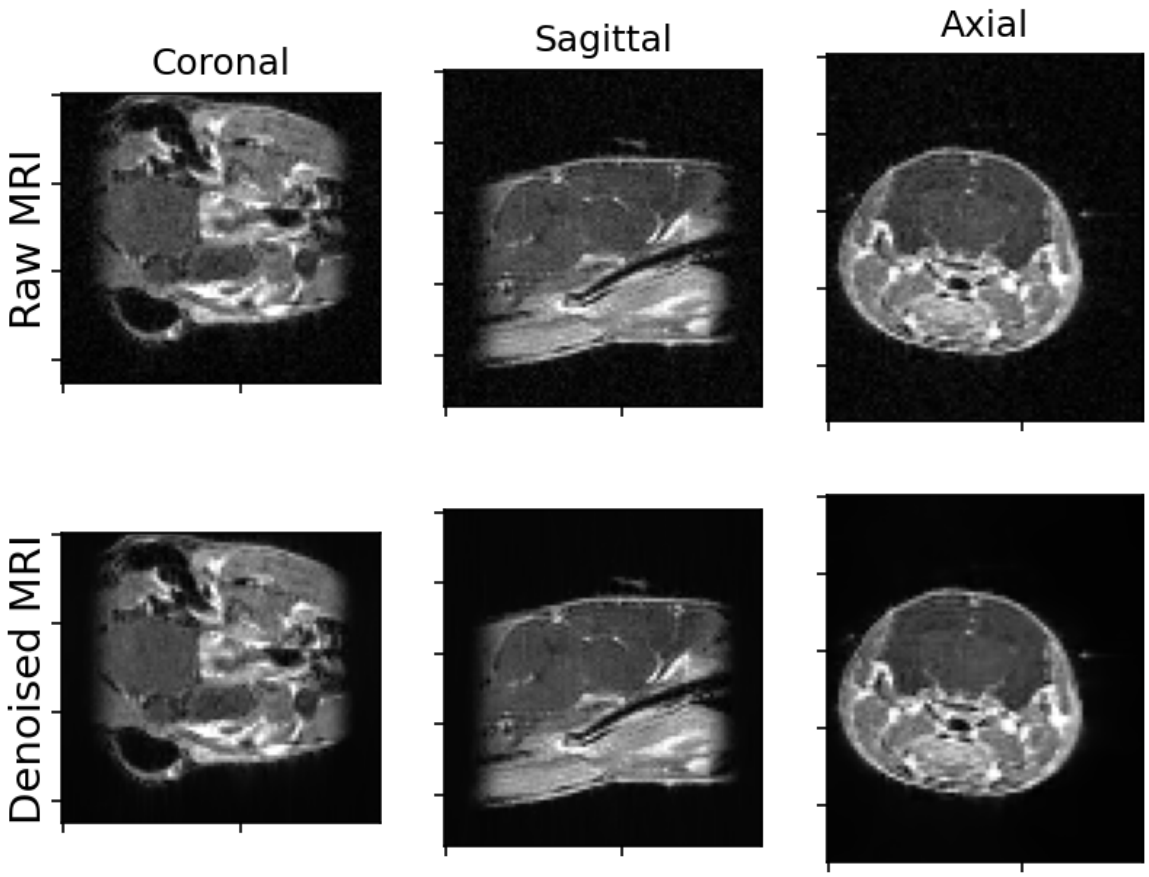


Figure 4.2: Raw and denoised MRI image, Timepoint:Week_01, Sequence type: T1, Signal-to-noise ratio (raw)= 43.94, Signal-to-Noise ratio (denoised) = 62.31

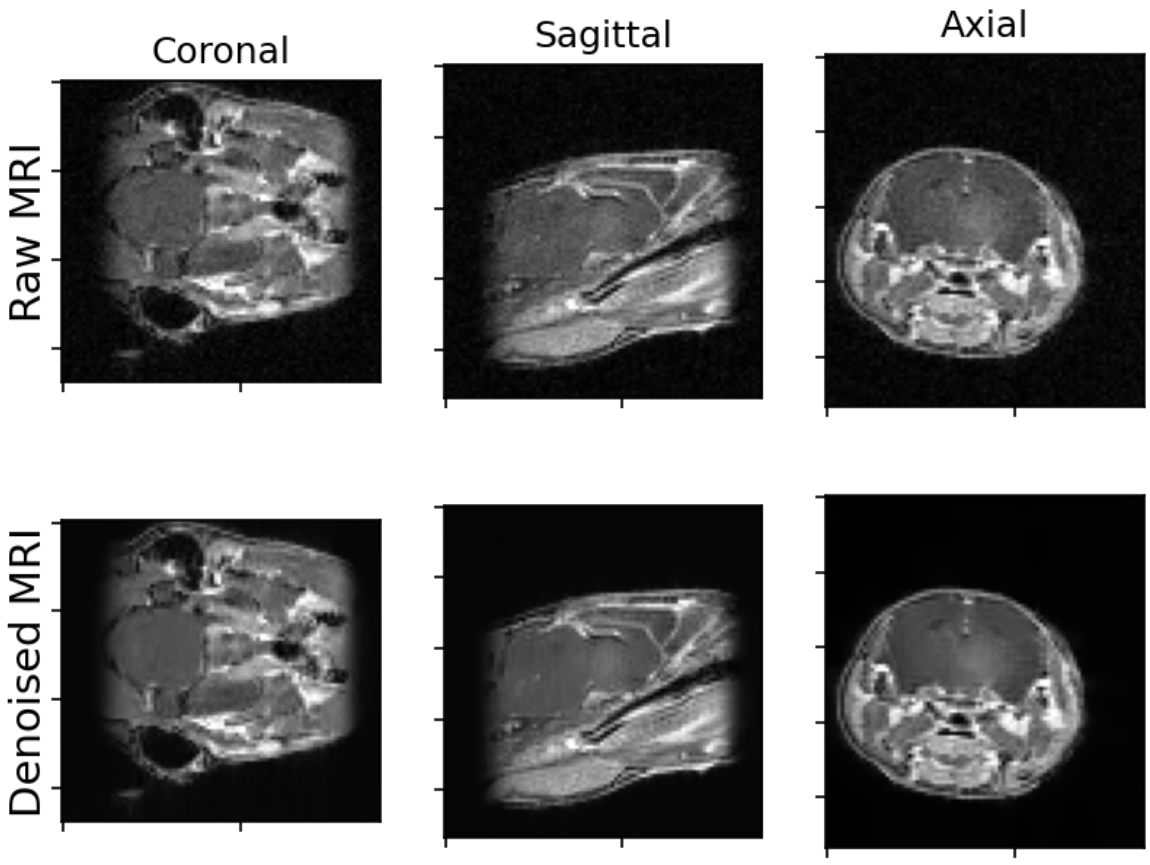


Figure 4.3: Raw and denoised MRI image, Timepoint:Week_03, Sequence type: T1, Signal-to-noise ratio (raw)= 42.10, Signal-to-Noise ratio (denoised) = 55.81

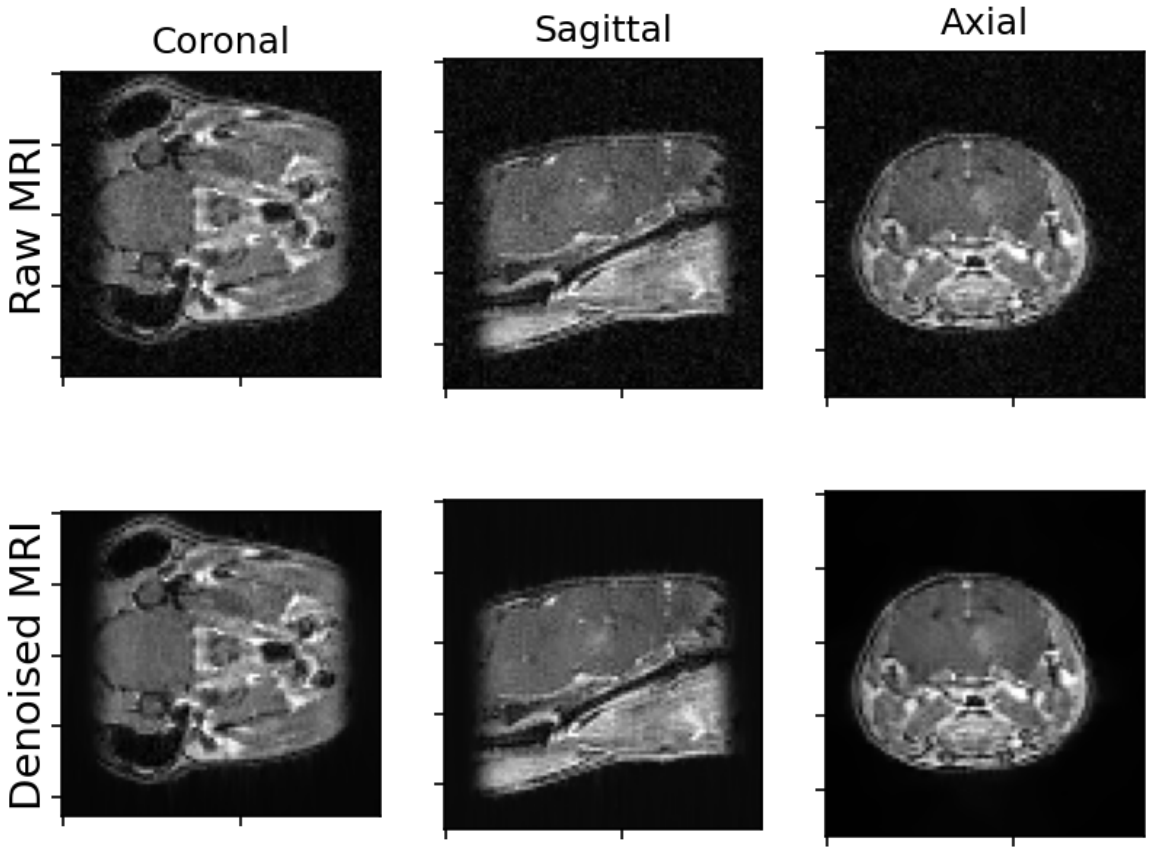


Figure 4.4: Raw and denoised MRI image, Timepoint:Week_05, Sequence type: T1, Signal-to-noise ratio (raw)= 41.84, Signal-to-Noise ratio (denoised) = 63.54

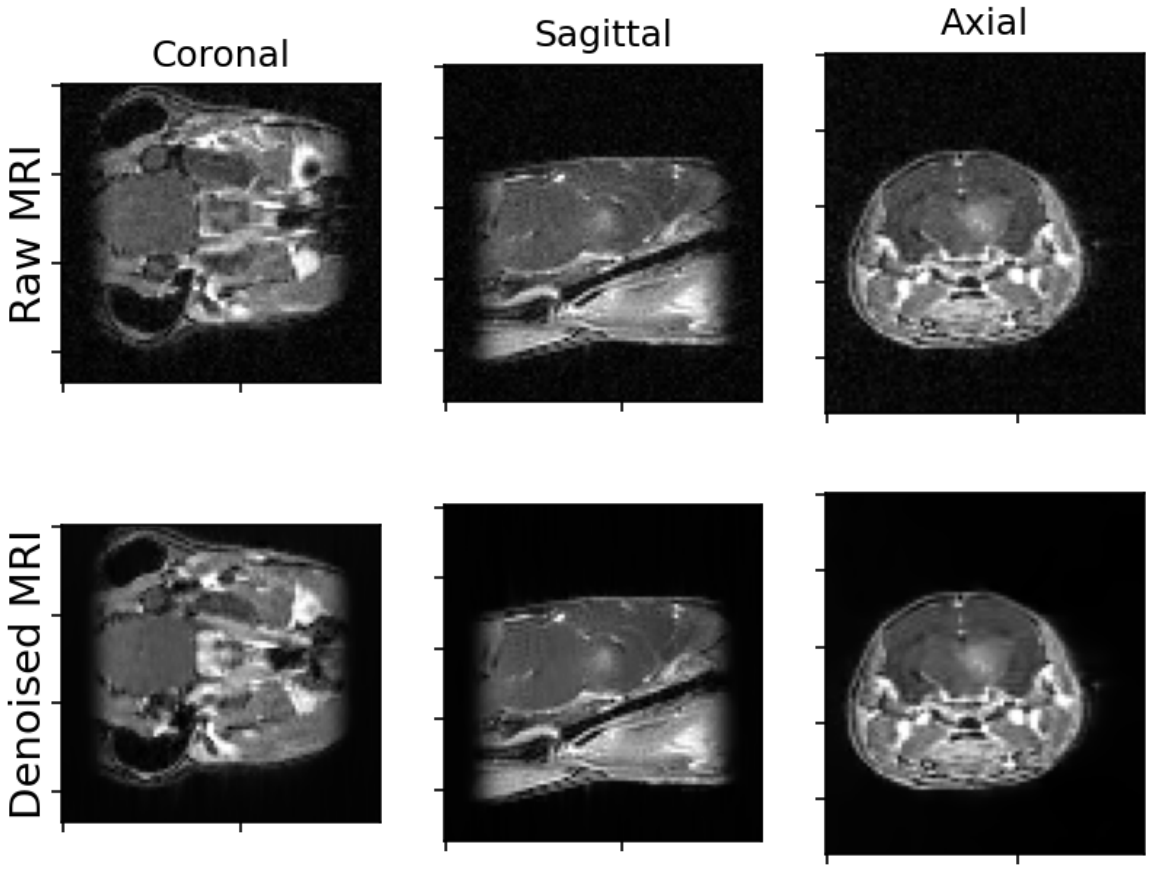


Figure 4.5: Raw and denoised MRI image, Timepoint:Week_07, Sequence type: T1, Signal-to-noise ratio (raw)= 46.45, Signal-to-Noise ratio (denoised) = 78.06

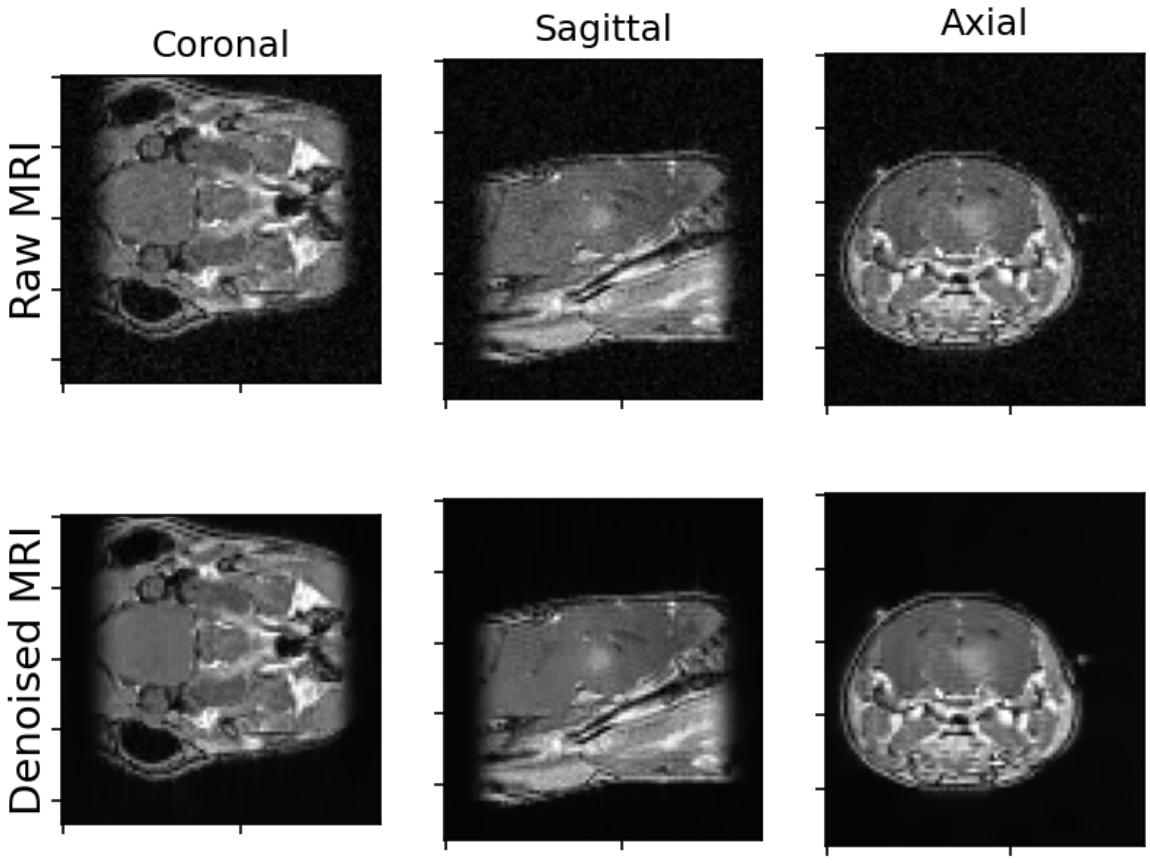


Figure 4.6: Raw and denoised MRI image, Timepoint:Week_09, Sequence type: T1, Signal-to-noise ratio (raw)= 43.61, Signal-to-Noise ratio (denoised) = 68.44

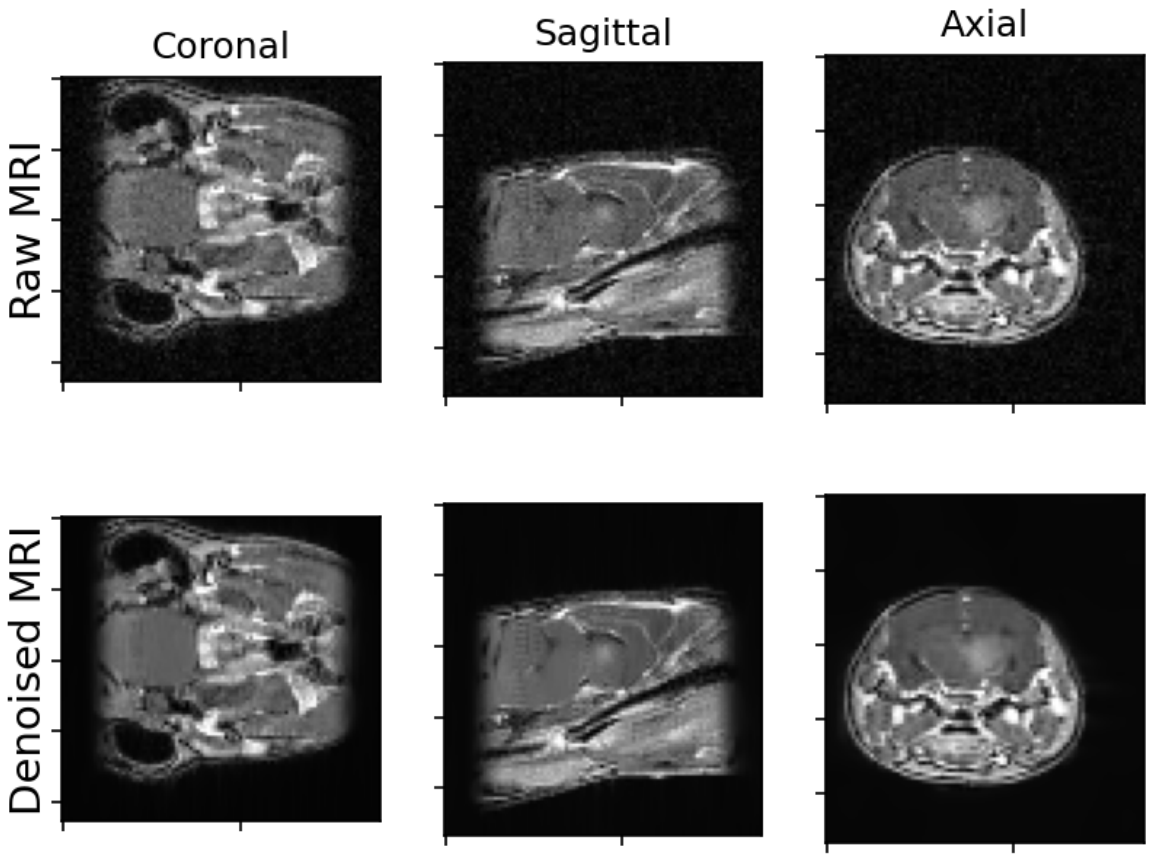


Figure 4.7: Raw and denoised MRI image, Timepoint:Week_11, Sequence type: T1, Signal-to-noise ratio (raw)= 41.24, Signal-to-Noise ratio (denoised) = 56.43

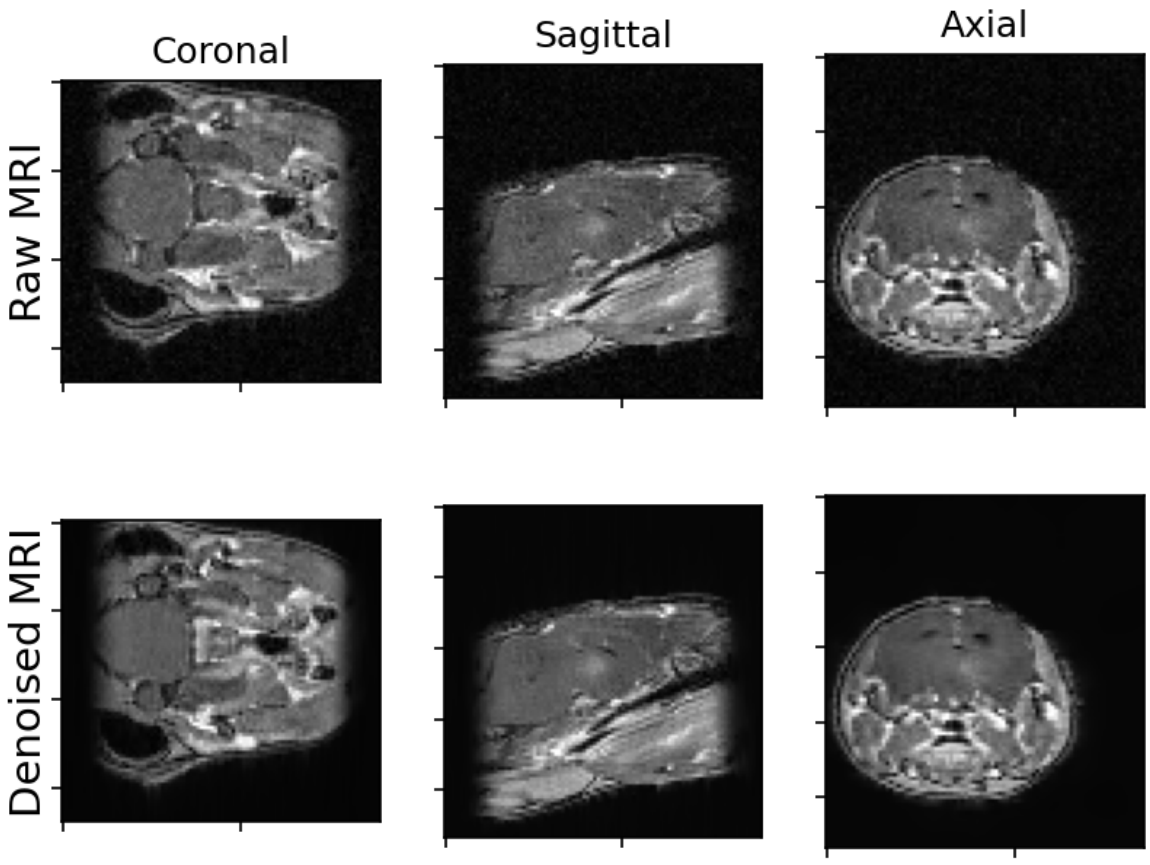


Figure 4.8: Raw and denoised MRI image, Timepoint:Week_13, Sequence type: T1, Signal-to-noise ratio (raw)= 39.42, Signal-to-Noise ratio (denoised) = 51.14

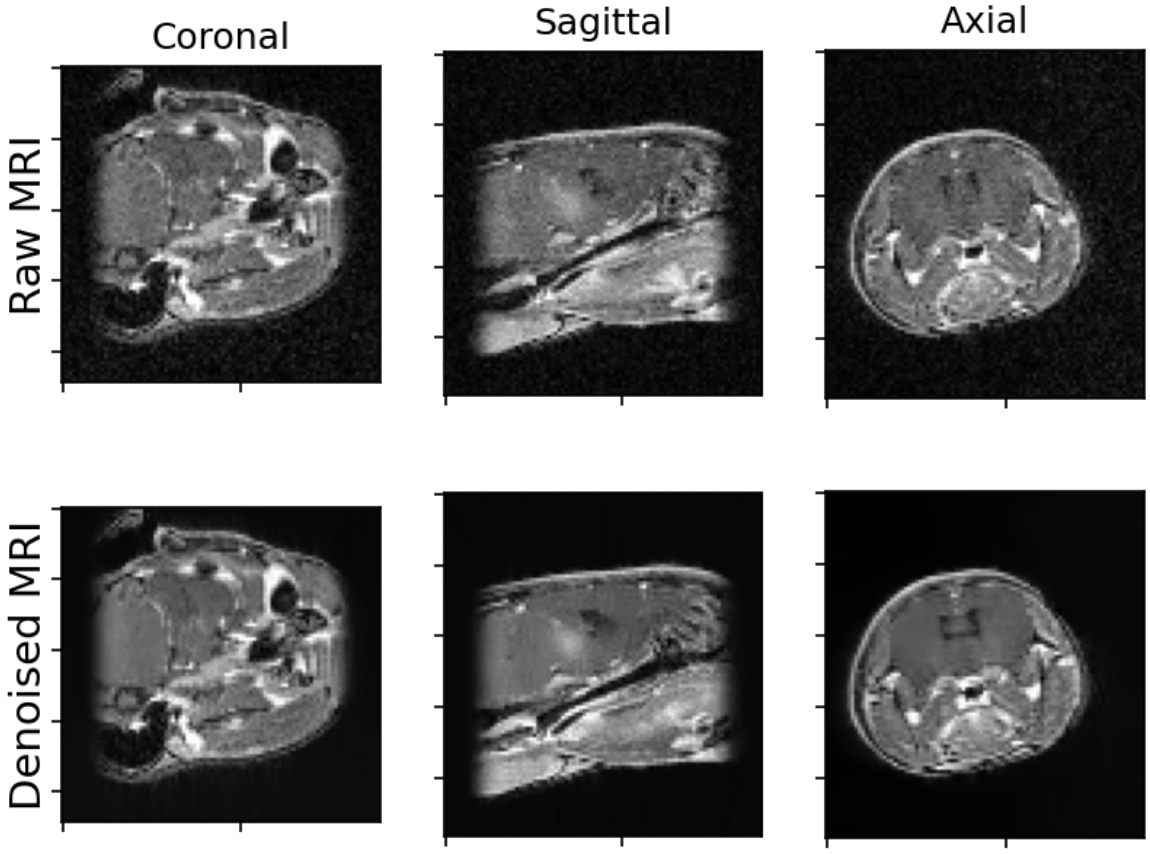


Figure 4.9: Raw and denoised MRI image, Timepoint:Week_15, Sequence type: T1, Signal-to-noise ratio (raw)= 46.44, Signal-to-Noise ratio (denoised) = 76.49

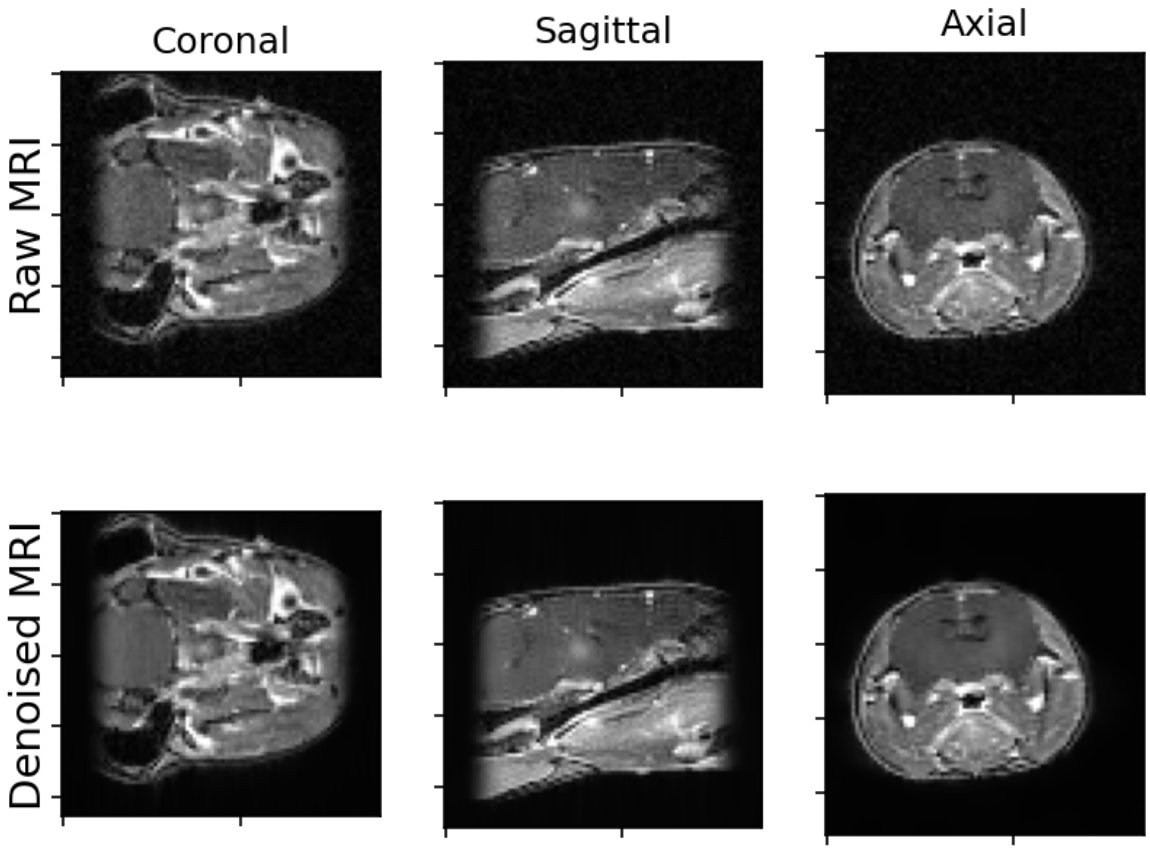


Figure 4.10: Raw and denoised MRI image, Timepoint:Week_17, Sequence type: T1, Signal-to-noise ratio (raw)= 42.63, Signal-to-Noise ratio (denoised) = 60.75

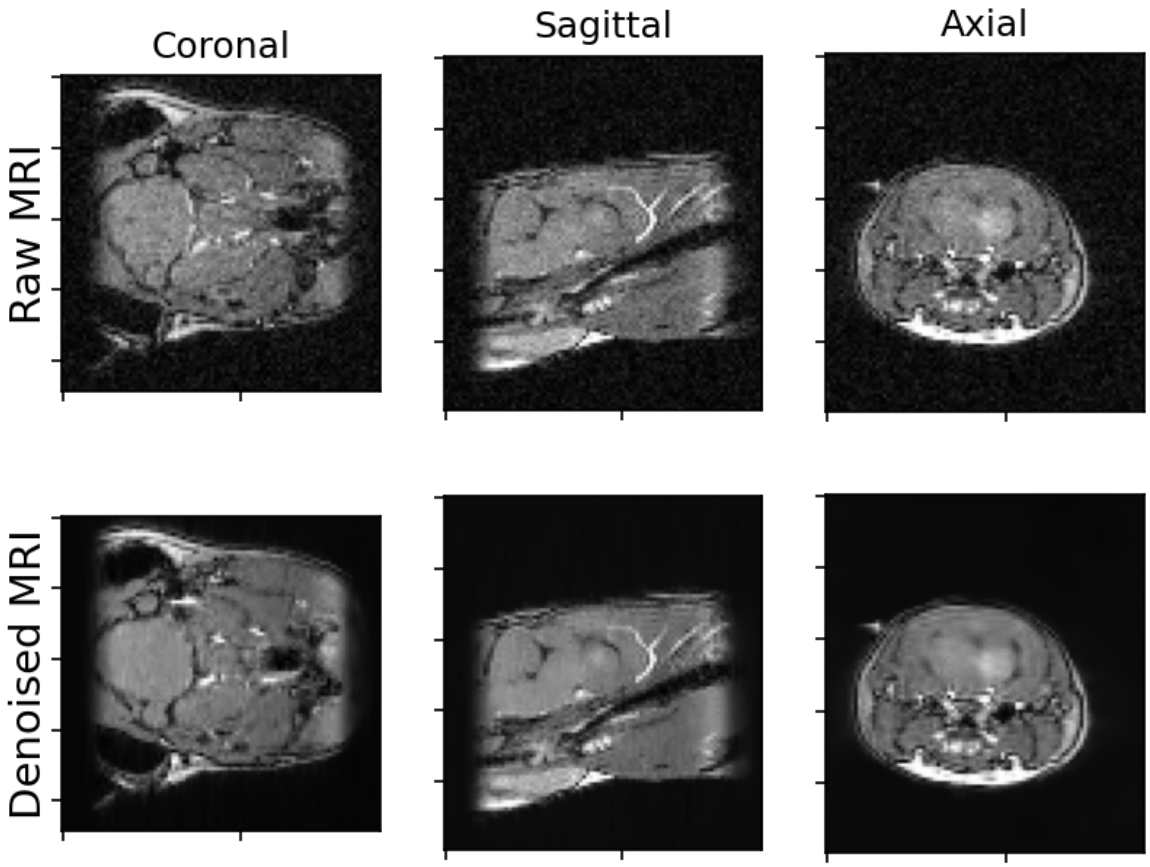


Figure 4.11: Raw and denoised MRI image, Timepoint:Week_19, Sequence type: T1, Signal-to-noise ratio (raw)= 42.39, Signal-to-Noise ratio (denoised) = 62.64

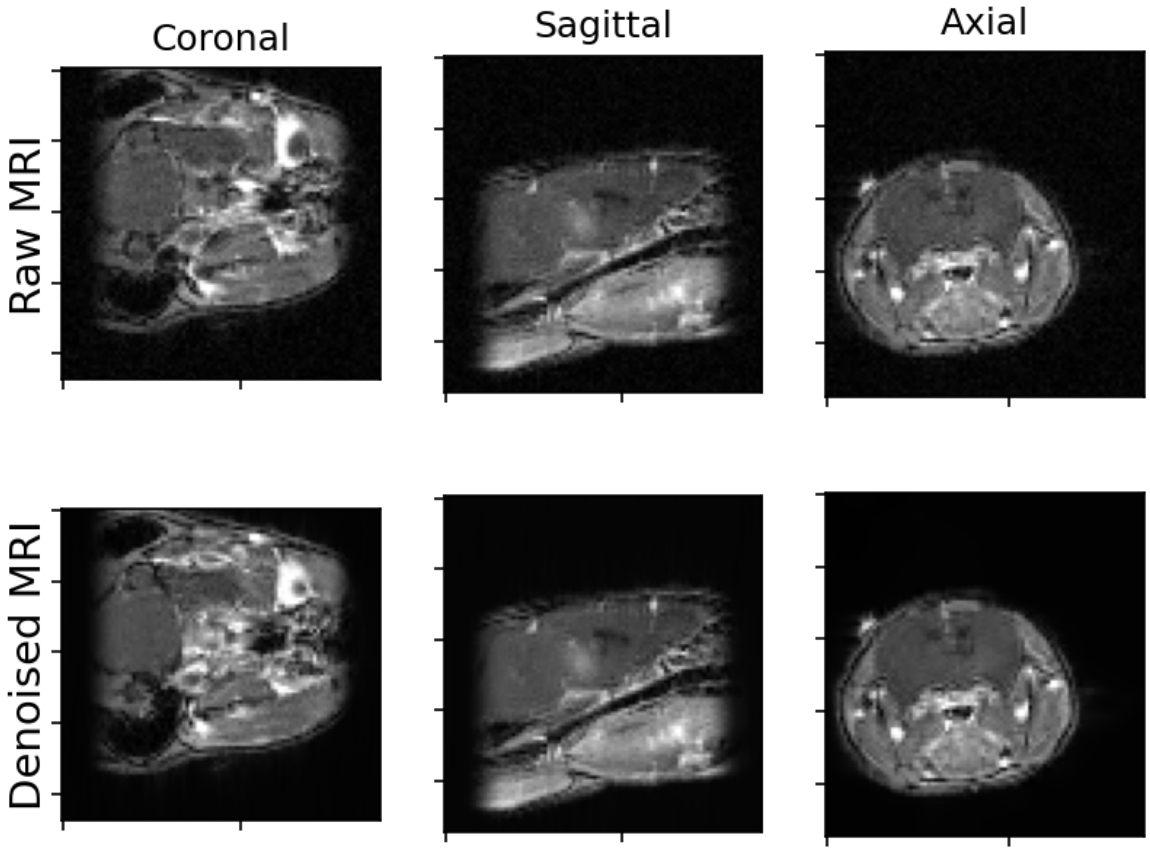


Figure 4.12: Raw and denoised MRI image, Timepoint:Week_21, Sequence type: T1, Signal-to-noise ratio (raw)= 42.07, Signal-to-Noise ratio (denoised) = 51.72

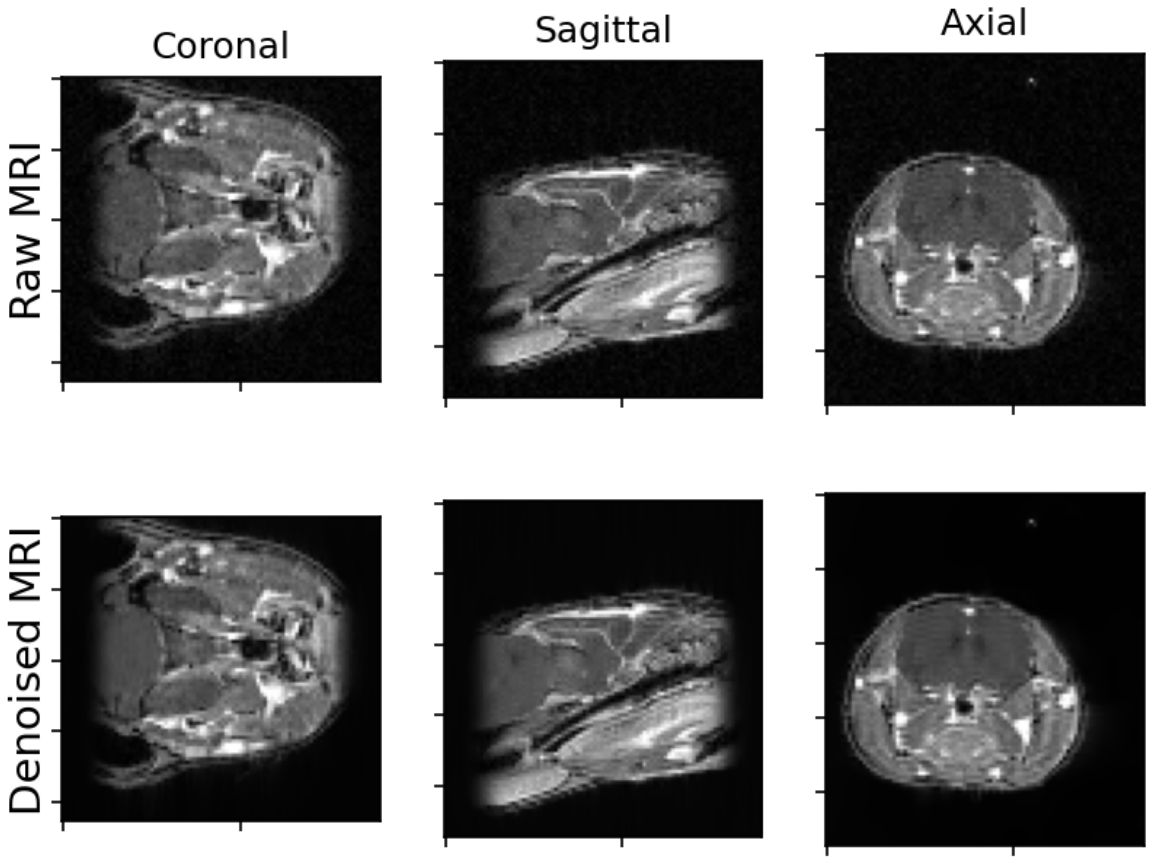


Figure 4.13: Raw and denoised MRI image, Timepoint:Week_23, Sequence type: T1, Signal-to-noise ratio (raw)= 43.05, Signal-to-Noise ratio (denoised) = 74.34

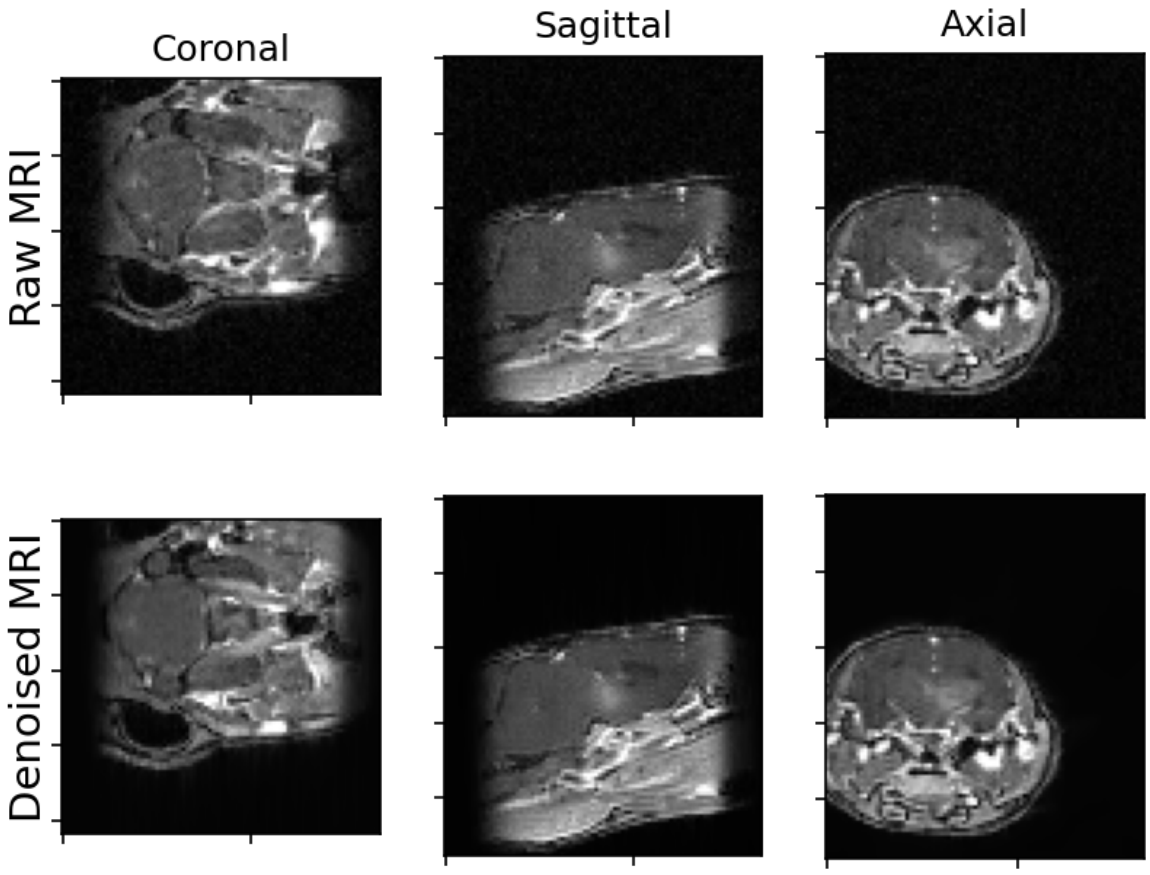


Figure 4.14: Raw and denoised MRI image, Timepoint:Week_25, Sequence type: T1, Signal-to-noise ratio (raw)= 41.78, Signal-to-Noise ratio (denoised) = 54.73

$SNR_{raw,T1} = 42.77 \pm 1.83$
$SNR_{denoised,T1} = 62.54 \pm 8.52$
$SNR_{denoised,T1} > SNR_{raw,T1}, (p < 5.8e - 09)$
$\Delta SNR = 19.77 \pm 7.02$

4.1.2 Sequence type: T2

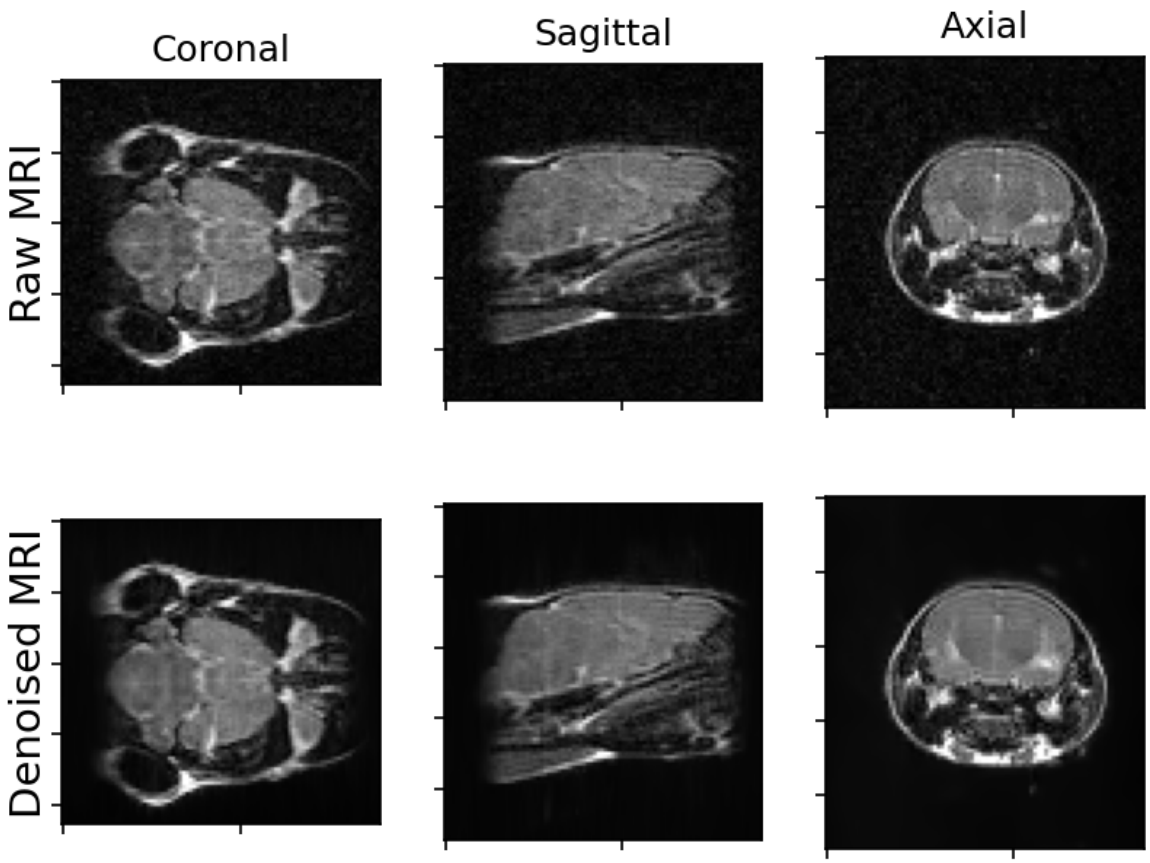


Figure 4.15: Raw and denoised MRI image, Timepoint:Week_00, Sequence type: T2, Signal-to-noise ratio (raw)= 121.30, Signal-to-Noise ratio (denoised) = 311.03

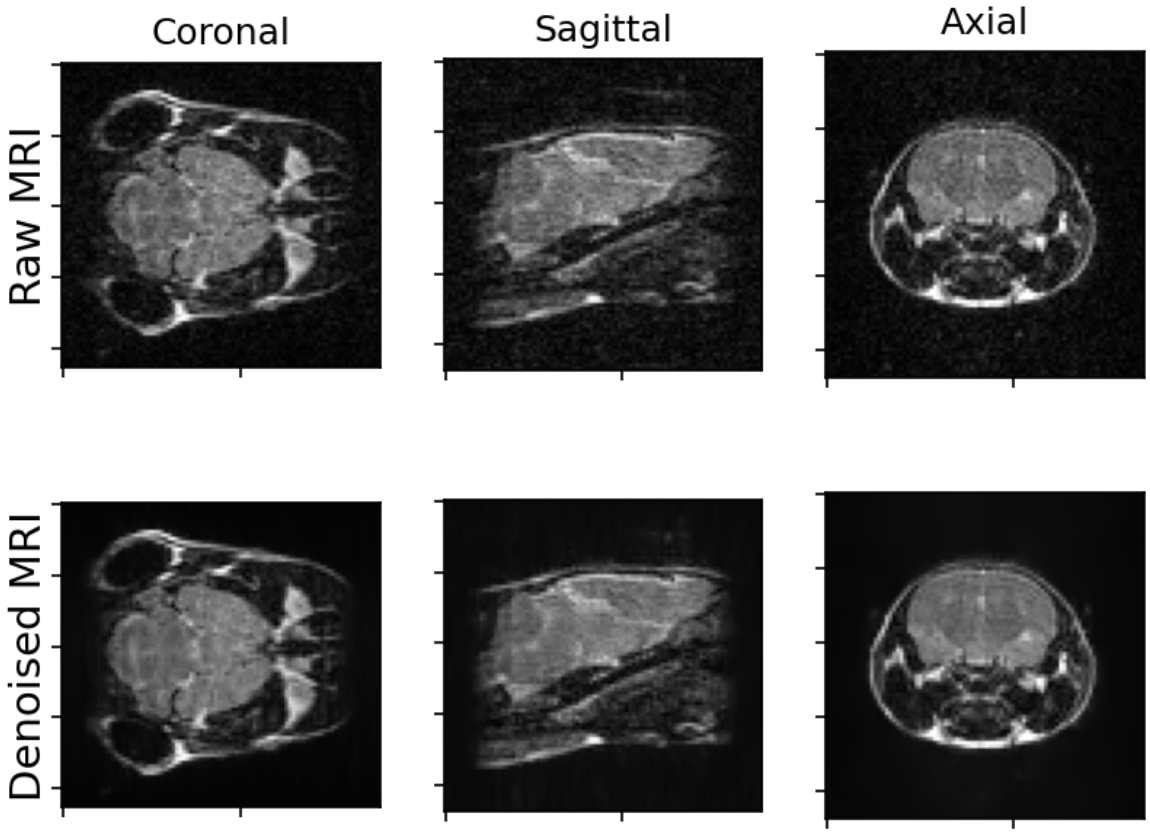


Figure 4.16: Raw and denoised MRI image, Timepoint:Week_01, Sequence type: T2, Signal-to-noise ratio (raw)= 126.16, Signal-to-Noise ratio (denoised) = 333.35

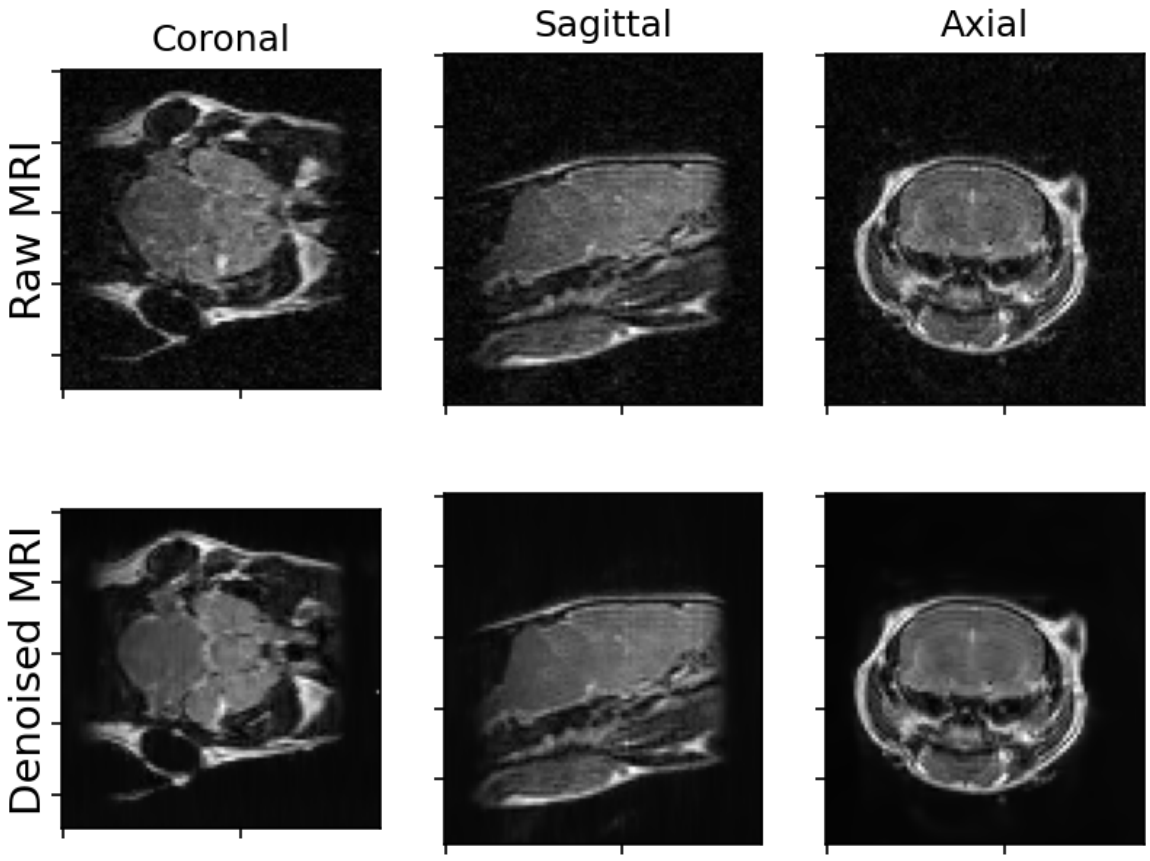


Figure 4.17: Raw and denoised MRI image, Timepoint:Week_03, Sequence type: T2, Signal-to-noise ratio (raw)= 126.96, Signal-to-Noise ratio (denoised) = 312.66

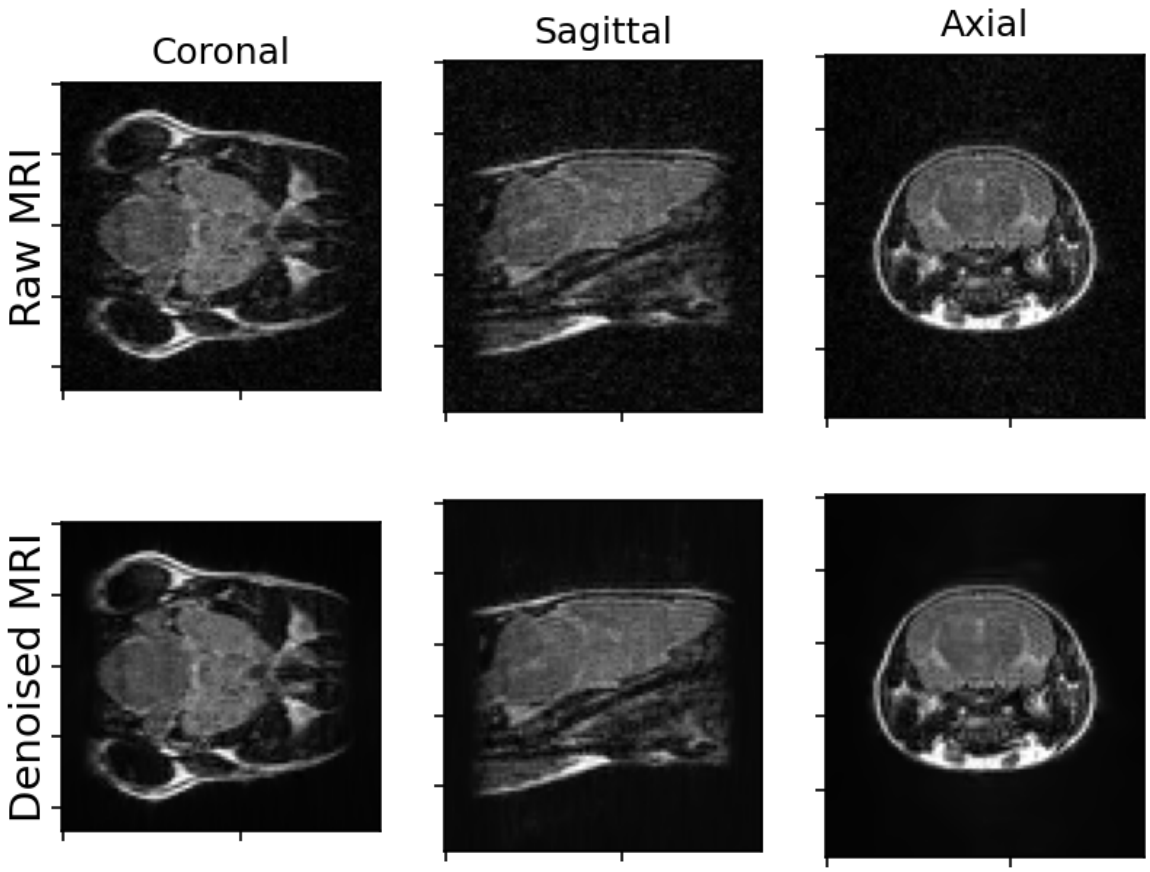


Figure 4.18: Raw and denoised MRI image, Timepoint:Week_05, Sequence type: T2, Signal-to-noise ratio (raw)= 136.54, Signal-to-Noise ratio (denoised) = 348.41

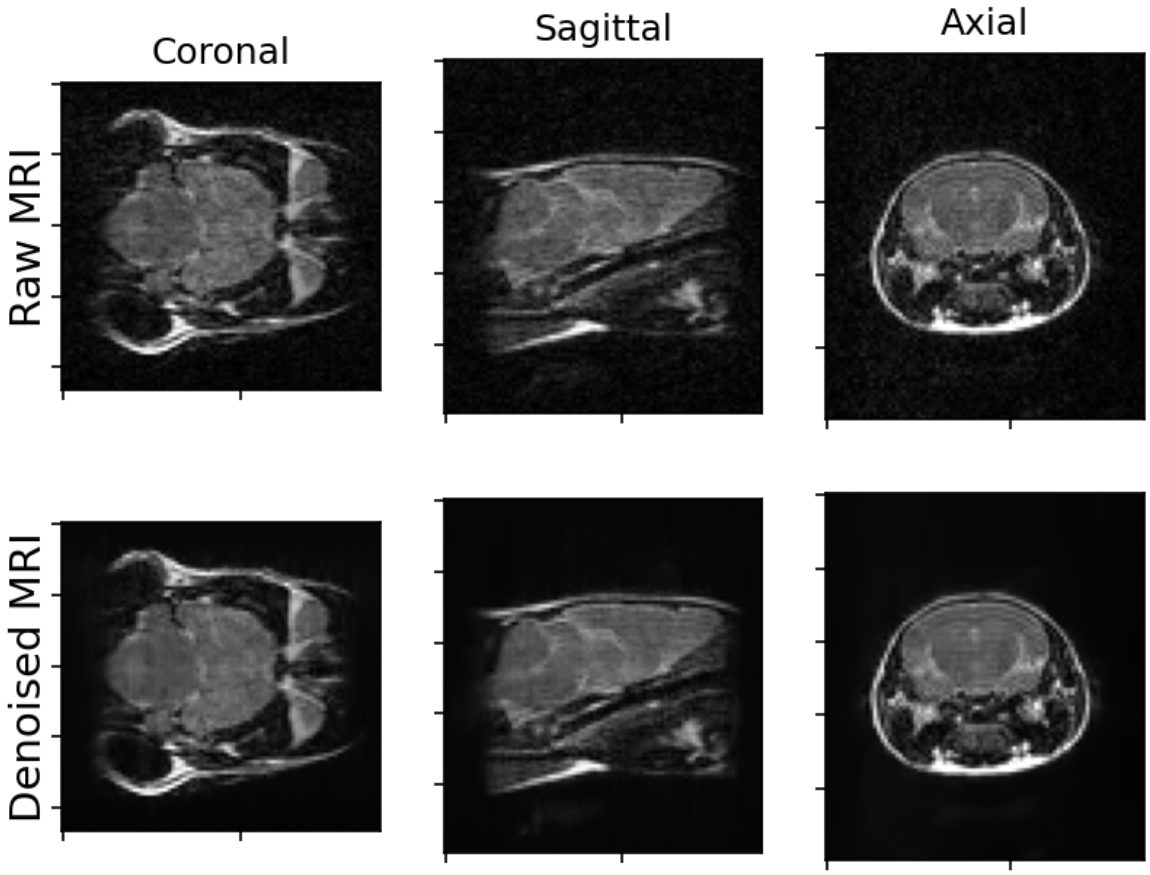


Figure 4.19: Raw and denoised MRI image, Timepoint:Week_07, Sequence type: T2, Signal-to-noise ratio (raw)= 126.56, Signal-to-Noise ratio (denoised) = 332.79

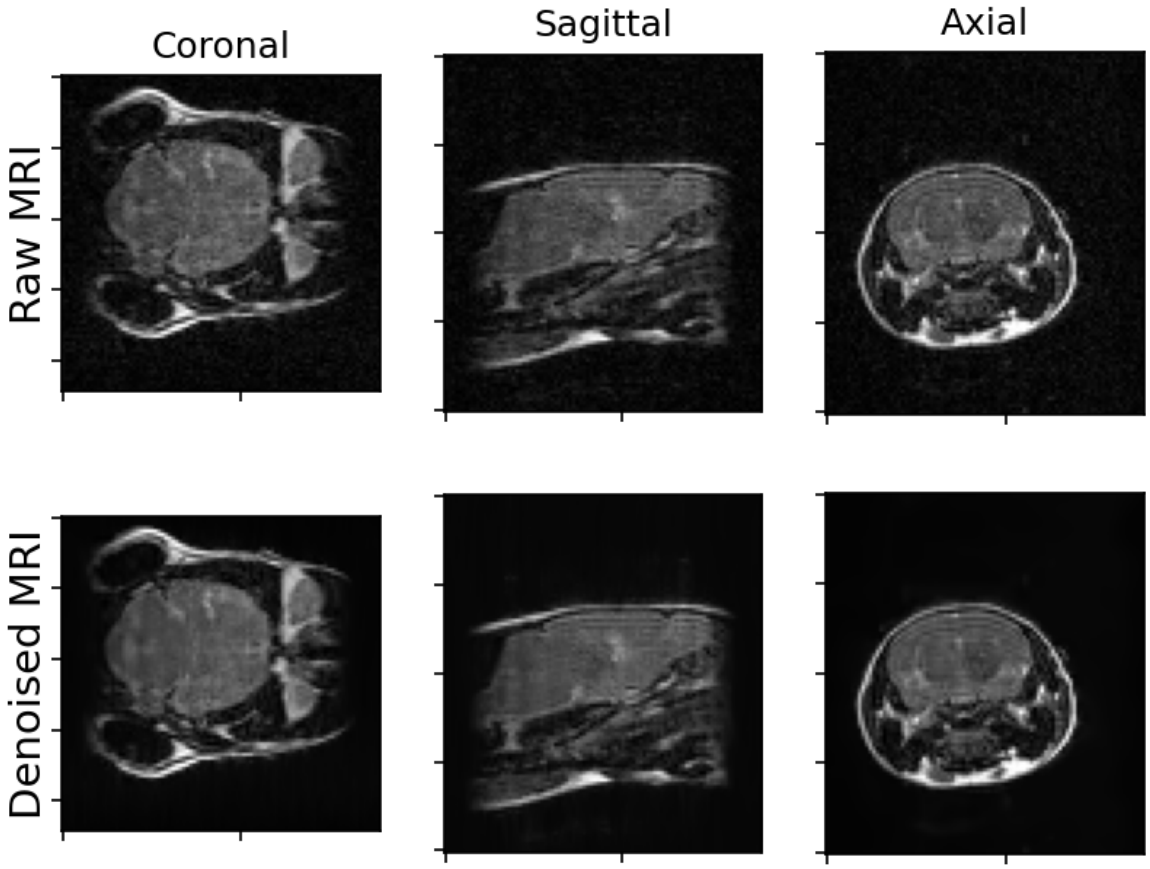


Figure 4.20: Raw and denoised MRI image, Timepoint:Week_09, Sequence type: T2, Signal-to-noise ratio (raw)= 131.71, Signal-to-Noise ratio (denoised) = 302.88

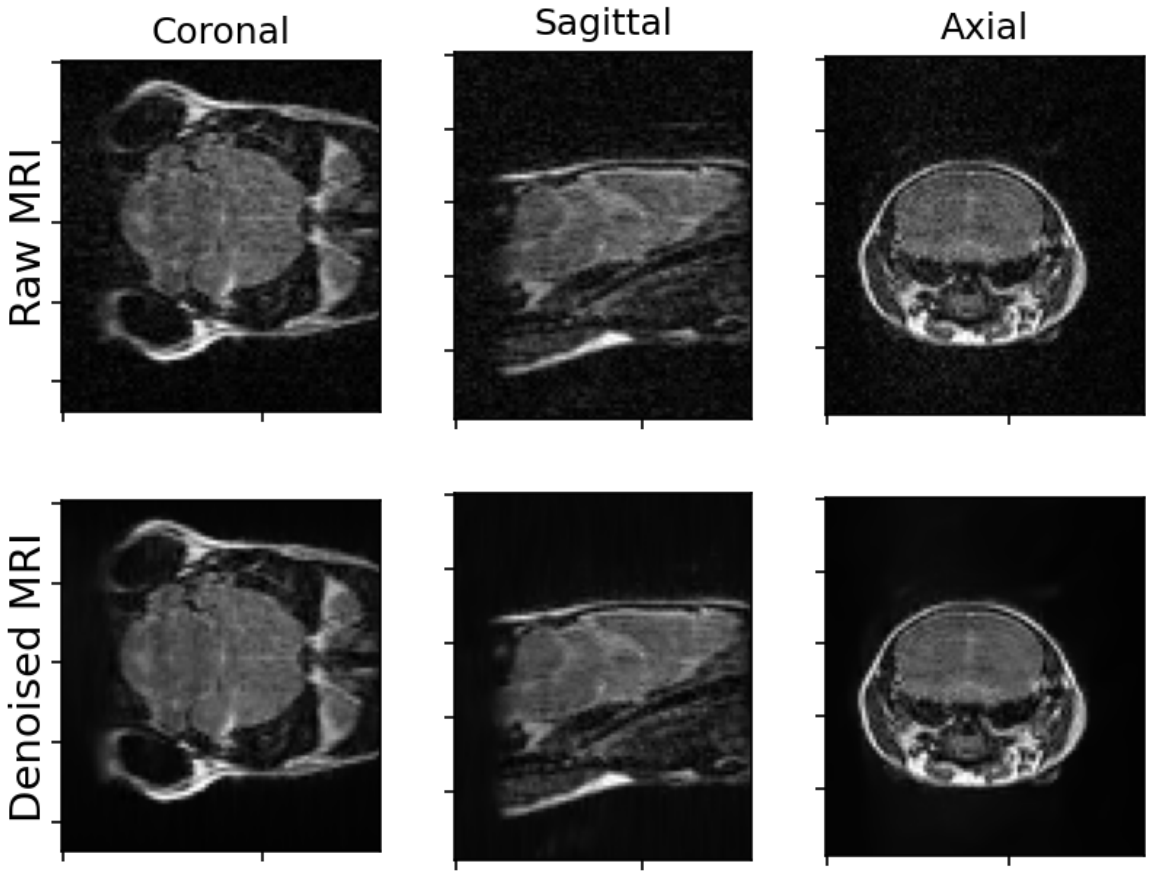


Figure 4.21: Raw and denoised MRI image, Timepoint:Week_11, Sequence type: T2, Signal-to-noise ratio (raw)= 131.78, Signal-to-Noise ratio (denoised) = 361.39

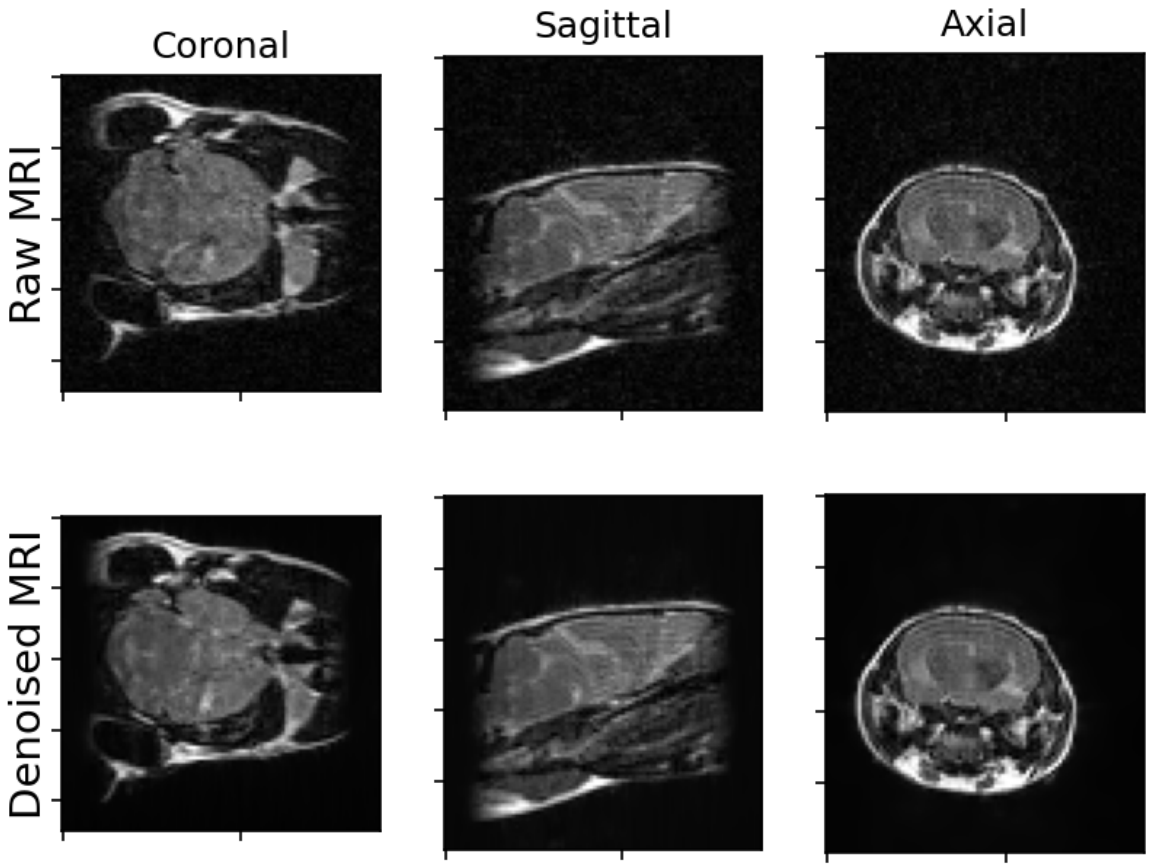


Figure 4.22: Raw and denoised MRI image, Timepoint:Week_13, Sequence type: T2, Signal-to-noise ratio (raw)= 144.62, Signal-to-Noise ratio (denoised) = 324.90

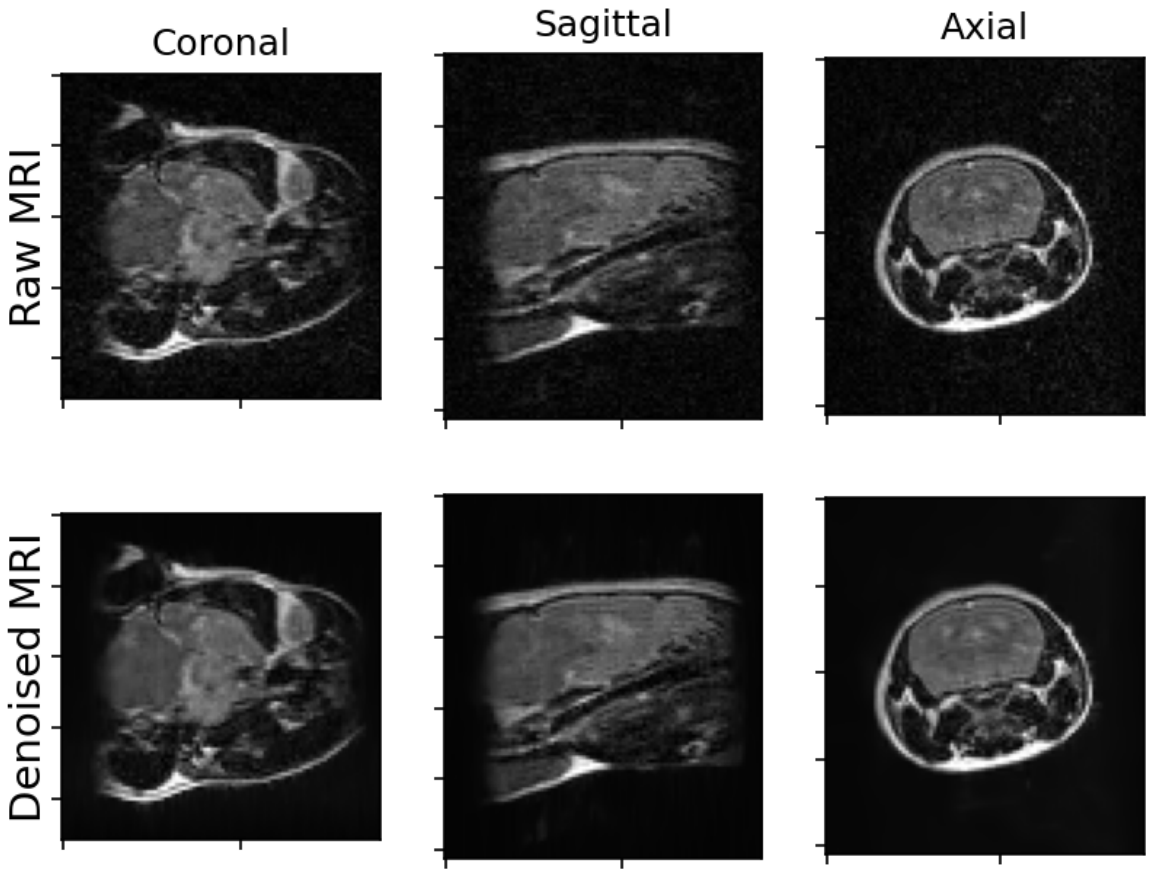


Figure 4.23: Raw and denoised MRI image, Timepoint:Week_15, Sequence type: T2, Signal-to-noise ratio (raw)= 139.52, Signal-to-Noise ratio (denoised) = 338.11

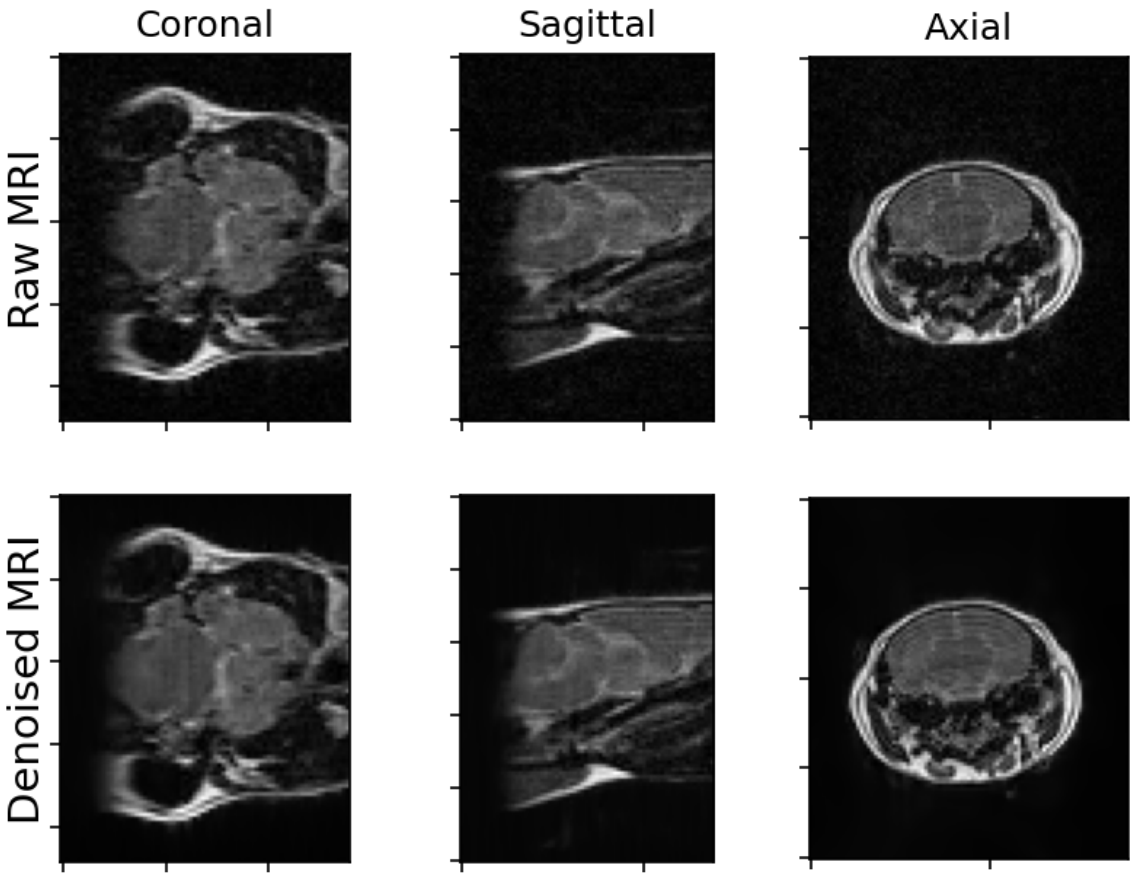


Figure 4.24: Raw and denoised MRI image, Timepoint:Week_17, Sequence type: T2, Signal-to-noise ratio (raw)= 143.02, Signal-to-Noise ratio (denoised) = 349.95

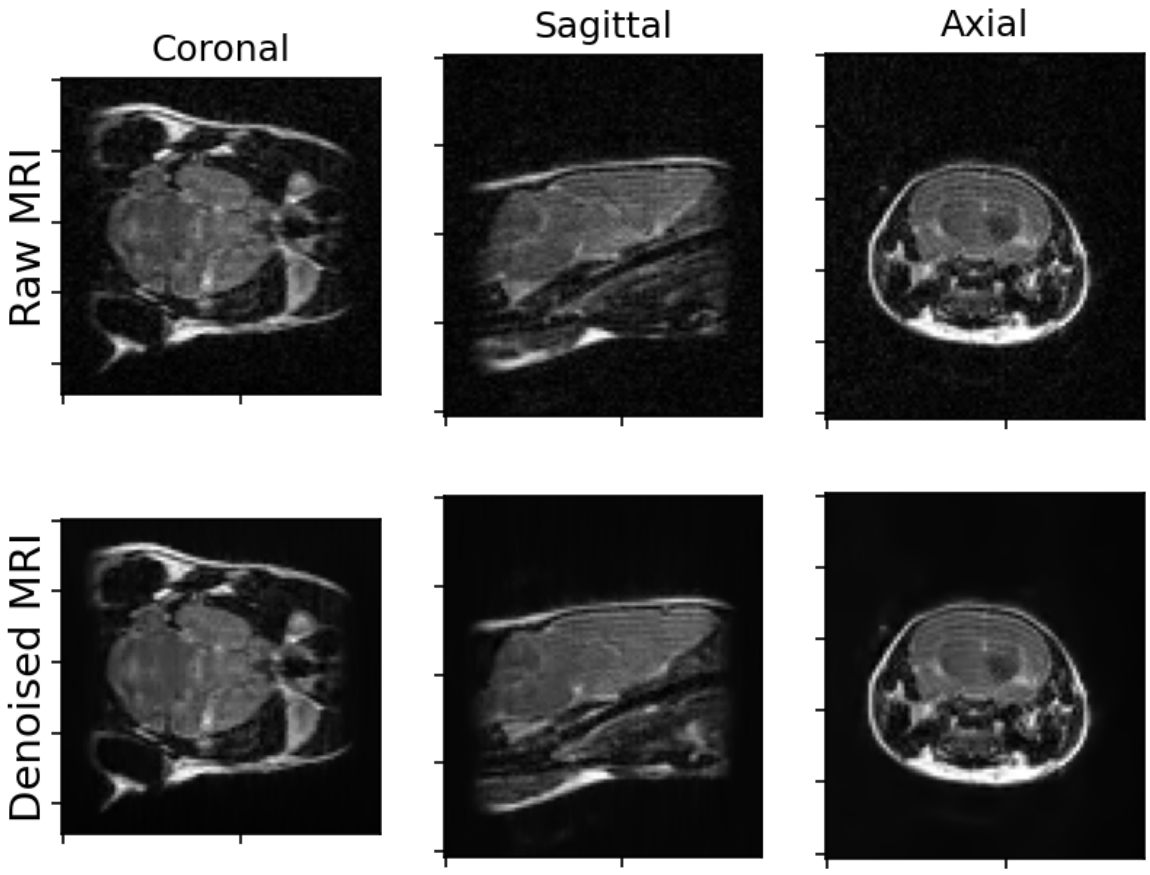


Figure 4.25: Raw and denoised MRI image, Timepoint:Week_19, Sequence type: T2, Signal-to-noise ratio (raw)= 134.27, Signal-to-Noise ratio (denoised) = 322.85

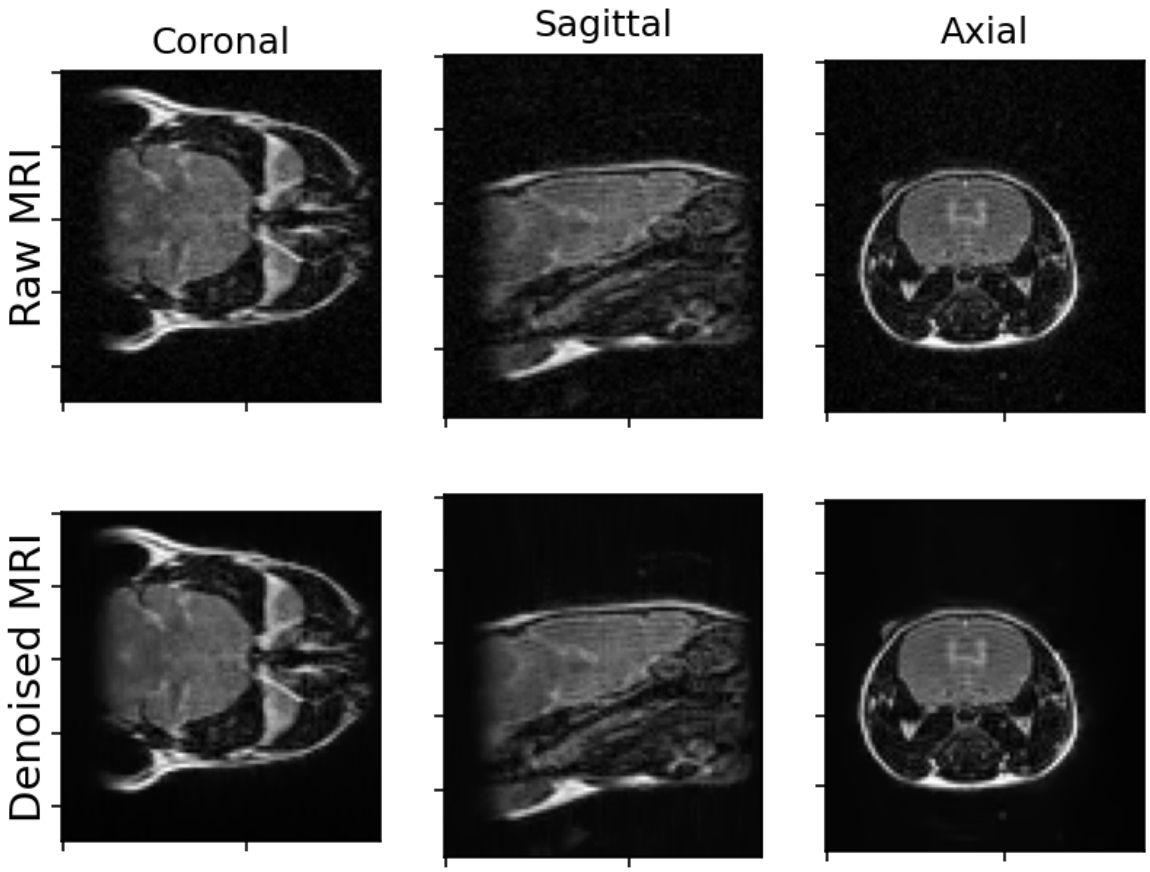


Figure 4.26: Raw and denoised MRI image, Timepoint:Week_21, Sequence type: T2, Signal-to-noise ratio (raw)= 149.27, Signal-to-Noise ratio (denoised) = 333.89

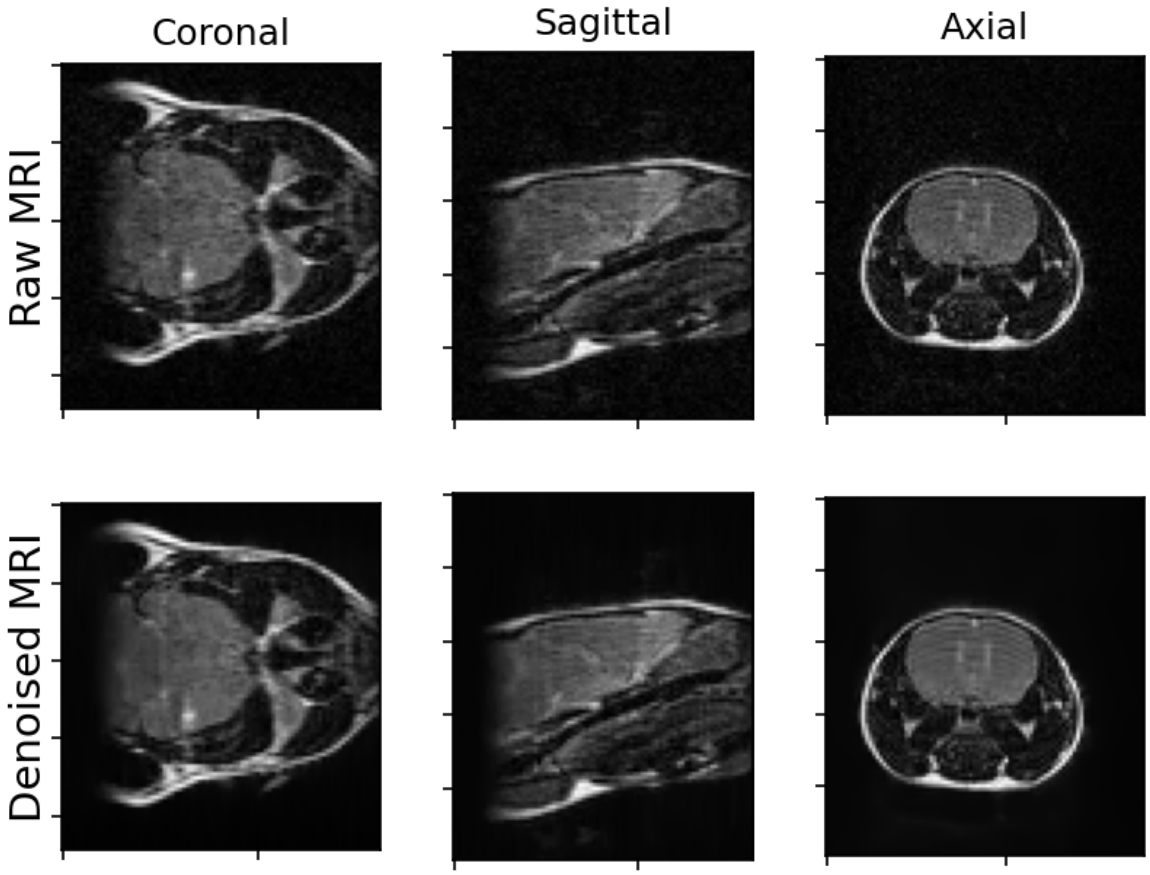


Figure 4.27: Raw and denoised MRI image, Timepoint:Week_23, Sequence type: T2, Signal-to-noise ratio (raw)= 140.25, Signal-to-Noise ratio (denoised) = 358.89

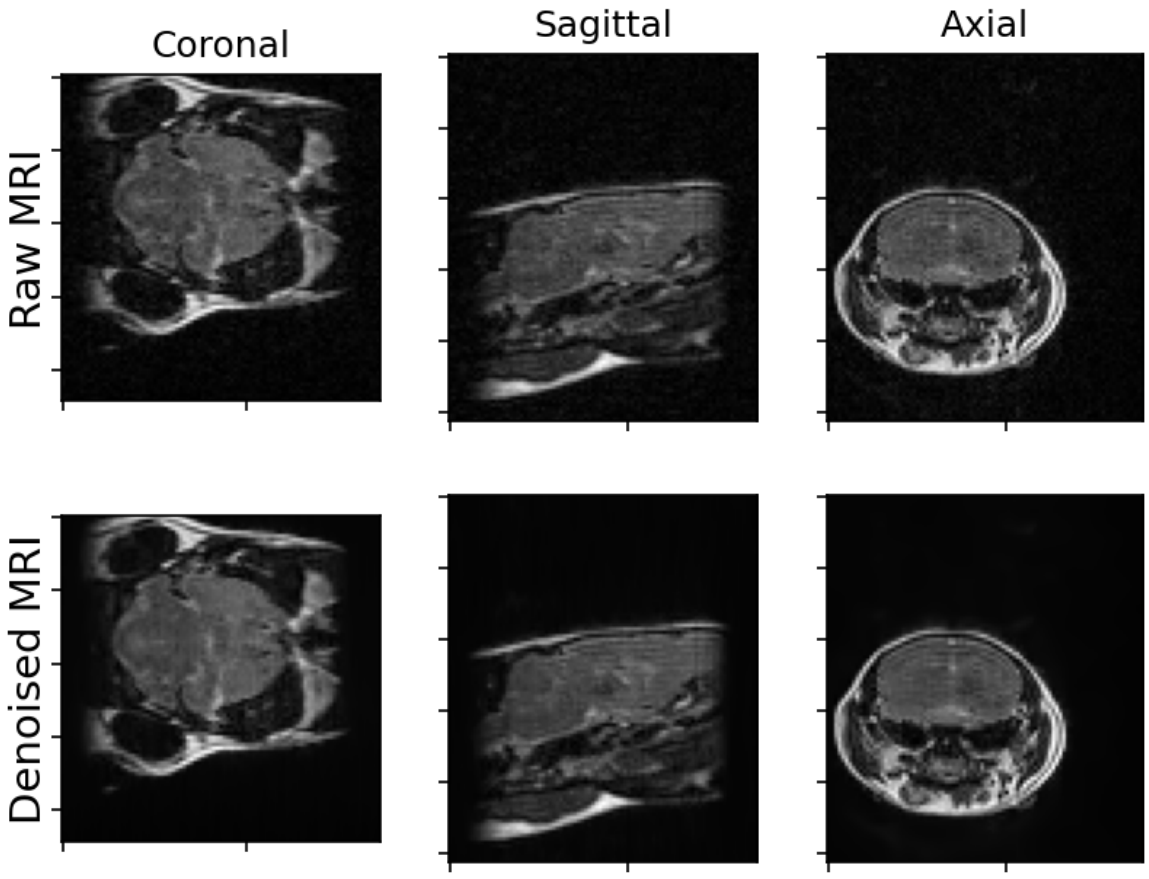


Figure 4.28: Raw and denoised MRI image, Timepoint:Week_25, Sequence type: T2, Signal-to-noise ratio (raw)= 162.11, Signal-to-Noise ratio (denoised) = 367.18

$SNR_{raw,T2} = 136.72 \pm 10.45$
$SNR_{denoised,T2} = 335.59 \pm 19.04$
$SNR_{denoised,T2} > SNR_{raw,T2}, (p < 4.7e - 23)$
$\Delta SNR = 198.87 \pm 15.61$

4.2 Registration (timepoints)

4.2.1 Sequence type: T1

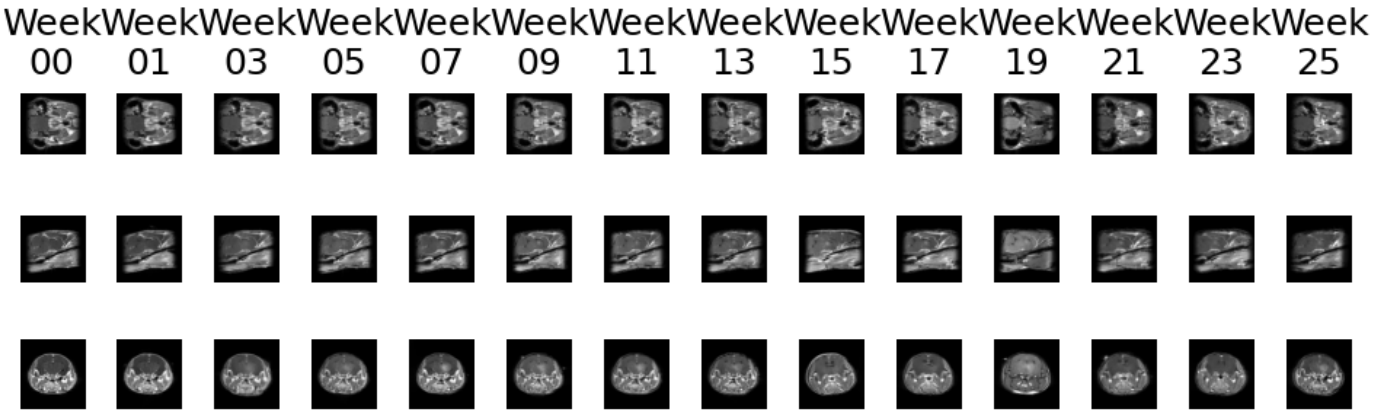


Figure 4.29: Gallery of registered MRI images , Sequence type: T1

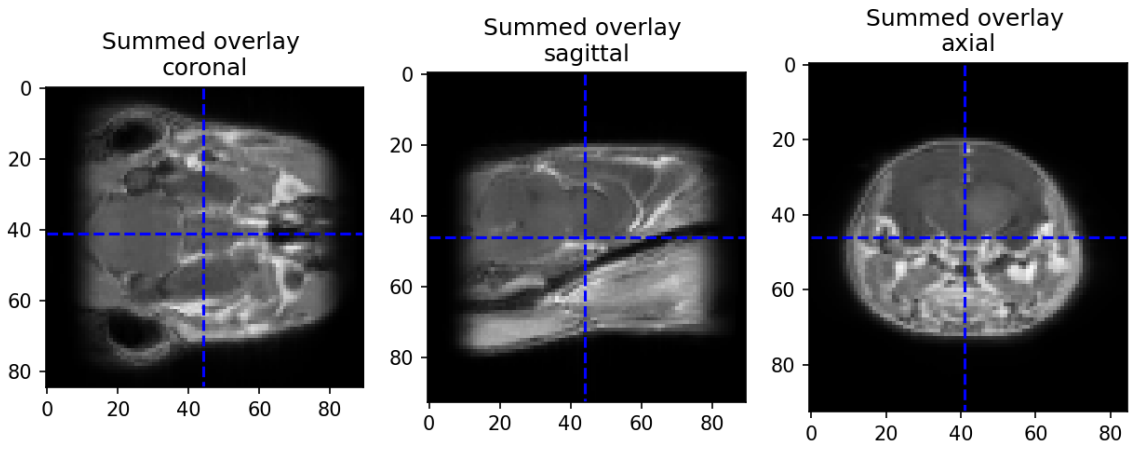


Figure 4.30: Summed overlay of registered MRI images , Sequence type: T1

4.2.2 Sequence type: T2

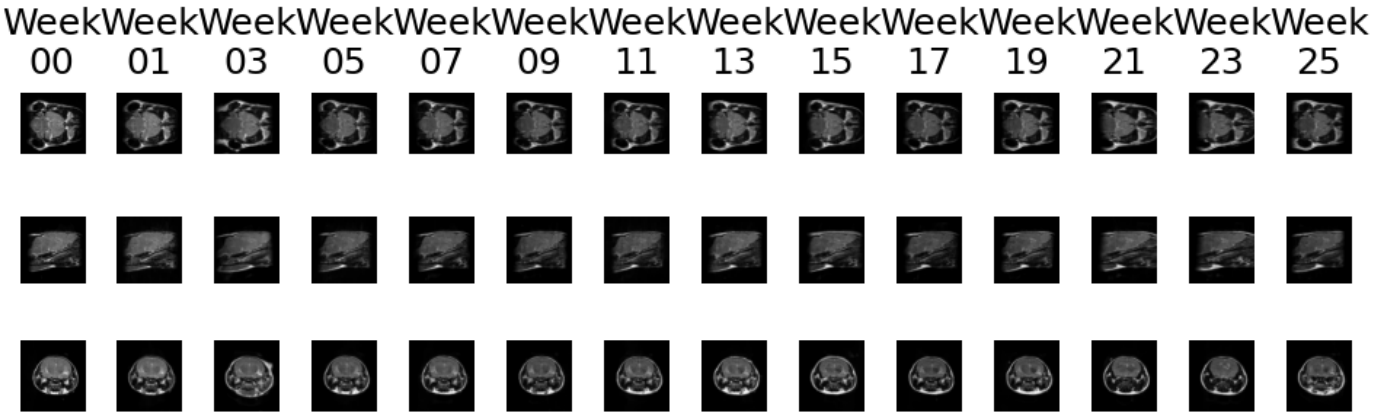


Figure 4.31: Gallery of registered MRI images , Sequence type: T2

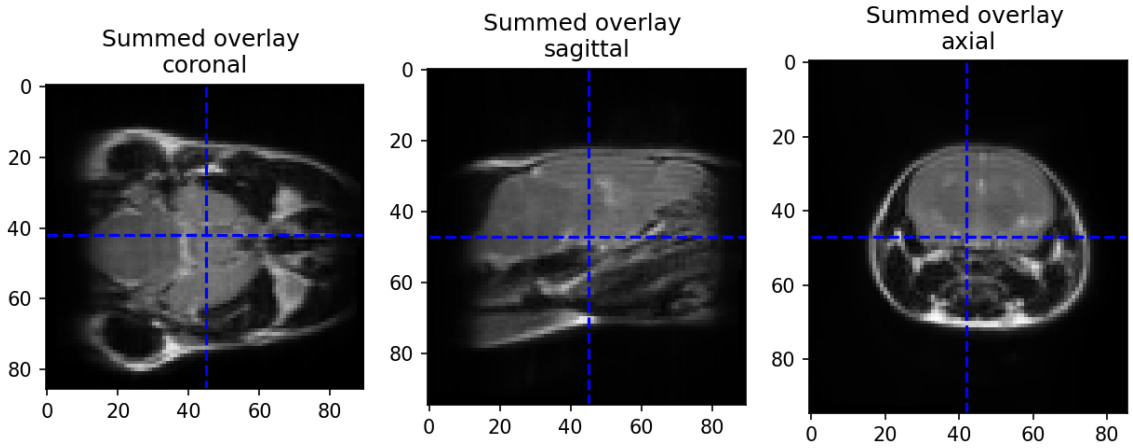


Figure 4.32: Summed overlay of registered MRI images , Sequence type: T2

4.3 Warping to CBCT

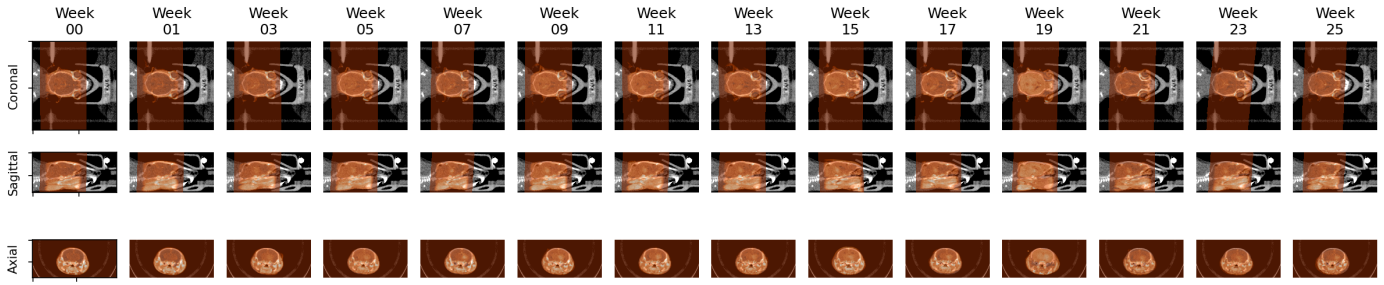


Figure 4.33: Gallery of CBCT (gray) and warped MRI images (orange) , Sequence type: T1

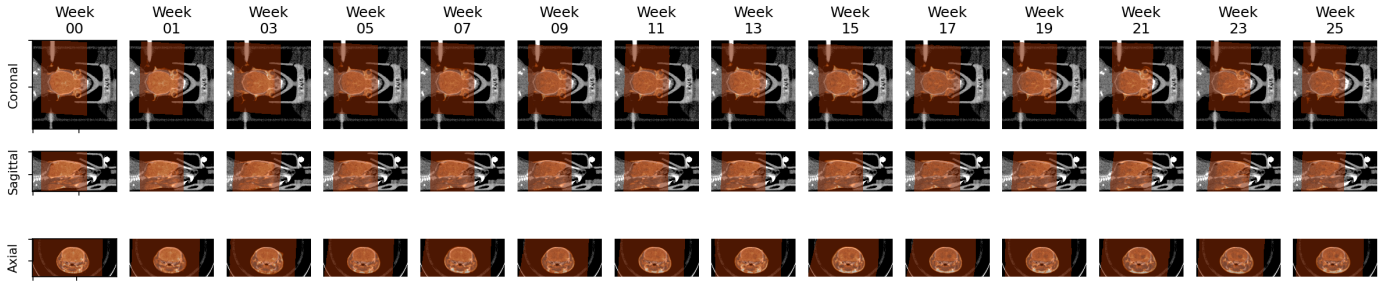


Figure 4.34: Gallery of CBCT (gray) and warped MRI images (orange) , Sequence type: T2

5 Histology image data

5.1 Bundle registration

Number of section locations:26
Stainings for this sample:

- HE: Hematoxylin & eosin staining
- NOK: NeuN, OSP, Ki-67 and DAPI
- GNI: GFAP, Nestin, Iba1 and DAPI

Note: Pairs of histochemical (e.g. HE) and immunofluorescent (e.g. GNI) images are registered with a contour-based technique, whereas pairs of immunofluorescent images (e.g. GNI and NOK) are registered with an intensity-based method. For the latter, the DAPI canal present in all immunofluorescent stainings serves as registration reference and is displayed in this overview.

5.1.1 0001_Scene_1

Raw images:

- 2020_04_25_GNI__0085-Scene-1.czi
- 2020_04_25_NOK__0111-Scene-1.czi
- P2A_C3H_M10_HE_0001-Scene-1-ScanRegion0.czi

Registered stainings: 3/3

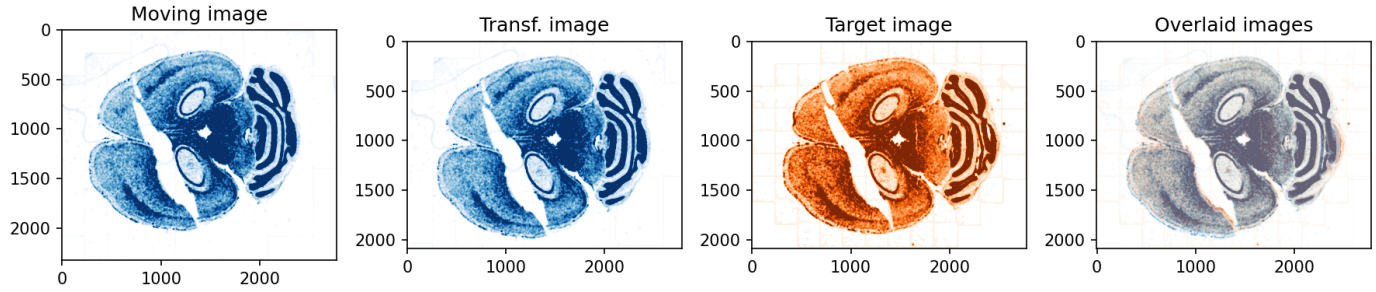


Figure 5.1: Results of registration of image 2020_04_25_NOK__0111-Scene-1 (Moving image) to 2020_04_25_GNI__0085-Scene-1 (Target image). $MI_norm = 0.99$

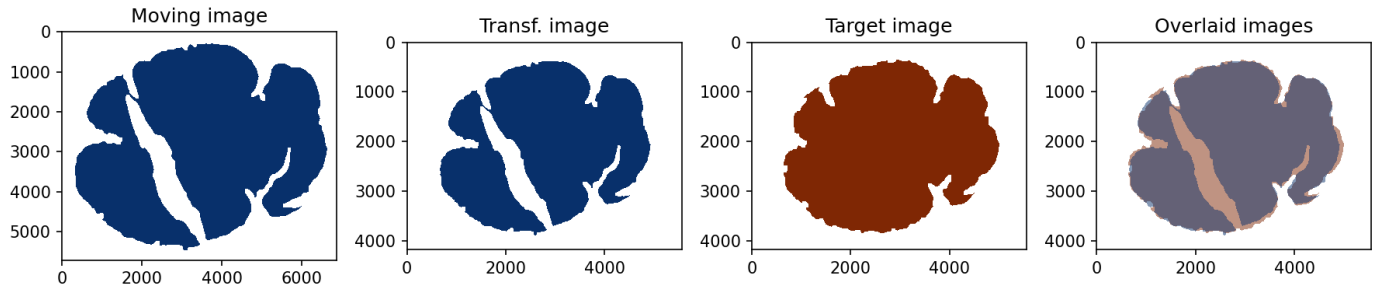


Figure 5.2: Results of registration of image P2A_C3H_M10_HE_0001-Scene-1-ScanRegion0 (Moving image) to 2020_04_25_GNI__0085-Scene-1 (Target image). Jaccard-coefficient = 0.88

5.1.2 0001_Scene_2

Raw images:

- 2020_04_25_GNI__0085-Scene-2.czi
- 2020_04_25_NOK__0111-Scene-2.czi
- P2A_C3H_M10_HE_0001-Scene-2-ScanRegion1.czi

Registered stainings: 3/3

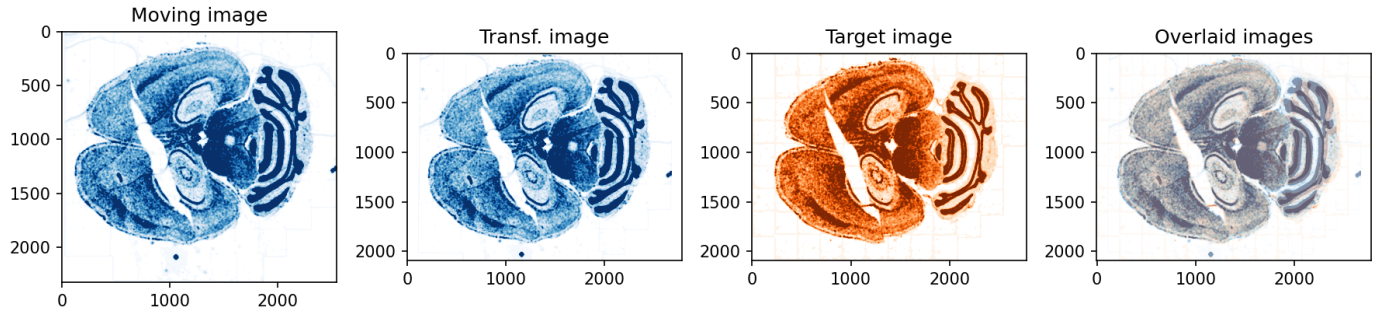


Figure 5.3: Results of registration of image 2020_04_25_NOK__0111-Scene-2 (Moving image) to 2020_04_25_GNI__0085-Scene-2 (Target image). $MI_norm = 0.98$

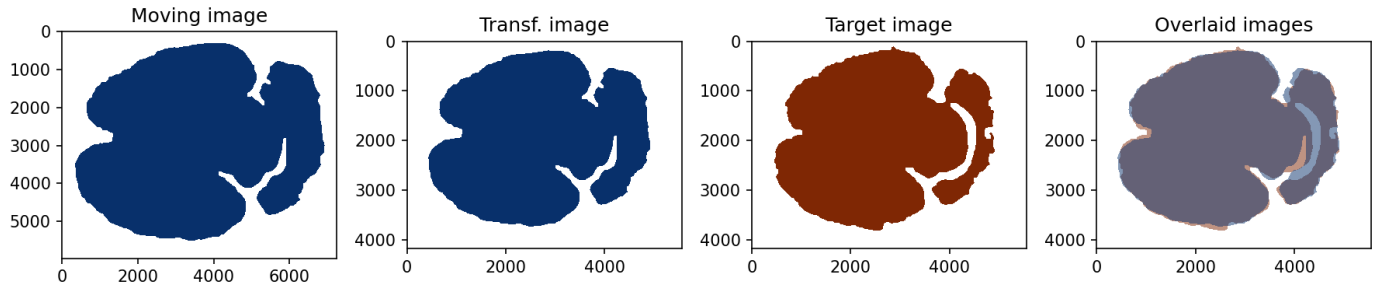


Figure 5.4: Results of registration of image P2A_C3H_M10_HE_0001-Scene-2-ScanRegion1 (Moving image) to 2020_04_25_GNI__0085-Scene-2 (Target image). Jaccard-coefficient = 0.93

5.1.3 0002_Scene_1

Raw images:

- 2020_04_25_GNI__0086-Scene-1.czi
- 2020_04_25_NOK__0112-Scene-1.czi
- P2A_C3H_M10_HE_0002-Scene-1-ScanRegion0.czi

Registered stainings: 3/3

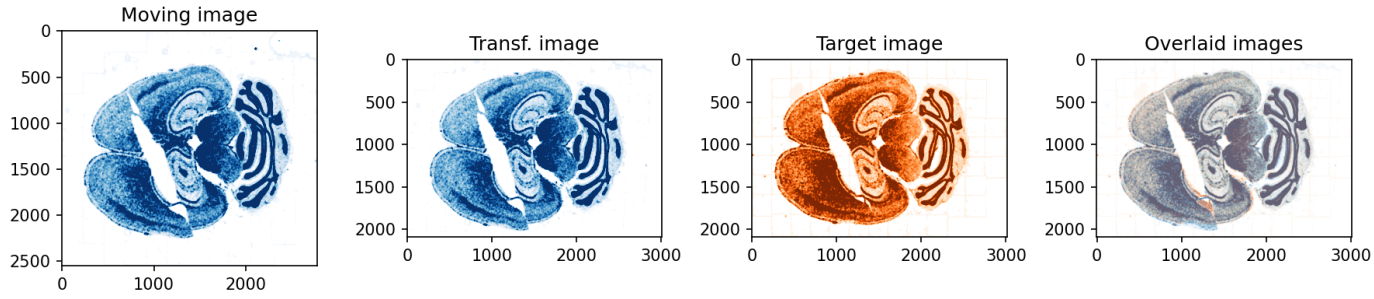


Figure 5.5: Results of registration of image 2020_04_25_NOK__0112-Scene-1 (Moving image) to 2020_04_25_GNI__0086-Scene-1 (Target image). $MI_norm = 0.97$

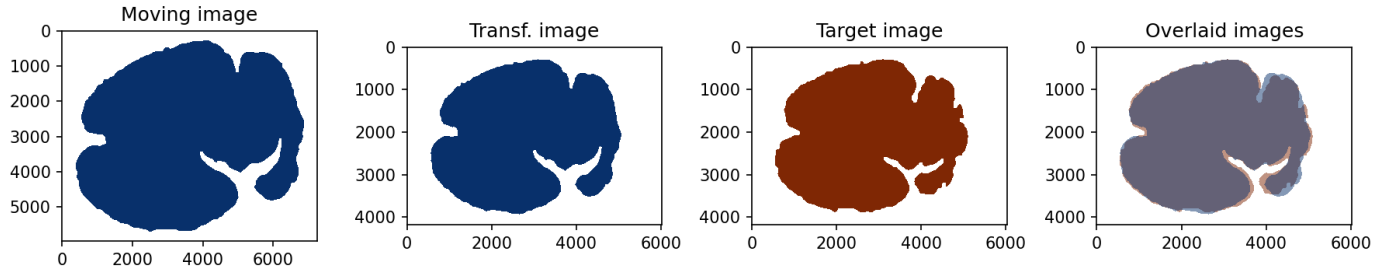


Figure 5.6: Results of registration of image P2A_C3H_M10_HE_0002-Scene-1-ScanRegion0 (Moving image) to 2020_04_25_GNI__0086-Scene-1 (Target image). Jaccard-coefficient = 0.94

5.1.4 0002_Scene_2

Raw images:

- 2020_04_25_GNI__0086-Scene-2.czi
- 2020_04_25_NOK__0112-Scene-2.czi
- P2A_C3H_M10_HE_0002-Scene-2-ScanRegion1.czi

Registered stainings: 3/3

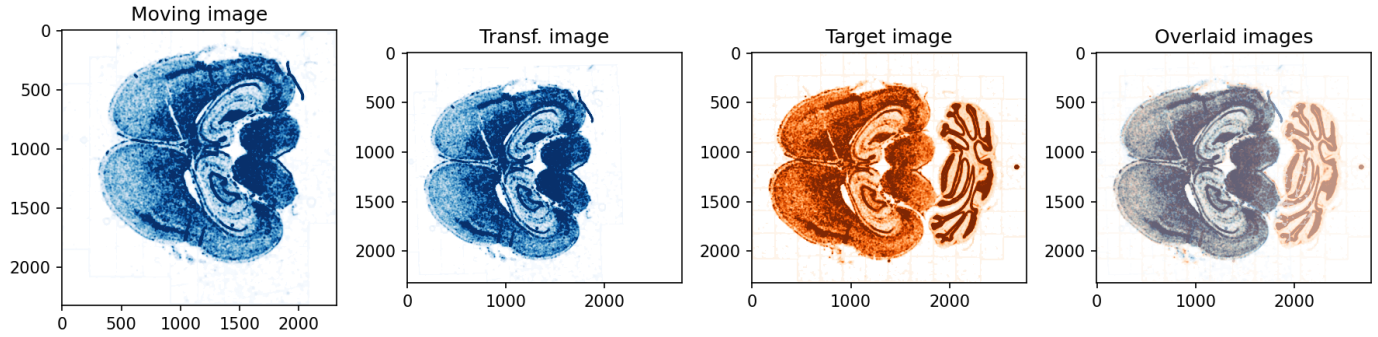


Figure 5.7: Results of registration of image 2020_04_25_NOK__0112-Scene-2 (Moving image) to 2020_04_25_GNI__0086-Scene-2 (Target image). $MI_norm = 0.00$

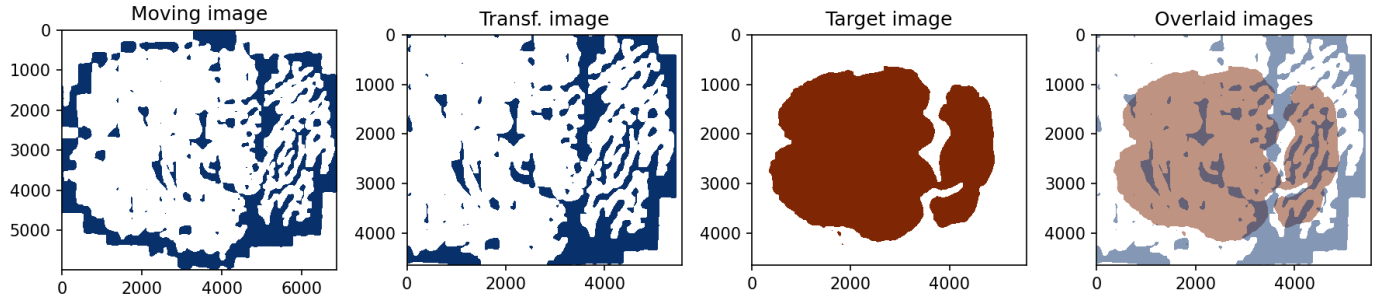


Figure 5.8: Results of registration of image P2A_C3H_M10_HE_0002-Scene-2-ScanRegion1 (Moving image) to 2020_04_25_GNI__0086-Scene-2 (Target image). Jaccard-coefficient = 0.18

5.1.5 0003_Scene_1

Raw images:

- 2020_04_25_GNI__0087-Scene-1.czi
- 2020_04_25_NOK__0113-Scene-1.czi
- P2A_C3H_M10_HE_0003-Scene-1-ScanRegion0.czi

Registered stainings: 3/3

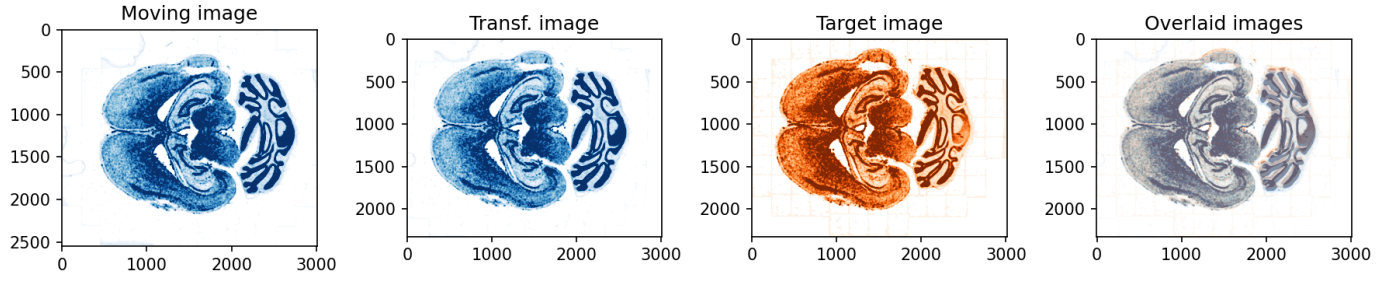


Figure 5.9: Results of registration of image 2020_04_25_NOK__0113-Scene-1 (Moving image) to 2020_04_25_GNI__0087-Scene-1 (Target image). $MI_norm = 0.97$

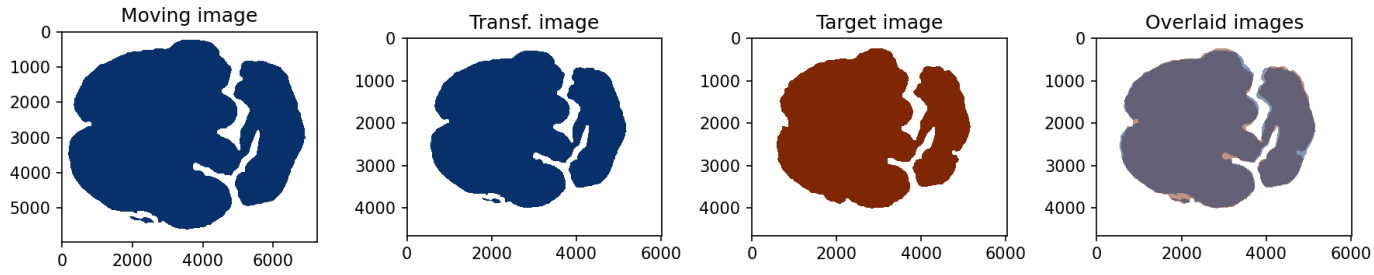


Figure 5.10: Results of registration of image P2A_C3H_M10_HE_0003-Scene-1-ScanRegion0 (Moving image) to 2020_04_25_GNI__0087-Scene-1 (Target image). Jaccard-coefficient = 0.95

5.1.6 0003_Scene_2

Raw images:

- 2020_04_25_GNI__0087-Scene-2.czi
- 2020_04_25_NOK__0113-Scene-2.czi
- P2A_C3H_M10_HE_0003-Scene-2-ScanRegion1.czi

Registered stainings: 3/3

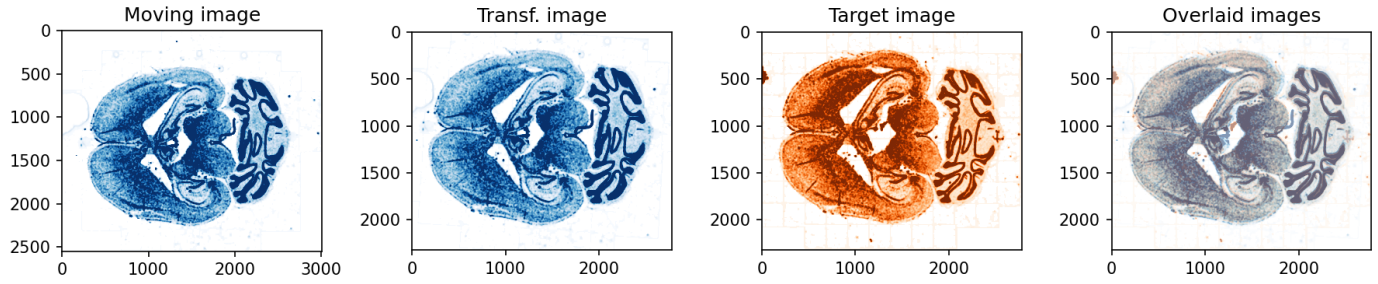


Figure 5.11: Results of registration of image 2020_04_25_NOK__0113-Scene-2 (Moving image) to 2020_04_25_GNI__0087-Scene-2 (Target image). $MI_norm = 0.93$

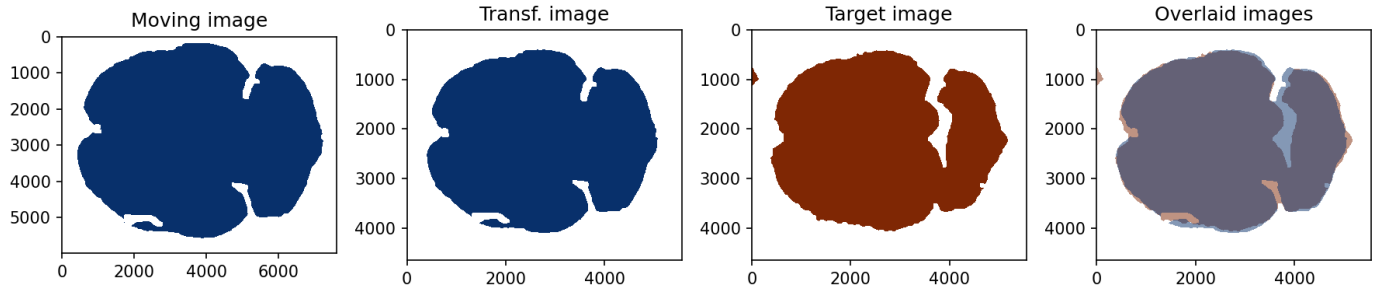


Figure 5.12: Results of registration of image P2A_C3H_M10_HE_0003-Scene-2-ScanRegion1 (Moving image) to 2020_04_25_GNI__0087-Scene-2 (Target image). Jaccard-coefficient = 0.93

5.1.7 0004_Scene_1

Raw images:

- 2020_04_25_GNI__0088-Scene-1.czi
- 2020_04_25_NOK__0114-Scene-1.czi
- P2A_C3H_M10_HE_0004-Scene-1-ScanRegion0.czi

Registered stainings: 3/3

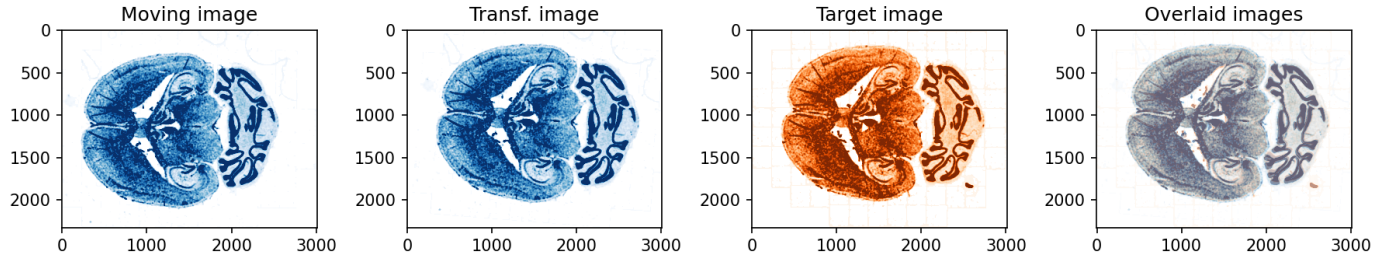


Figure 5.13: Results of registration of image 2020_04_25_NOK__0114-Scene-1 (Moving image) to 2020_04_25_GNI__0088-Scene-1 (Target image). $MI_norm = 0.99$

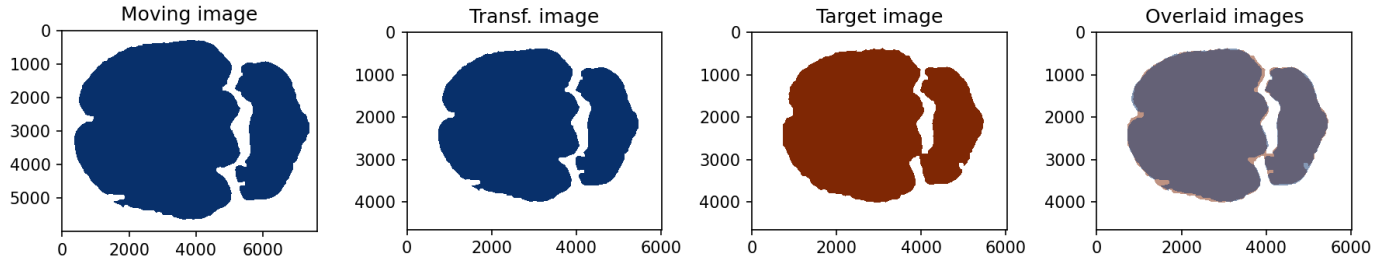


Figure 5.14: Results of registration of image P2A_C3H_M10_HE_0004-Scene-1-ScanRegion0 (Moving image) to 2020_04_25_GNI__0088-Scene-1 (Target image). Jaccard-coefficient = 0.96

5.1.8 0004_Scene_2

Raw images:

- 2020_04_25_GNI__0088-Scene-2.czi
- 2020_04_25_NOK__0114-Scene-2.czi
- P2A_C3H_M10_HE_0004-Scene-2-ScanRegion1.czi

Registered stainings: 3/3

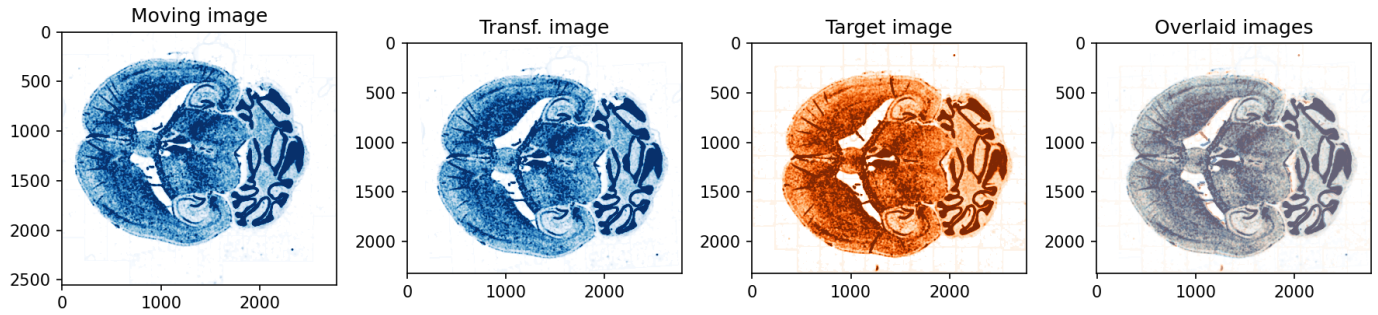


Figure 5.15: Results of registration of image 2020_04_25_NOK__0114-Scene-2 (Moving image) to 2020_04_25_GNI__0088-Scene-2 (Target image). $MI_norm = 0.87$

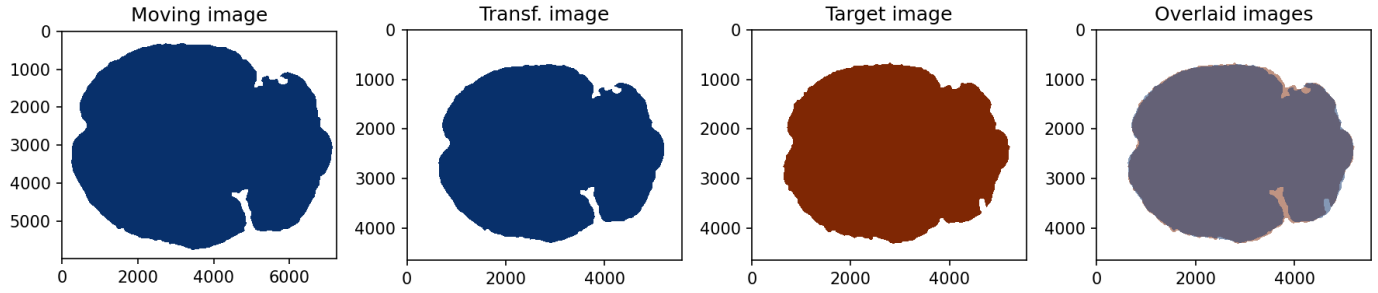


Figure 5.16: Results of registration of image P2A_C3H_M10_HE_0004-Scene-2-ScanRegion1 (Moving image) to 2020_04_25_GNI__0088-Scene-2 (Target image). Jaccard-coefficient = 0.97

5.1.9 0005_Scene_1

Raw images:

- 2020_04_25_GNI__0089-Scene-1.czi
- 2020_04_25_NOK__0115-Scene-1.czi
- P2A_C3H_M10_HE_0005-Scene-1-ScanRegion0.czi

Registered stainings: 2/3

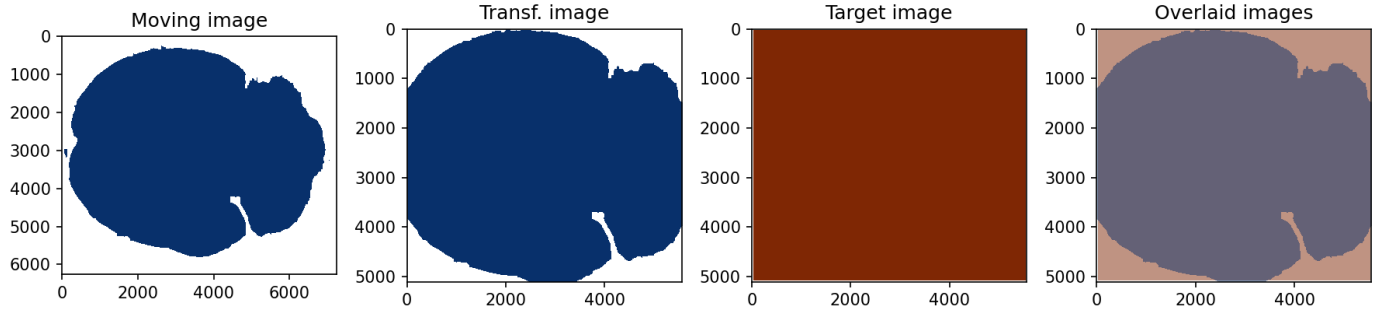


Figure 5.17: Results of registration of image P2A_C3H_M10_HE_0005-Scene-1-ScanRegion0 (Moving image) to 2020_04_25_GNI__0089-Scene-1 (Target image). Jaccard-coefficient = 0.85

5.1.10 0005_Scene_2

Raw images:

- 2020_04_25_GNI__0089-Scene-2.czi
- 2020_04_25_NOK__0115-Scene-2.czi
- P2A_C3H_M10_HE_0005-Scene-2-ScanRegion1.czi

Registered stainings: 3/3

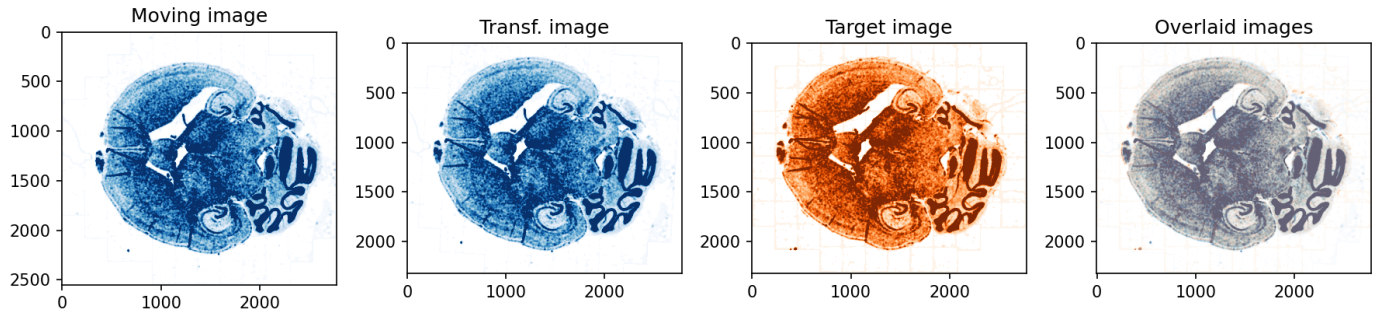


Figure 5.18: Results of registration of image 2020_04_25_NOK__0115-Scene-2 (Moving image) to 2020_04_25_GNI__0089-Scene-2 (Target image). $MI_norm = 0.96$

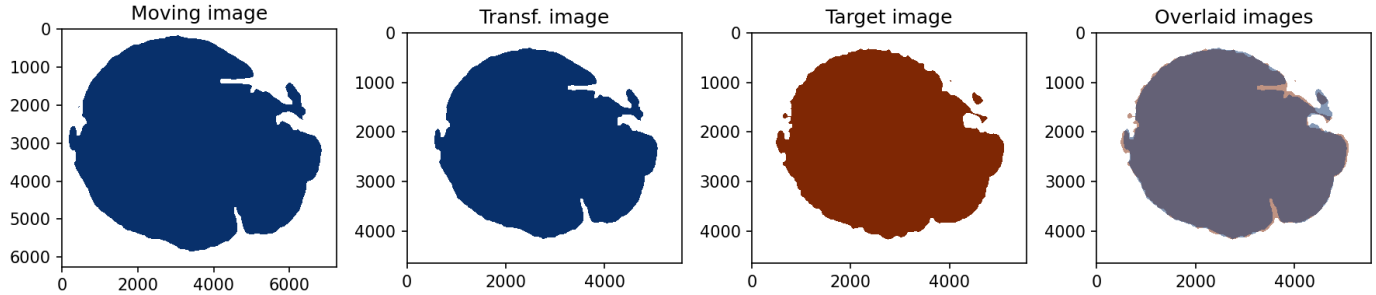


Figure 5.19: Results of registration of image P2A_C3H_M10_HE_0005-Scene-2-ScanRegion1 (Moving image) to 2020_04_25_GNI__0089-Scene-2 (Target image). Jaccard-coefficient = 0.96

5.1.11 0006_Scene_1

Raw images:

- 2020_04_25_GNI__0090-Scene-1.czi
- 2020_04_25_NOK__0116-Scene-1.czi
- P2A_C3H_M10_HE_0006-Scene-1-ScanRegion0.czi

Registered stainings: 3/3

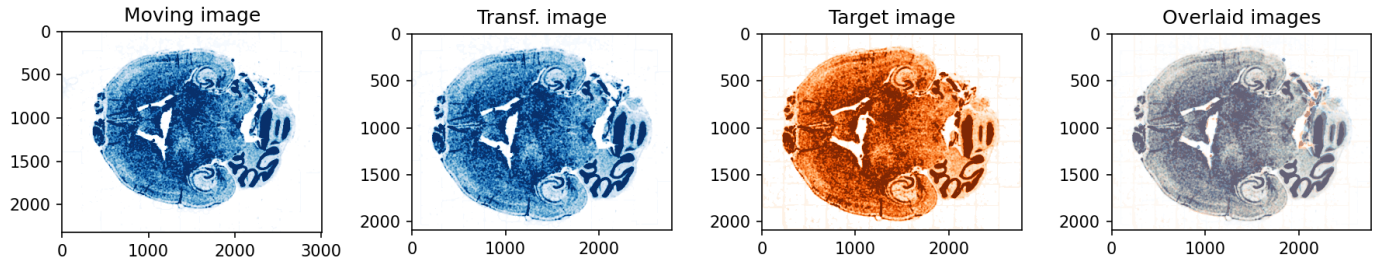


Figure 5.20: Results of registration of image 2020_04_25_NOK__0116-Scene-1 (Moving image) to 2020_04_25_GNI__0090-Scene-1 (Target image). $MI_norm = 0.98$

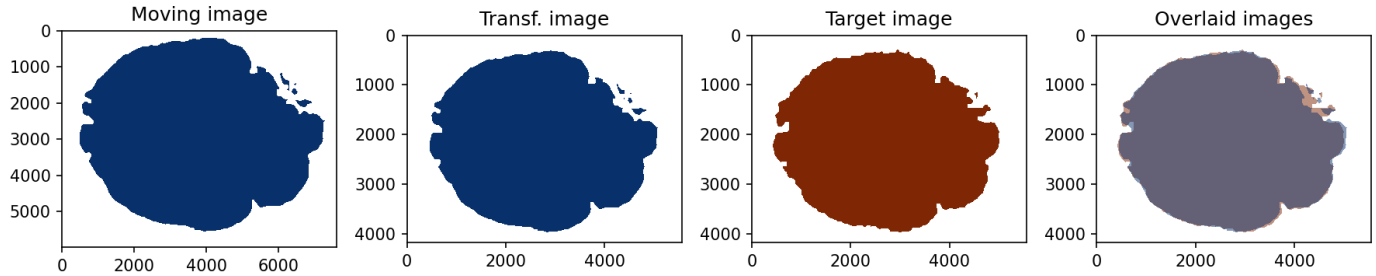


Figure 5.21: Results of registration of image P2A_C3H_M10_HE_0006-Scene-1-ScanRegion0 (Moving image) to 2020_04_25_GNI__0090-Scene-1 (Target image). Jaccard-coefficient = 0.97

5.1.12 0006_Scene_2

Raw images:

- 2020_04_25_GNI__0090-Scene-2.czi
- 2020_04_25_NOK__0116-Scene-2.czi
- P2A_C3H_M10_HE_0006-Scene-2-ScanRegion1.czi

Registered stainings: 3/3

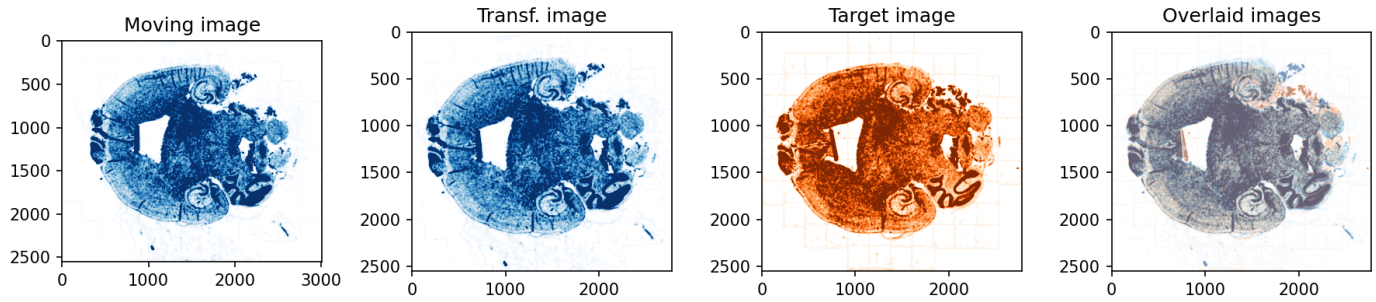


Figure 5.22: Results of registration of image 2020_04_25_NOK__0116-Scene-2 (Moving image) to 2020_04_25_GNI__0090-Scene-2 (Target image). $MI_norm = 0.81$

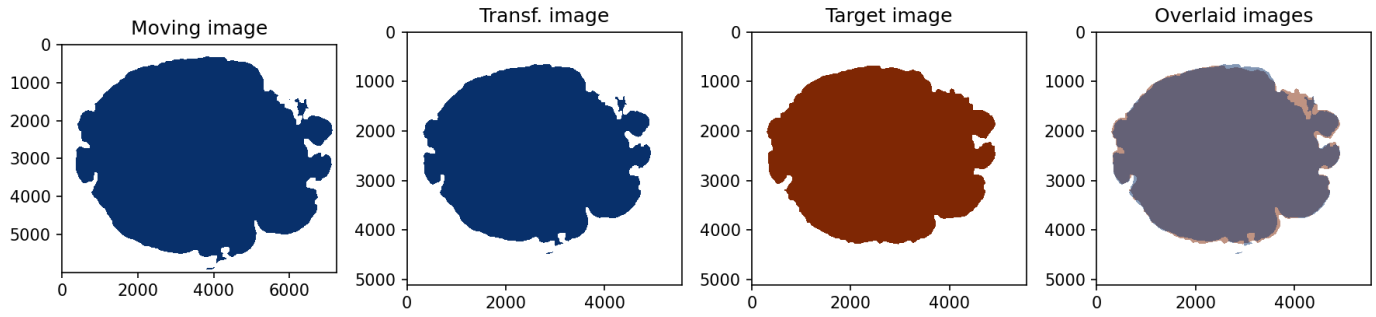


Figure 5.23: Results of registration of image P2A_C3H_M10_HE_0006-Scene-2-ScanRegion1 (Moving image) to 2020_04_25_GNI__0090-Scene-2 (Target image). Jaccard-coefficient = 0.96

5.1.13 0007_Scene_1

Raw images:

- 2020_04_25_GNI__0091-Scene-1.czi
- 2020_04_25_NOK__0117-Scene-1.czi
- P2A_C3H_M10_HE_0007-Scene-1-ScanRegion0.czi

Registered stainings: 3/3

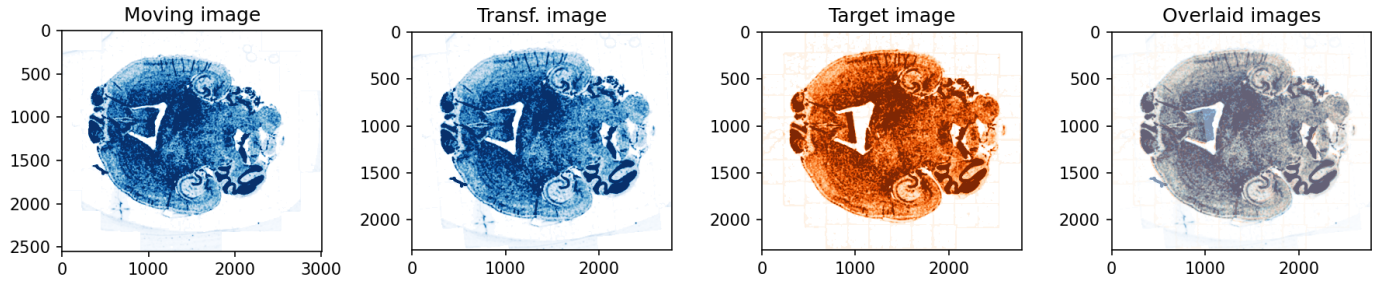


Figure 5.24: Results of registration of image 2020_04_25_NOK__0117-Scene-1 (Moving image) to 2020_04_25_GNI__0091-Scene-1 (Target image). $MI_norm = 0.98$

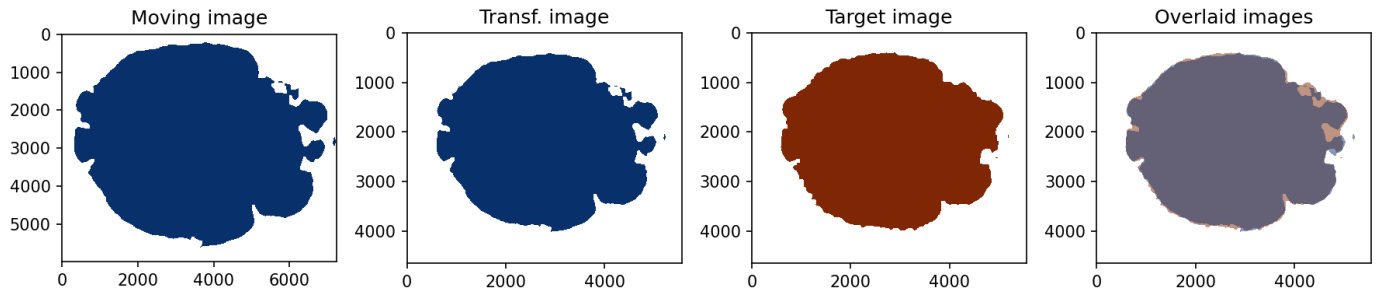


Figure 5.25: Results of registration of image P2A_C3H_M10_HE_0007-Scene-1-ScanRegion0 (Moving image) to 2020_04_25_GNI__0091-Scene-1 (Target image). Jaccard-coefficient = 0.96

5.1.14 0007_Scene_2

Raw images:

- 2020_04_25_GNI__0091-Scene-2.czi
- 2020_04_25_NOK__0117-Scene-2.czi
- P2A_C3H_M10_HE_0007-Scene-2-ScanRegion1.czi

Registered stainings: 3/3

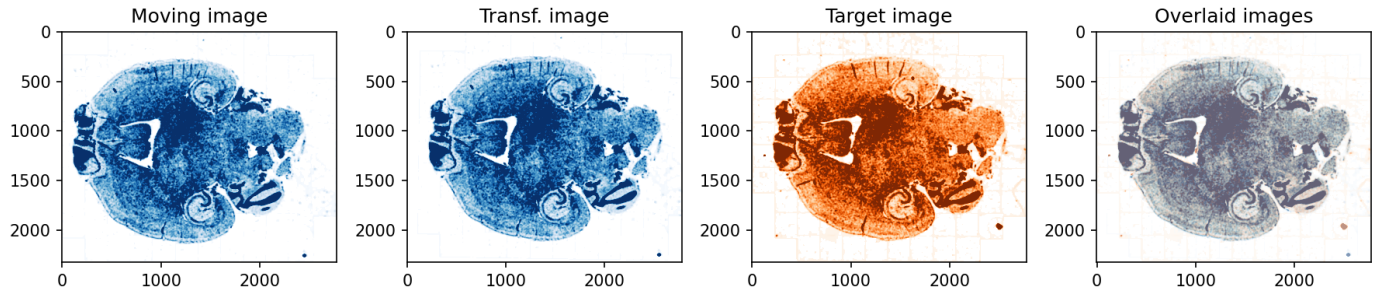


Figure 5.26: Results of registration of image 2020_04_25_NOK__0117-Scene-2 (Moving image) to 2020_04_25_GNI__0091-Scene-2 (Target image). $MI_norm = 0.94$

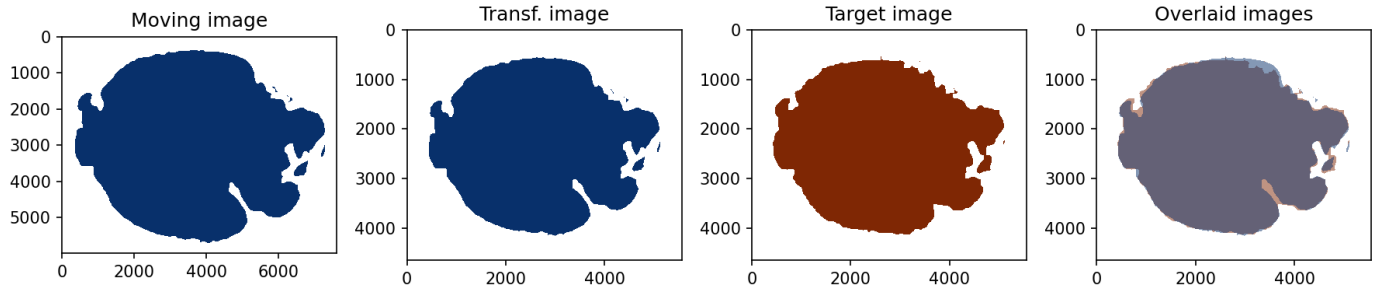


Figure 5.27: Results of registration of image P2A_C3H_M10_HE_0007-Scene-2-ScanRegion1 (Moving image) to 2020_04_25_GNI__0091-Scene-2 (Target image). Jaccard-coefficient = 0.96

5.1.15 0008_Scene_1

Raw images:

- 2020_04_25_GNI__0092-Scene-1.czi
- 2020_04_25_NOK__0118-Scene-1.czi
- P2A_C3H_M10_HE_0008-Scene-1-ScanRegion0.czi

Registered stainings: 3/3

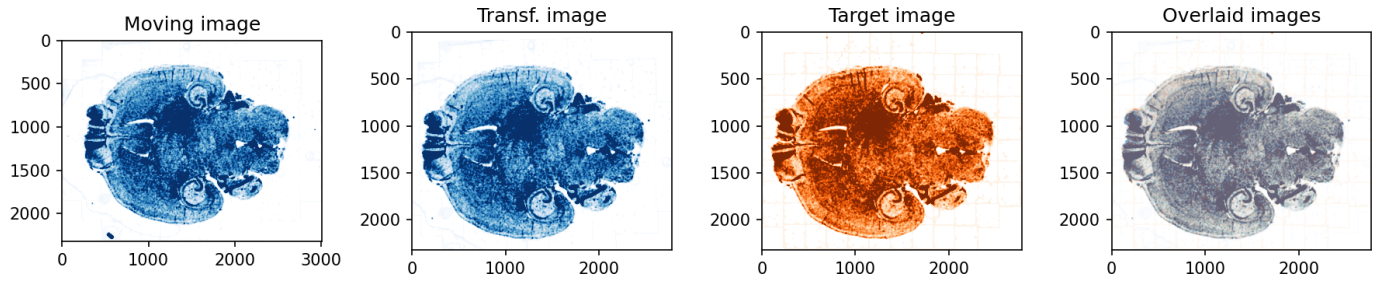


Figure 5.28: Results of registration of image 2020_04_25_NOK__0118-Scene-1 (Moving image) to 2020_04_25_GNI__0092-Scene-1 (Target image). $MI_norm = 0.00$

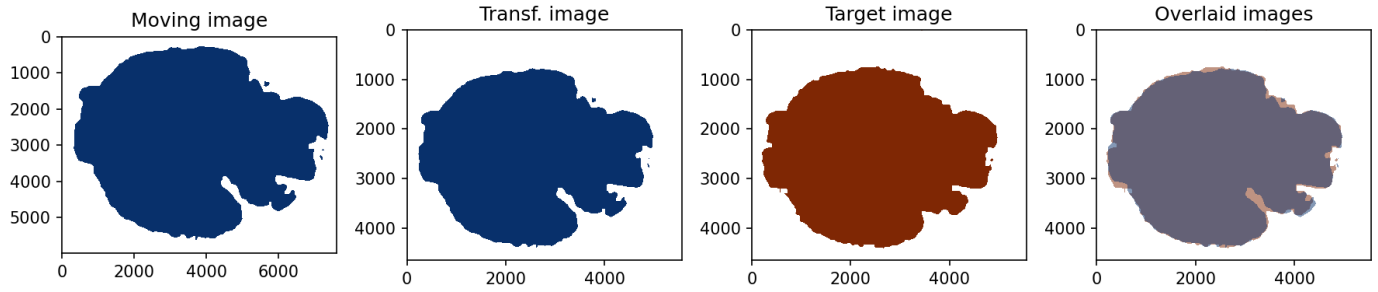


Figure 5.29: Results of registration of image P2A_C3H_M10_HE_0008-Scene-1-ScanRegion0 (Moving image) to 2020_04_25_GNI__0092-Scene-1 (Target image). Jaccard-coefficient = 0.96

5.1.16 0008_Scene_2

Raw images:

- 2020_04_25_GNI__0092-Scene-2.czi
- 2020_04_25_NOK__0118-Scene-2.czi
- P2A_C3H_M10_HE_0008-Scene-2-ScanRegion1.czi

Registered stainings: 3/3

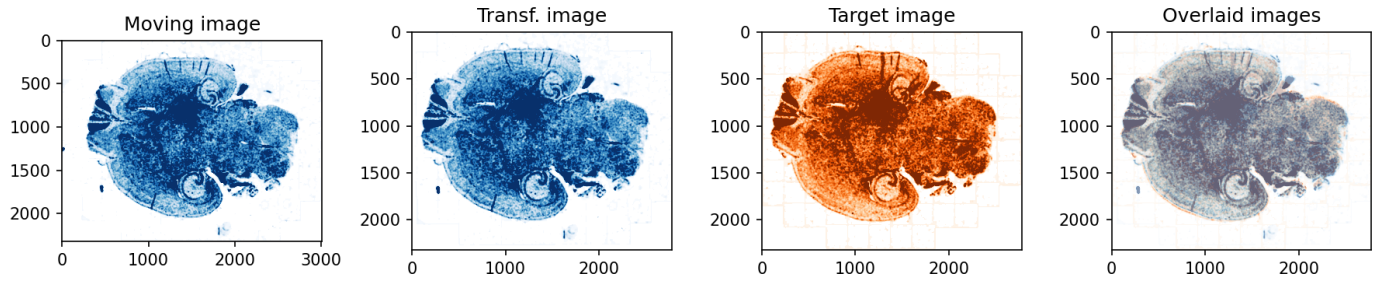


Figure 5.30: Results of registration of image 2020_04_25_NOK__0118-Scene-2 (Moving image) to 2020_04_25_GNI__0092-Scene-2 (Target image). $MI_norm = 0.97$

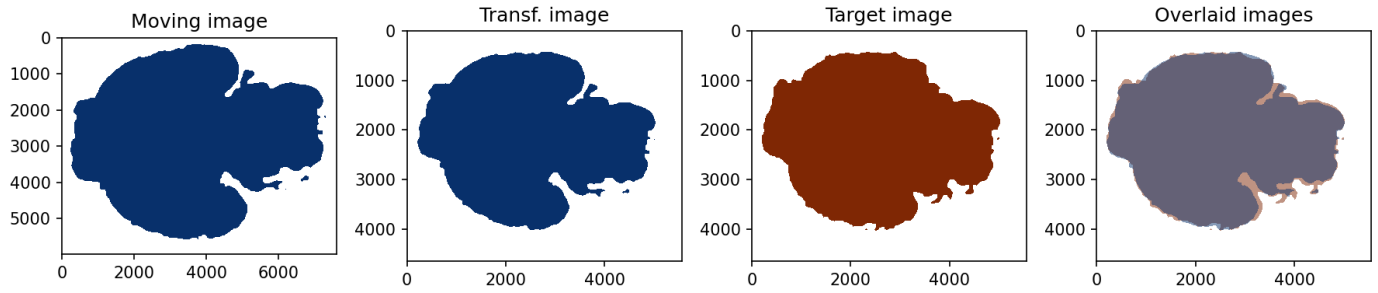


Figure 5.31: Results of registration of image P2A_C3H_M10_HE_0008-Scene-2-ScanRegion1 (Moving image) to 2020_04_25_GNI__0092-Scene-2 (Target image). Jaccard-coefficient = 0.95

5.1.17 0009_Scene_1

Raw images:

- 2020_04_25_GNI__0093-Scene-1.czi
- 2020_04_25_NOK__0119-Scene-1.czi
- P2A_C3H_M10_HE_0009-Scene-1-ScanRegion0.czi

Registered stainings: 3/3

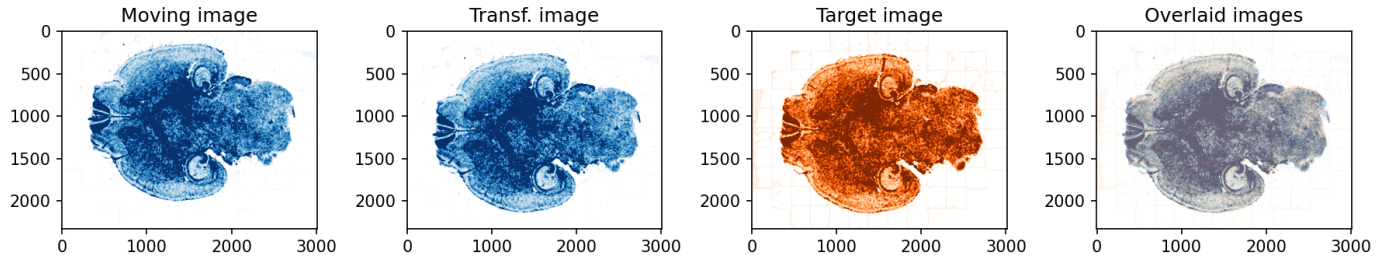


Figure 5.32: Results of registration of image 2020_04_25_NOK__0119-Scene-1 (Moving image) to 2020_04_25_GNI__0093-Scene-1 (Target image). $MI_norm = 0.00$

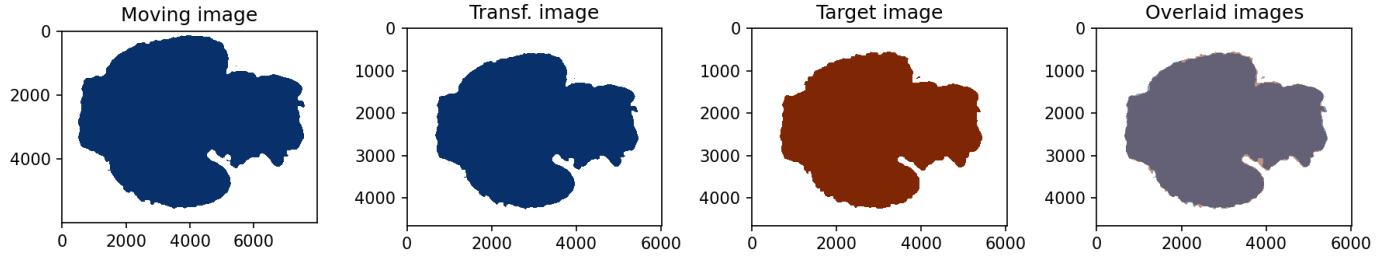


Figure 5.33: Results of registration of image P2A_C3H_M10_HE_0009-Scene-1-ScanRegion0 (Moving image) to 2020_04_25_GNI__0093-Scene-1 (Target image). Jaccard-coefficient = 0.97

5.1.18 0009_Scene_2

Raw images:

- 2020_04_25_GNI__0093-Scene-2.czi
- 2020_04_25_NOK__0119-Scene-2.czi
- P2A_C3H_M10_HE_0009-Scene-2-ScanRegion1.czi

Registered stainings: 3/3

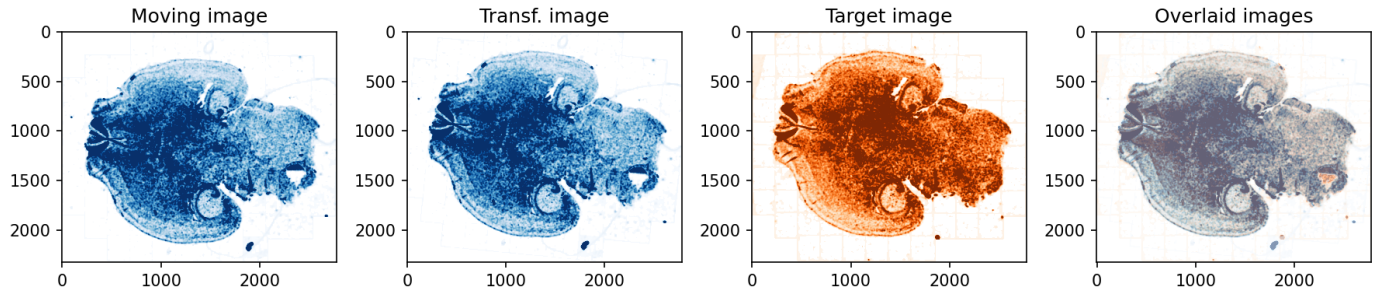


Figure 5.34: Results of registration of image 2020_04_25_NOK__0119-Scene-2 (Moving image) to 2020_04_25_GNI__0093-Scene-2 (Target image). $MI_norm = 0.90$

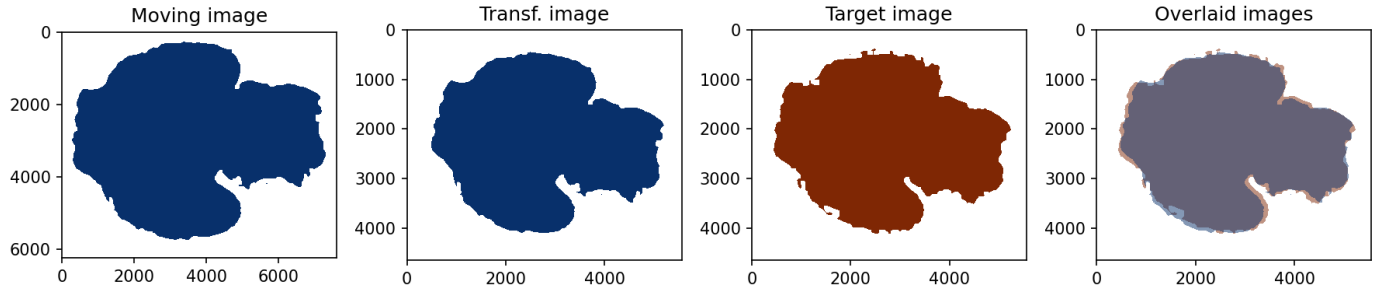


Figure 5.35: Results of registration of image P2A_C3H_M10_HE_0009-Scene-2-ScanRegion1 (Moving image) to 2020_04_25_GNI__0093-Scene-2 (Target image). Jaccard-coefficient = 0.94

5.1.19 0010_Scene_1

Raw images:

- 2020_04_25_GNI__0094-Scene-1.czi
- 2020_04_25_NOK__0120-Scene-1.czi
- P2A_C3H_M10_HE_0010-Scene-1-ScanRegion0.czi

Registered stainings: 3/3

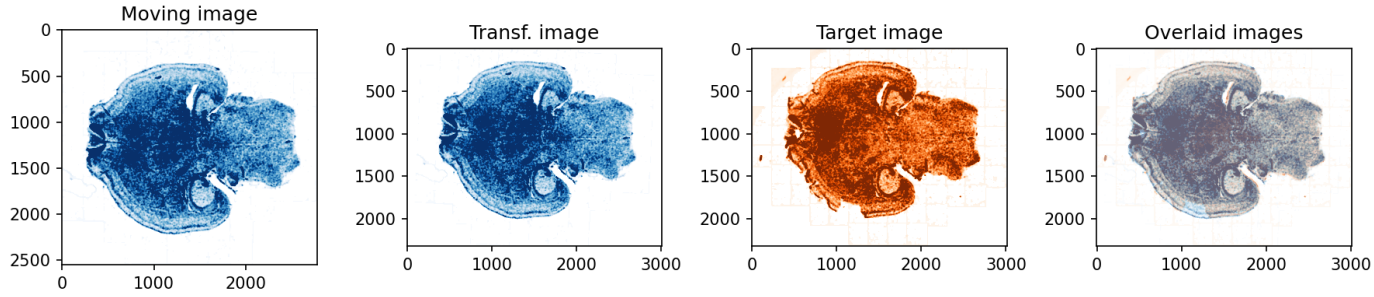


Figure 5.36: Results of registration of image 2020_04_25_NOK__0120-Scene-1 (Moving image) to 2020_04_25_GNI__0094-Scene-1 (Target image). $MI_norm = 0.93$

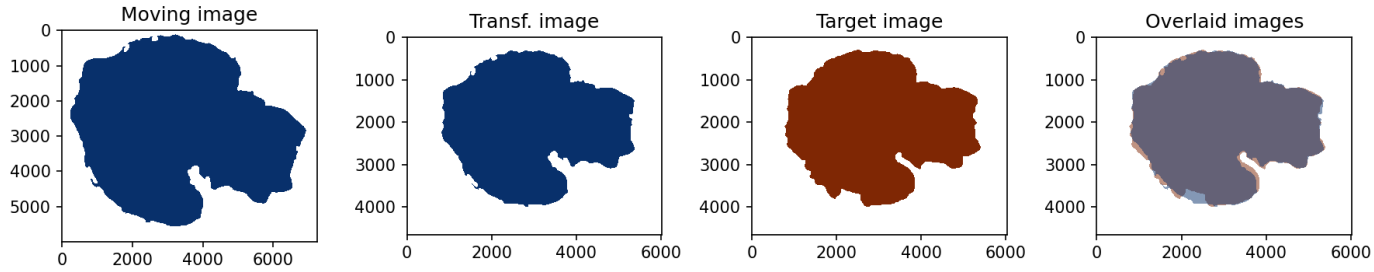


Figure 5.37: Results of registration of image P2A_C3H_M10_HE_0010-Scene-1-ScanRegion0 (Moving image) to 2020_04_25_GNI__0094-Scene-1 (Target image). Jaccard-coefficient = 0.95

5.1.20 0010_Scene_2

Raw images:

- 2020_04_25_GNI__0094-Scene-2.czi
- 2020_04_25_NOK__0120-Scene-2.czi
- P2A_C3H_M10_HE_0010-Scene-2-ScanRegion1.czi

Registered stainings: 3/3

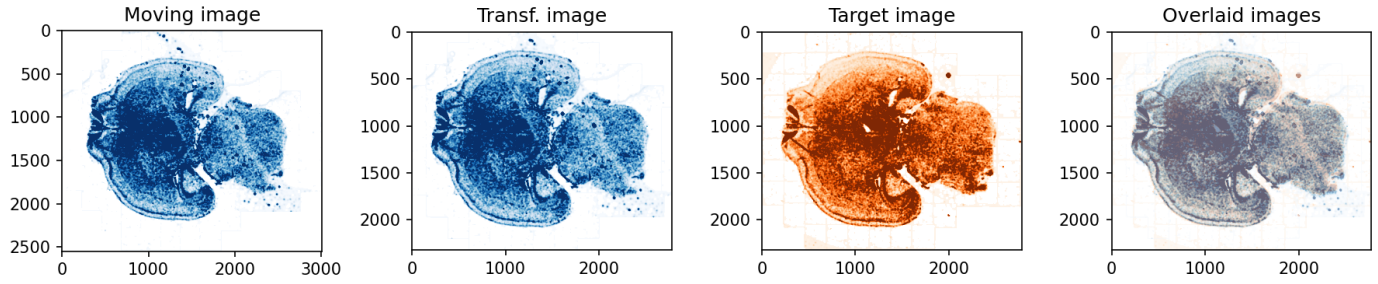


Figure 5.38: Results of registration of image 2020_04_25_NOK__0120-Scene-2 (Moving image) to 2020_04_25_GNI__0094-Scene-2 (Target image). $MI_norm = 0.93$

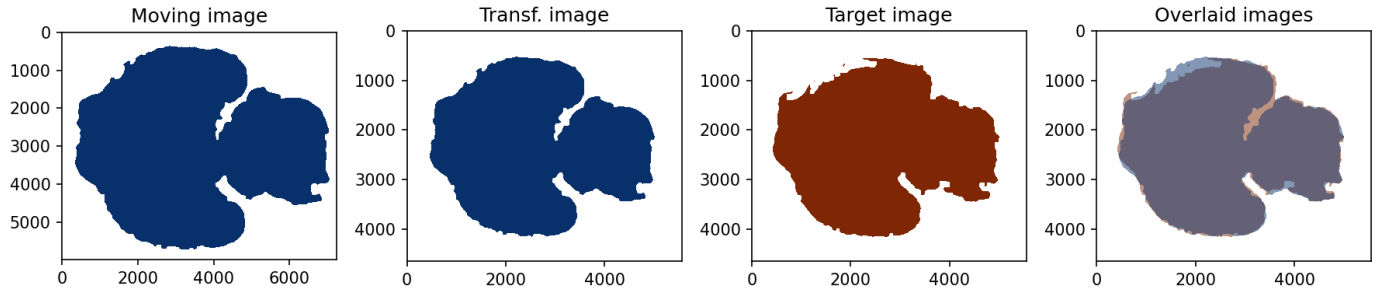


Figure 5.39: Results of registration of image P2A_C3H_M10_HE_0010-Scene-2-ScanRegion1 (Moving image) to 2020_04_25_GNI__0094-Scene-2 (Target image). Jaccard-coefficient = 0.93

5.1.21 0011_Scene_1

Raw images:

- 2020_04_25_GNI__0095-Scene-1.czi
- 2020_04_25_NOK__0121-Scene-1.czi
- P2A_C3H_M10_HE_0011-Scene-1-ScanRegion0.czi

Registered stainings: 3/3

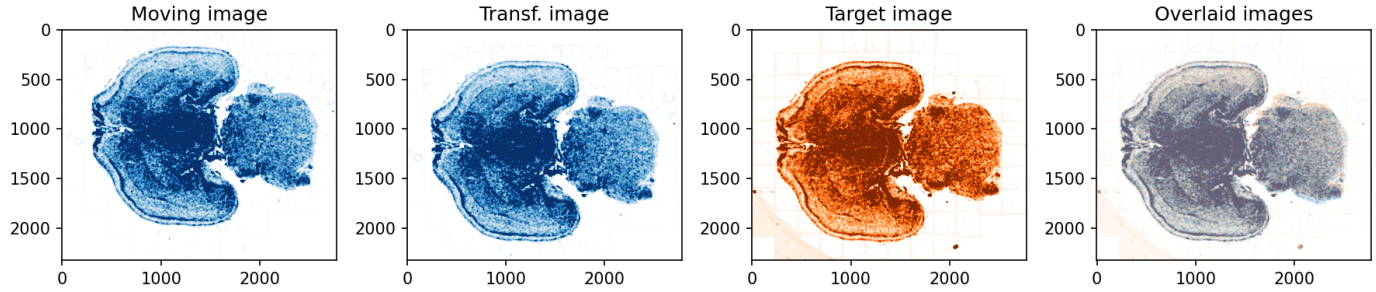


Figure 5.40: Results of registration of image 2020_04_25_NOK__0121-Scene-1 (Moving image) to 2020_04_25_GNI__0095-Scene-1 (Target image). $MI_norm = 0.00$

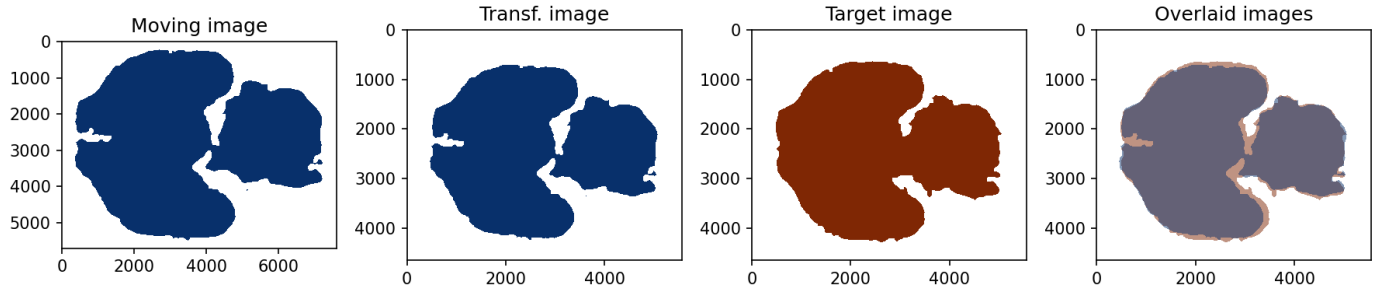


Figure 5.41: Results of registration of image P2A_C3H_M10_HE_0011-Scene-1-ScanRegion0 (Moving image) to 2020_04_25_GNI__0095-Scene-1 (Target image). Jaccard-coefficient = 0.92

5.1.22 0011_Scene_2

Raw images:

- 2020_04_25_GNI__0095-Scene-2.czi
- 2020_04_25_NOK__0121-Scene-2.czi
- P2A_C3H_M10_HE_0011-Scene-2-ScanRegion1.czi

Registered stainings: 3/3

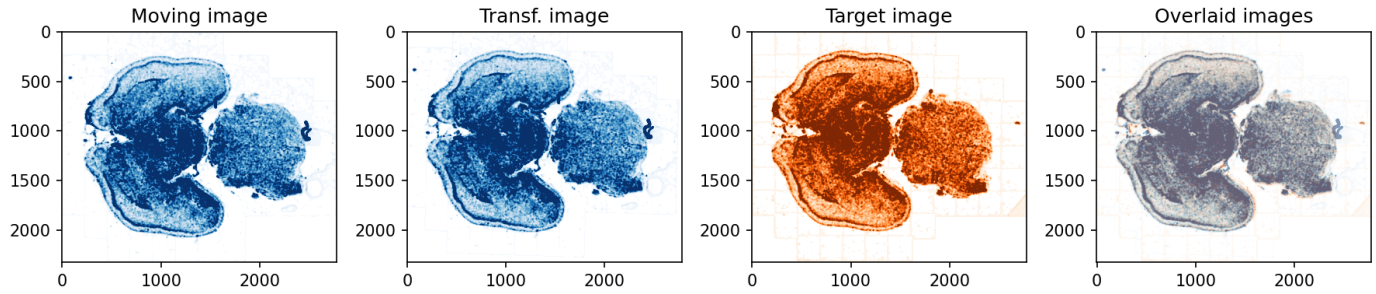


Figure 5.42: Results of registration of image 2020_04_25_NOK__0121-Scene-2 (Moving image) to 2020_04_25_GNI__0095-Scene-2 (Target image). $MI_norm = 0.86$

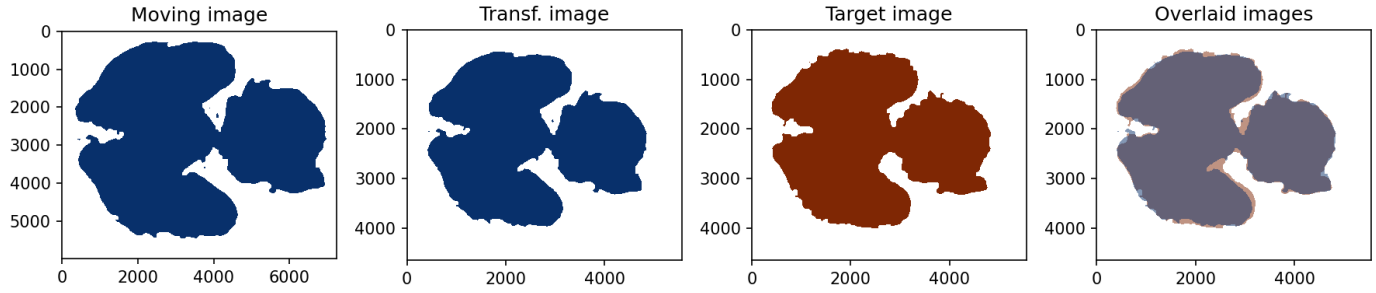


Figure 5.43: Results of registration of image P2A_C3H_M10_HE_0011-Scene-2-ScanRegion1 (Moving image) to 2020_04_25_GNI__0095-Scene-2 (Target image). Jaccard-coefficient = 0.94

5.1.23 0012_Scene_1

Raw images:

- 2020_04_25_GNI__0096-Scene-1.czi
- 2020_04_25_NOK__0122-Scene-1.czi
- P2A_C3H_M10_HE_0012-Scene-1-ScanRegion0.czi

Registered stainings: 3/3

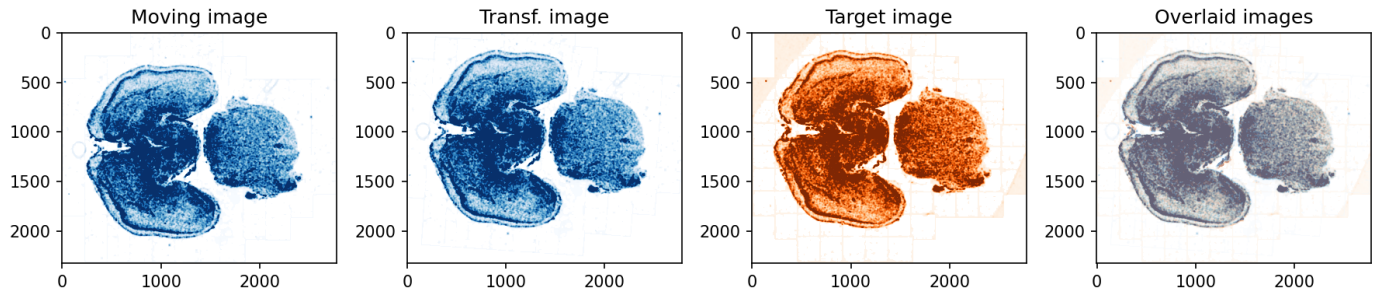


Figure 5.44: Results of registration of image 2020_04_25_NOK__0122-Scene-1 (Moving image) to 2020_04_25_GNI__0096-Scene-1 (Target image). $MI_norm = 0.94$

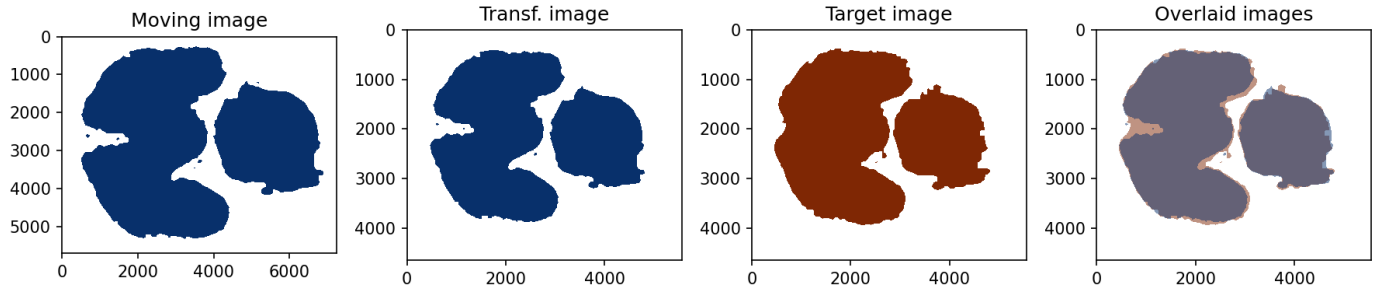


Figure 5.45: Results of registration of image P2A_C3H_M10_HE_0012-Scene-1-ScanRegion0 (Moving image) to 2020_04_25_GNI__0096-Scene-1 (Target image). Jaccard-coefficient = 0.93

5.1.24 0012_Scene_2

Raw images:

- 2020_04_25_GNI__0096-Scene-2.czi
- 2020_04_25_NOK__0122-Scene-2.czi
- P2A_C3H_M10_HE_0012-Scene-2-ScanRegion1.czi

Registered stainings: 3/3

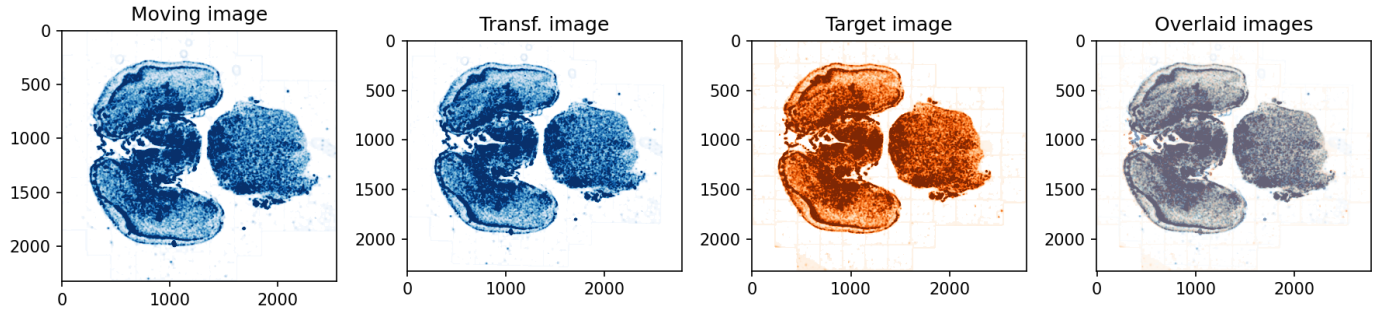


Figure 5.46: Results of registration of image 2020_04_25_NOK__0122-Scene-2 (Moving image) to 2020_04_25_GNI__0096-Scene-2 (Target image). $MI_norm = 0.94$

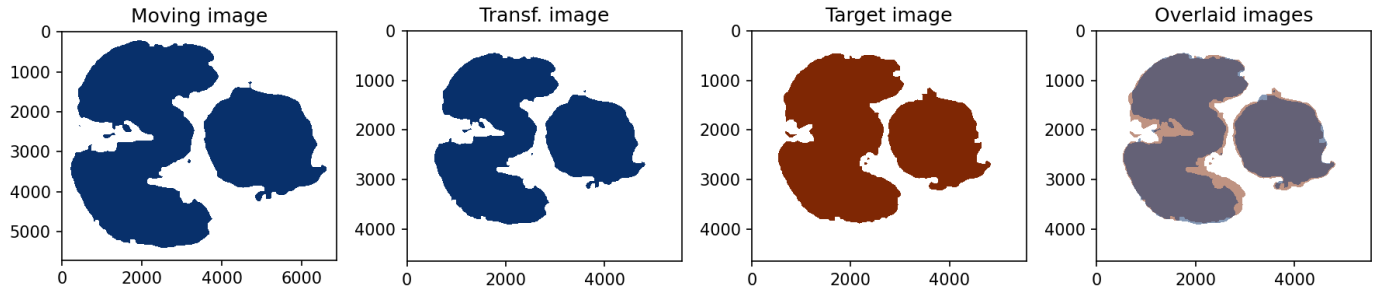


Figure 5.47: Results of registration of image P2A_C3H_M10_HE_0012-Scene-2-ScanRegion1 (Moving image) to 2020_04_25_GNI__0096-Scene-2 (Target image). Jaccard-coefficient = 0.89

5.1.25 0013_Scene_1

Raw images:

- 2020_04_25_NOK__0123-Scene-1.czi
- P2A_C3H_M10_HE_0013-Scene-1-ScanRegion0.czi

Registered stainings: 2/3

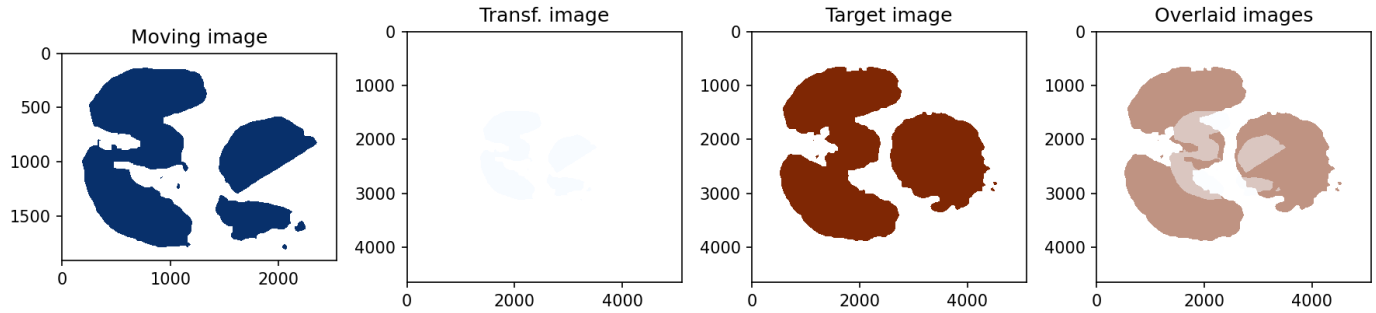


Figure 5.48: Results of registration of image P2A_C3H_M10_HE_0013-Scene-1-ScanRegion0 (Moving image) to 2020_04_25_NOK__0123-Scene-1 (Target image). Jaccard-coefficient = 0.19

5.1.26 0013_Scene_2

Raw images:

- 2020_04_25_NOK__0123-Scene-2.czi
- P2A_C3H_M10_HE_0013-Scene-2-ScanRegion1.czi

Registered stainings: 2/3

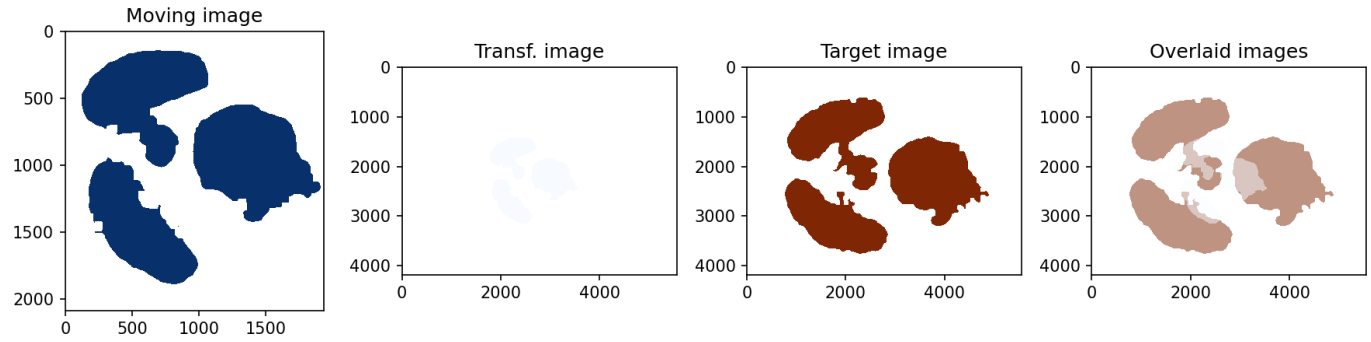


Figure 5.49: Results of registration of image P2A_C3H_M10_HE_0013-Scene-2-ScanRegion1 (Moving image) to 2020_04_25_NOK__0123-Scene-2 (Target image). Jaccard-coefficient = 0.12

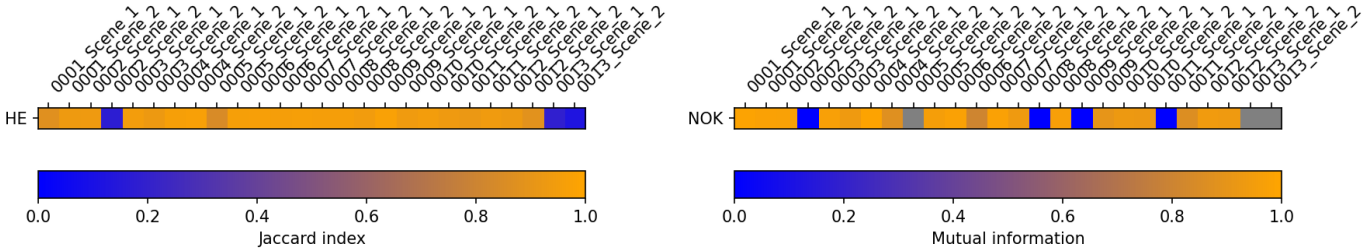


Figure 5.50: Separate Jaccard index (JC) and normalized mutual information (MI) for every histology bundle and registration step.

Overall quantified intensity-based registration quality:
Normalized mutual information for intensity-based registrations $MI_{norm} = 0.78 \pm 0.36$, Jaccard-coefficient (JC) for contour-based registrations $JC = 0.85 \pm 0.25$

5.2 Slice2Volume

Forward transformation files: 23/26
Inverse transformation files: 23/26

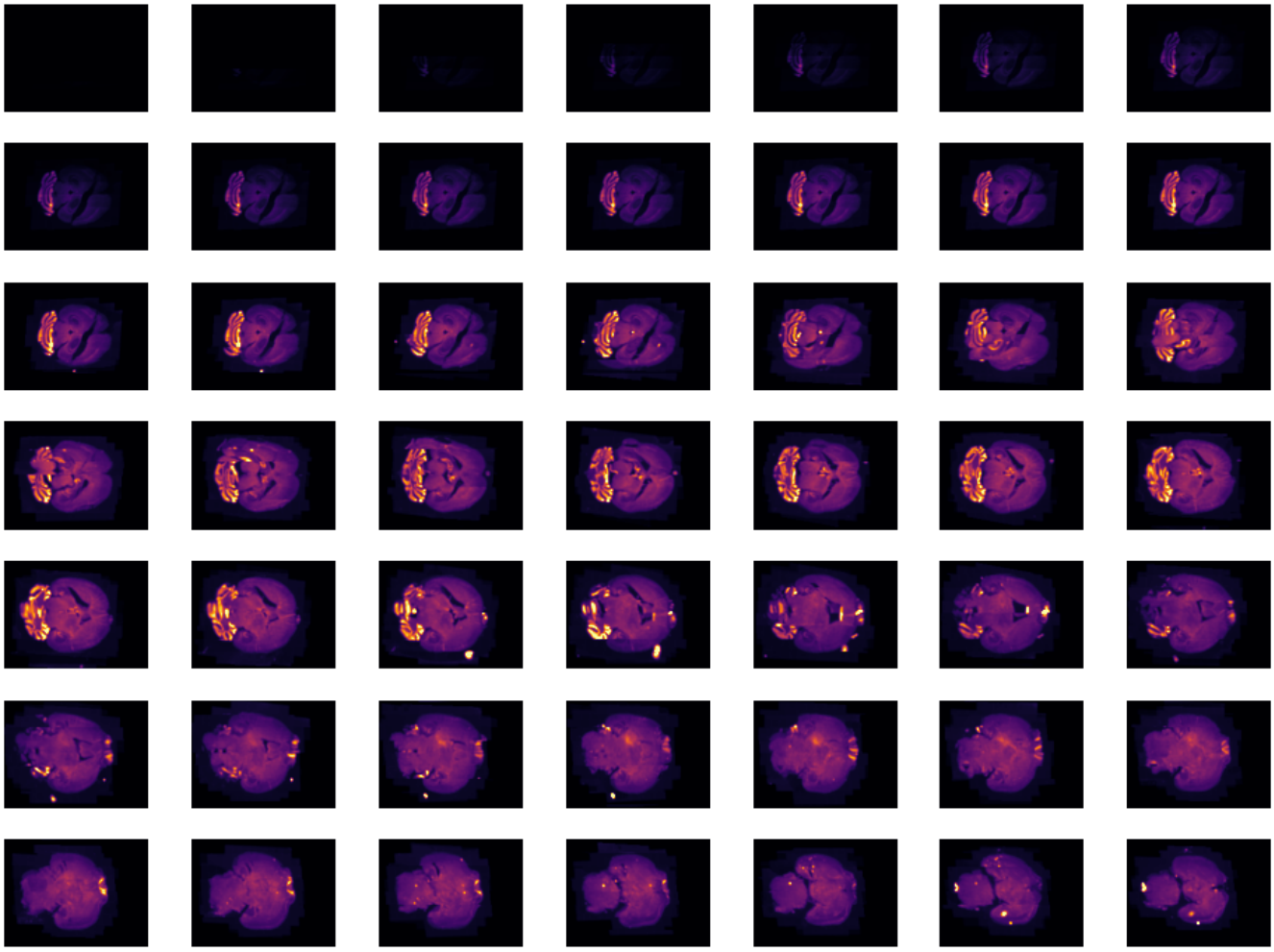


Figure 5.51: Sequence of coronal DAPI images that were transformed with Slice2Volume. This view allows to evaluate the consistency of subsequent slices.

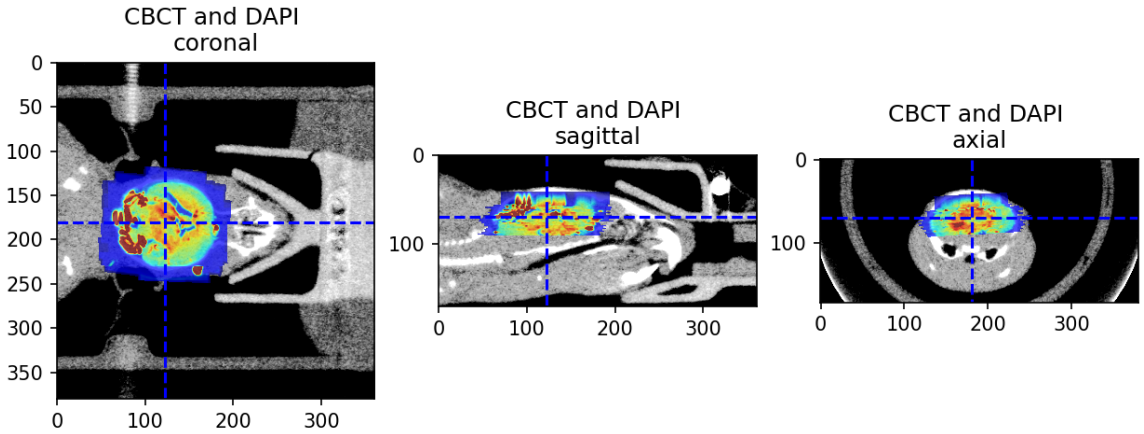


Figure 5.52: Overlay of downsampled and transformed histological image (transformed_DAPI) and CBCT

5.3 Histology close-up

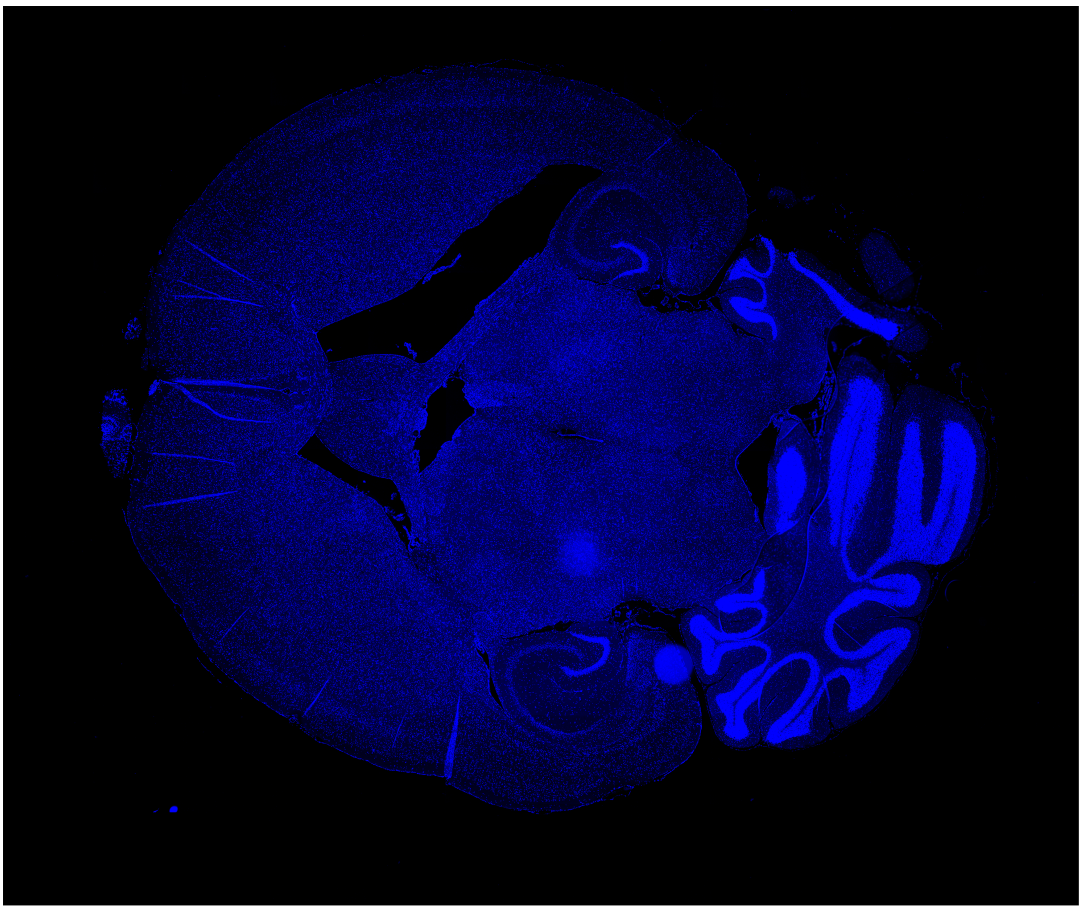


Figure 5.53: DAPI-staining from plane 0005_Scene_2

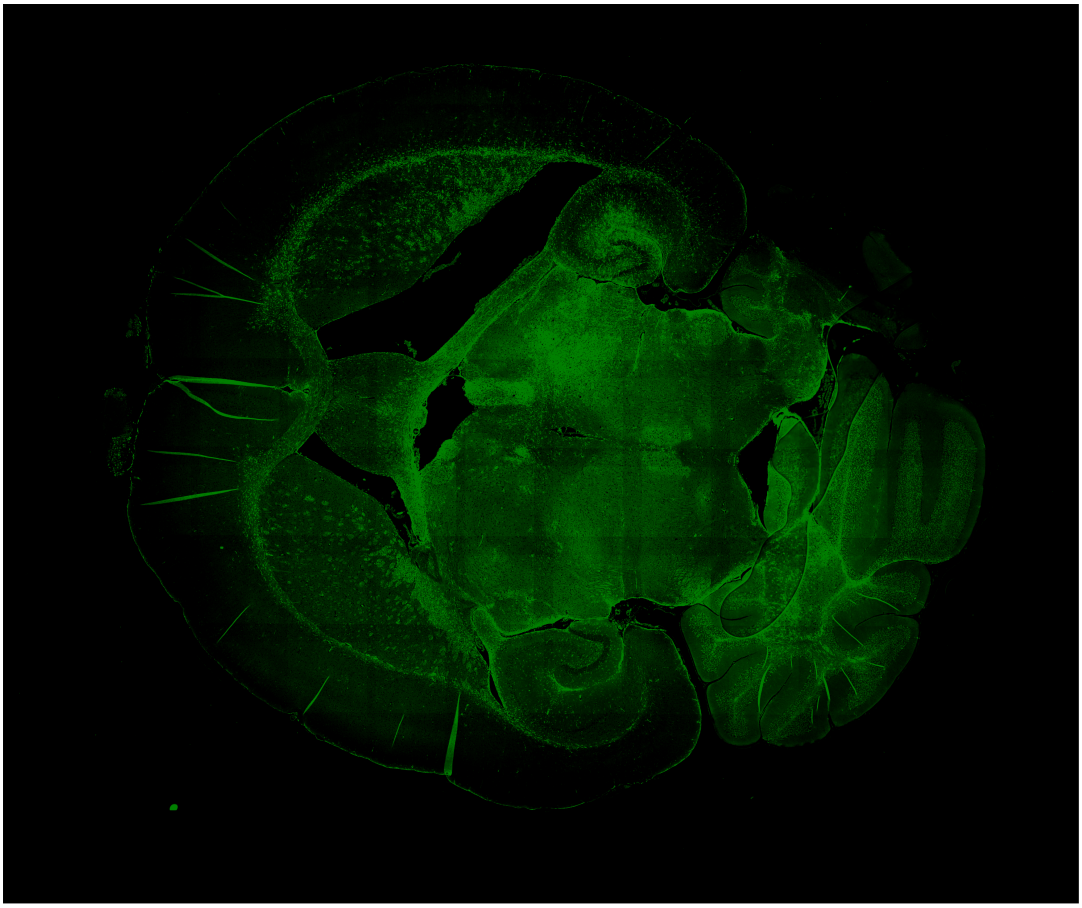


Figure 5.54: GFAP-staining from plane 0005_Scene_2

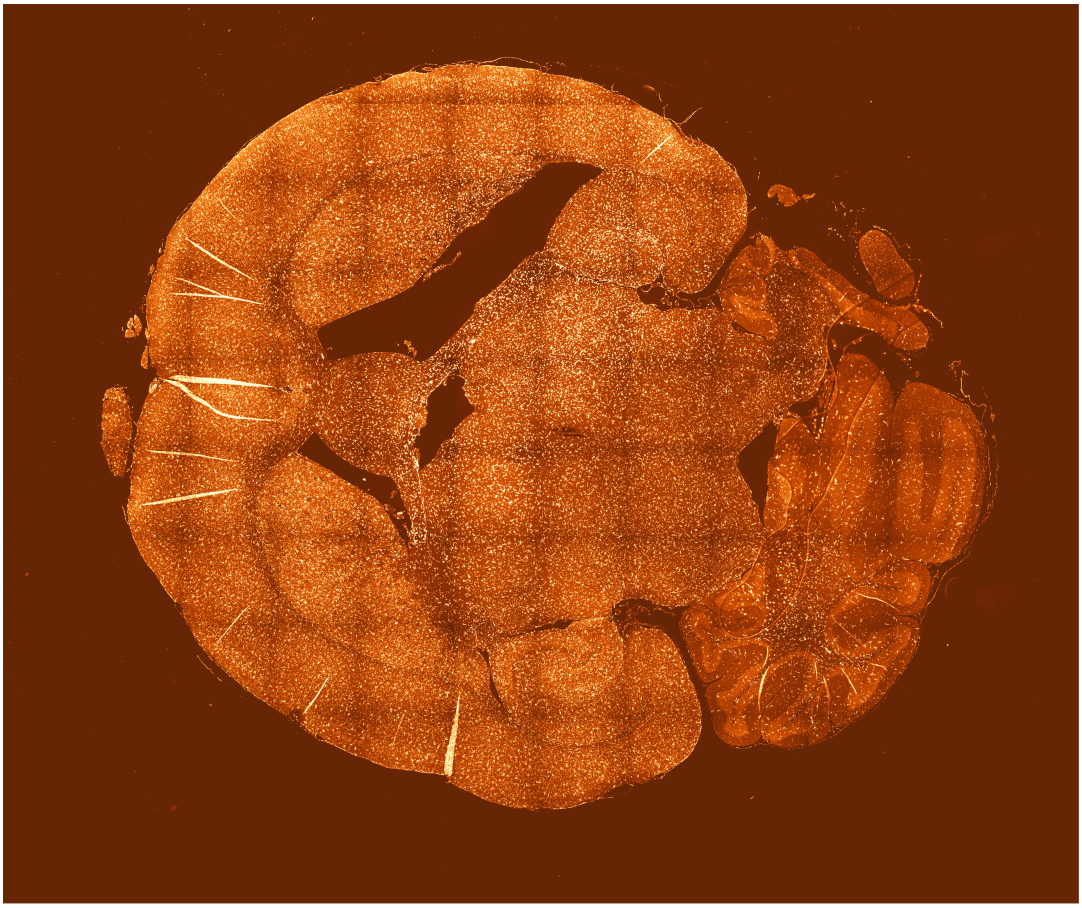


Figure 5.55: Iba1-staining from plane 0005_Scene_2

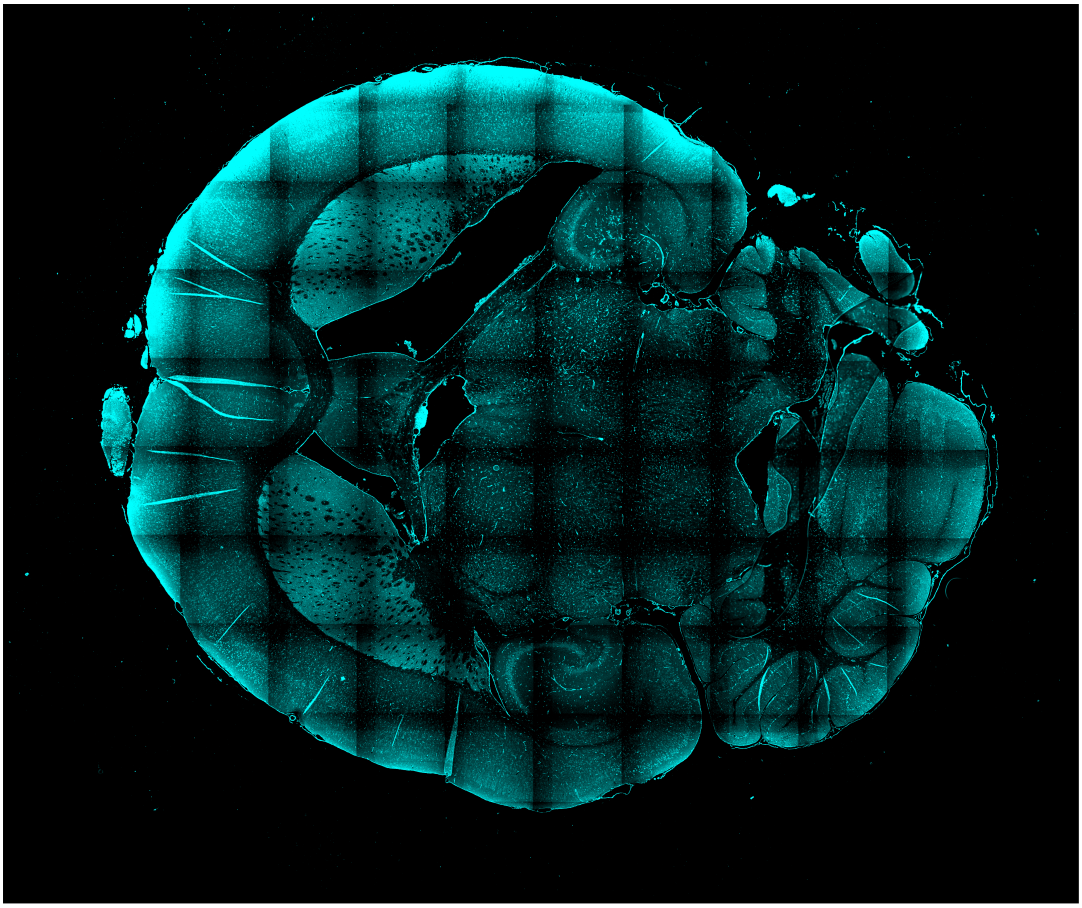


Figure 5.56: Nestin-staining from plane 0005_Scene_2

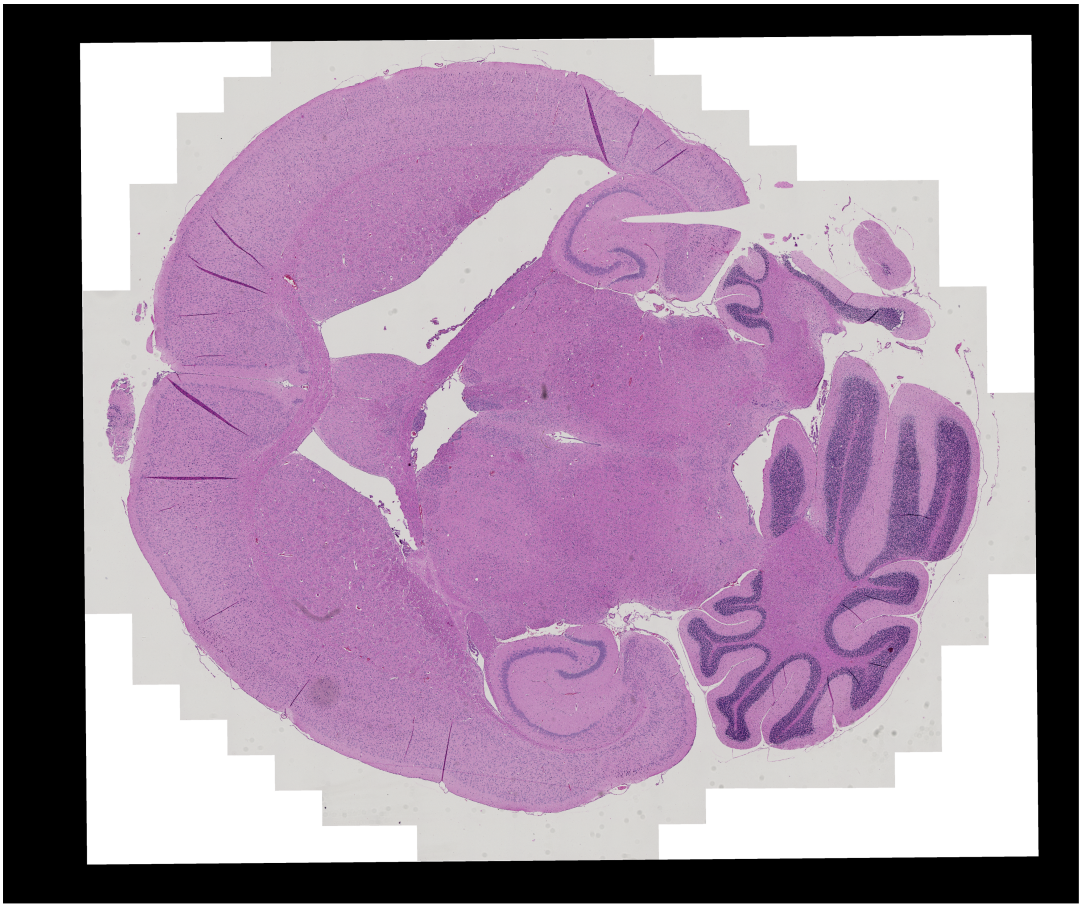


Figure 5.57: HE-staining from plane 0005_Scene_2

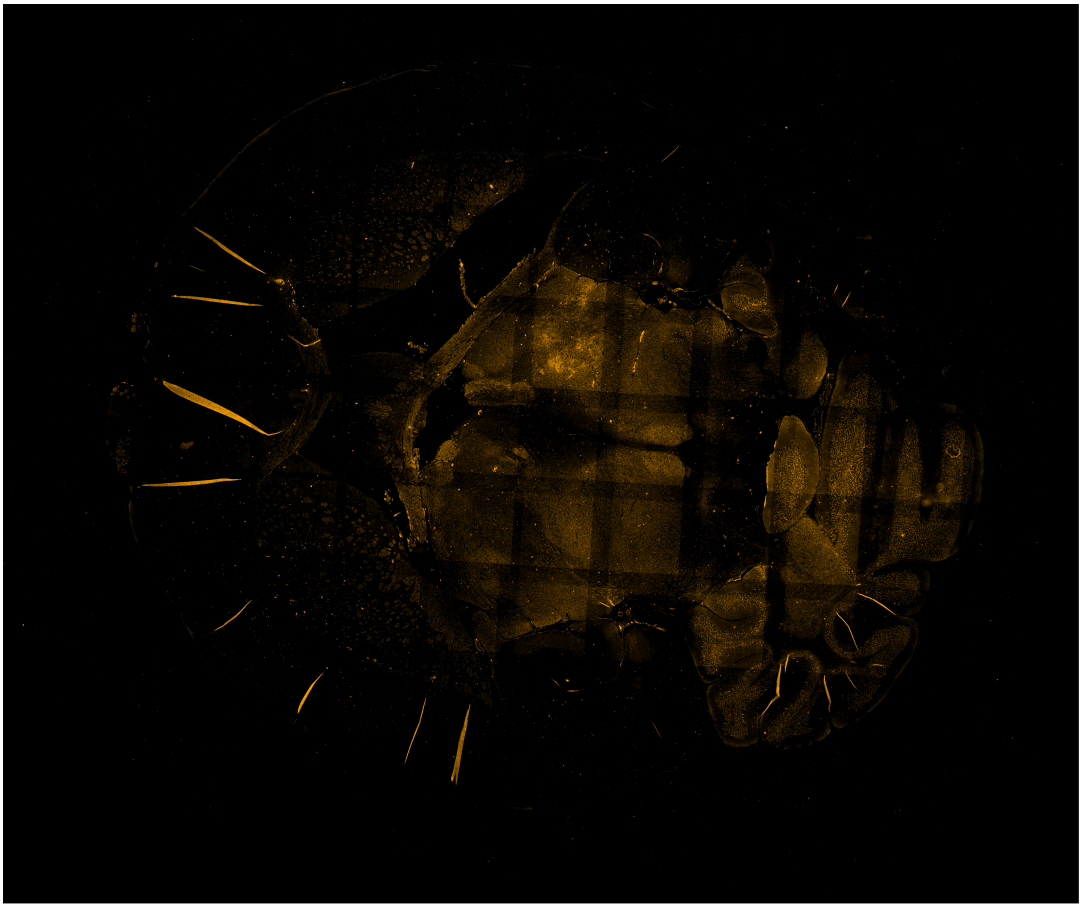


Figure 5.58: Ki67-staining from plane 0005_Scene_2

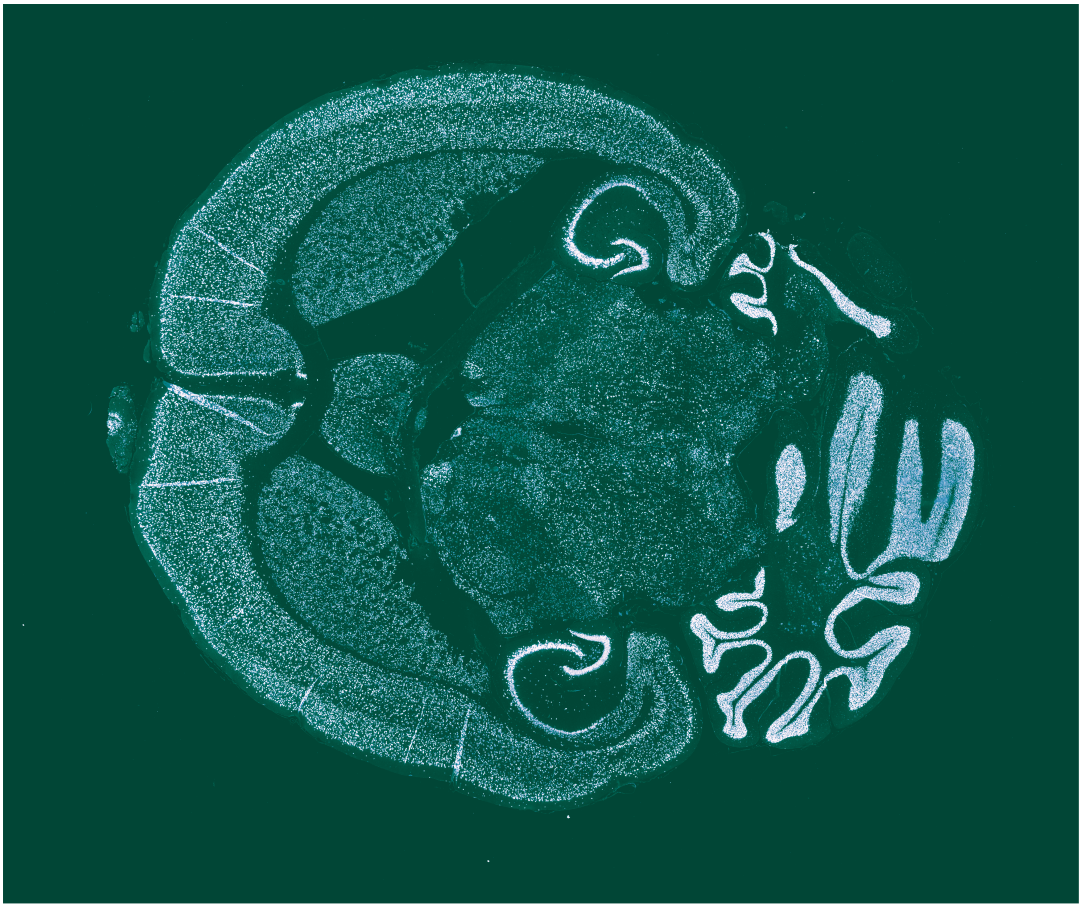


Figure 5.59: NeuN-staining from plane 0005_Scene_2

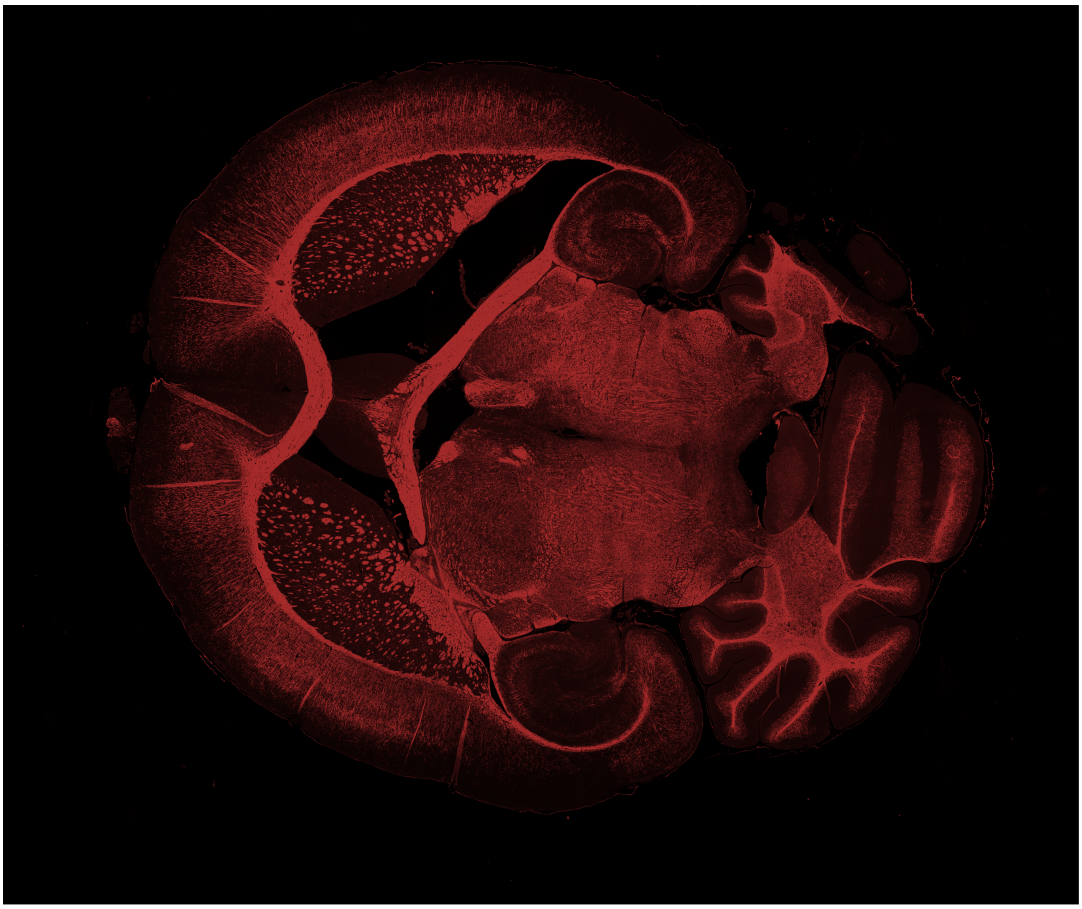


Figure 5.60: OSP-staining from plane 0005_Scene_2

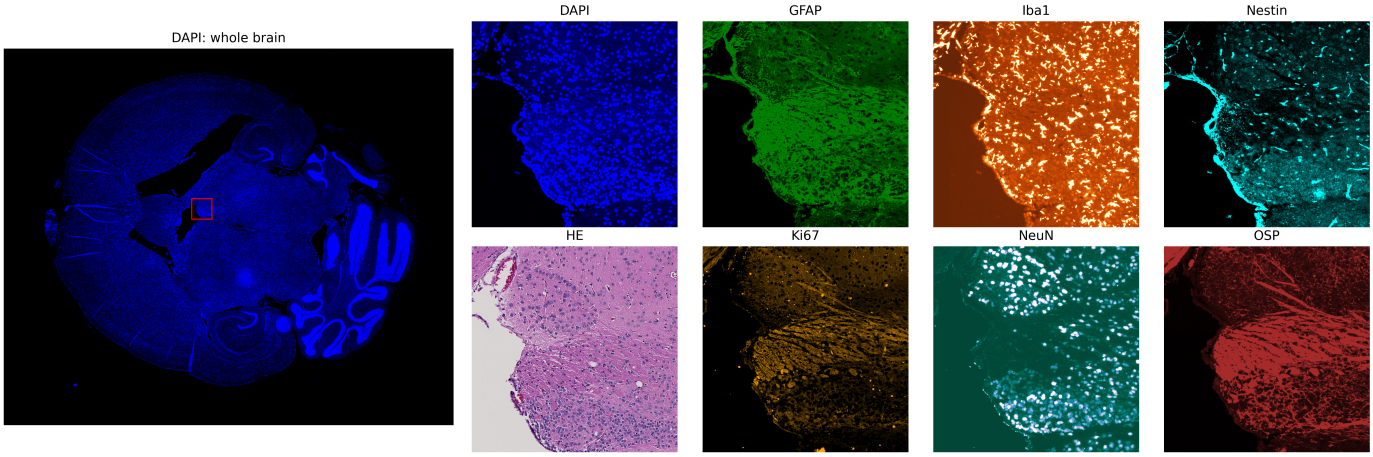


Figure 5.61: Selection of image details of the various co-aligned stainings. The position of the image detail is indicated by the red rectangle in the whole-brain DAPI image. The selected section for this overview was 0005_Scene_2.

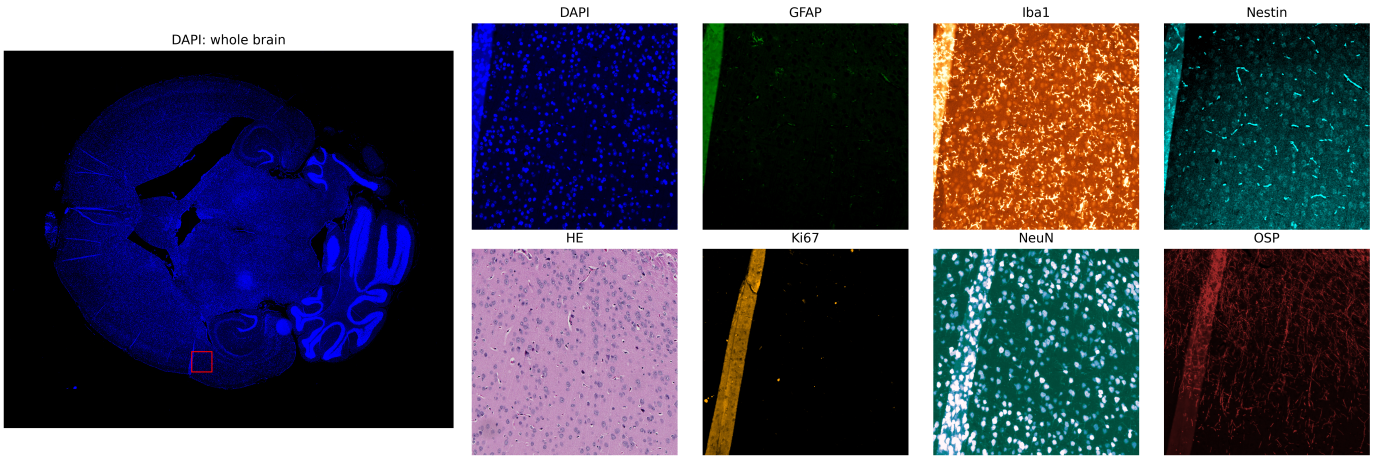


Figure 5.62: Selection of image details of the various co-aligned stainings. The position of the image detail is indicated by the red rectangle in the whole-brain DAPI image. The selected section for this overview was 0005_Scene_2.